



**Università  
degli Studi  
di Ferrara**

DOCTORAL COURSE IN  
“Molecular Medicine”

CYCLE XXXIV

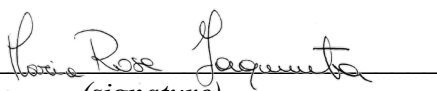
COORDINATOR Prof. Francesco Di Virgilio

***In vitro* mesenchymal stem cell osteogenic differentiation and  
immunomodulation, and bone regrowth in patients,  
are induced by innovative biomaterials**

Scientific/Disciplinary Sector (SDS) BIO/13


**Candidate**

Dr. Iaquina Maria Rosa

  
(signature)

**Supervisor**

Prof. Martini Fernanda

  
(signature)

Years 2018/2021

## INDEX

<b>1. INTRODUCTION</b> .....	3
<b>1.1. General introduction</b> .....	4
<b>1.2. Bone remodelling</b> .....	5
<b>1.3. Bone fracture and fracture healing</b> .....	6
<b>1.4. Stem cells</b> .....	7
<b>1.4.1. hMSC osteogenic differentiation</b> .....	9
<b>1.5. Biomaterials</b> .....	9
<b>1.5.1. Ceramic Biomaterials</b> .....	10
<b>1.5.2. Polymers</b> .....	12
<b>1.5.3. Composite Biomaterials</b> .....	13
<b>2. AIMS</b> .....	14
<b>3. MATERIALS AND METHODS</b> .....	17
<b>3.1. Biomaterials</b> .....	18
<b>3.1.1. Pro Osteon® 200/Avitene™ composite biomaterial</b> .....	18
<b>3.1.2. Bio-Oss®/Avitene™ composite biomaterial</b> .....	18
<b>3.1.3. Bioceramic biomorphic hydroxlyapatite</b> .....	18
<b>3.2. Cell culture</b> .....	18
<b>3.3. Microstructural Analysis</b> .....	19
<b>3.4. Cell Morphology</b> .....	19
<b>3.5. Cytoskeleton Architecture</b> .....	20
<b>3.6. Cell Proliferation Assay</b> .....	20
<b>3.7. Matrix Mineralization</b> .....	20
<b>3.8. Alkaline phosphatase protein expression</b> .....	20
<b>3.9. Osteocalcin protein expression</b> .....	21
<b>3.10. Cytokine/Chemokine and Osteogenic gene expression</b> .....	21
<b>3.11. Statistical Analysis</b> .....	21
<b>3.12. <i>In vivo</i> evaluation</b> .....	22
<b>4. RESULTS</b> .....	23
<b>4.1. Pro Osteon® 200/Avitene™ composite biomaterial</b> .....	24
<b>4.2. Bio-Oss®/Avitene™ composite biomaterial</b> .....	36
<b>4.3. Biomorphic hydroxlyapatite</b> .....	44
<b>5. DISCUSSION</b> .....	51
<b>5.1. Pro Osteon 200/Avitene and Bio-Oss®/Avitene™ composite biomaterials</b> .....	52
<b>5.2. Biomorphic hydroxylapatite scaffold</b> .....	61
<b>6. CONCLUSIONS</b> .....	66
<b>7. Research activity at AO RESEARCH INSTITUTE</b> .....	68
<b>7.1. INTRODUCTION</b> .....	69
<b>7.2. MATERIALS AND METHODS</b> .....	72
<b>7.3. RESULTS</b> .....	75
<b>7.4. DISCUSSION</b> .....	81
<b>8. REFERENCES</b> .....	84
<b>9. SCIENTIFIC CONTRIBUTION</b> .....	98

# **1. INTRODUCTION**

## 1.1. General introduction

Bone is a rigid and highly dynamic structure that supports and protects several organs of the body. Furthermore, bone tissue produces red and white blood cells, plays an important role in mineral homeostasis, such as calcium and phosphorus, and gives a solid ground to skeletal muscles [1]. In bone tissue, two different phases can be distinguished: bone matrix and an organic phase [2] (**Figure 1**). Bone matrix is a dynamic system that represents the intercellular substance of bone tissue. It is composed of several organic and inorganic components, such as collagen type I (which represents the most abundant protein in bone tissue), elastin, polysaccharides, and calcium phosphate [3–5]. Among the principal non-collagenous proteins of the bone matrix there are osteonectin (ON), osteopontin (OPN), and osteocalcin (OCN)[6], which contain aspartic acid (Asp) and glutamic acid (Glu) residues, with a high affinity for calcium ions ( $\text{Ca}^{2+}$ ) due to their charged carboxyl groups [6]. The inorganic component of bone matrix is an ion reservoir [7]. Hydroxylapatite (HA;  $\text{Ca}_{10}(\text{PO}_4)_6(\text{OH})_2$ ) is the major inorganic crystal phase, with citrate, carbonate and several ions [8], such as  $\text{F}^-$ ,  $\text{K}^+$ ,  $\text{Sr}^{2+}$ ,  $\text{Pb}^{2+}$ ,  $\text{Zn}^{2+}$ ,  $\text{Cu}^{2+}$ , and  $\text{Fe}^{2+}$ .

In the organic phase, osteoblasts and osteoclasts represent the majority bone tissue cells [9]. The specialised cells that resorb bone [10], the osteoclasts, derive from the myeloid lineage of hematopoietic precursors of bone marrow, can also circulate in the bloodstream. On the other hand, osteoblasts derived from human mesenchymal stem cells (hMSCs) in bone marrow, blood and also from pericytes are implicated in bone formation and substitute bone removed by osteoclasts [11]. The hMSC migration to the bone surface is a complex mechanism, as well as an important step in both bone formation and fracture healing. Indeed, alterations in MSC migration can lead to abnormal bone imbalances [12].

Other osteoblast-derived cells exist in bone tissue, such as bone lining cells and osteocytes. Bone lining cells cover the bone surface, where bone resorption or bone formation is not requested [13], while osteocytes derived from osteoblasts that interrupt their activity when buried in the matrix. Osteocytes recognize old or damaged bone areas and recruit osteoclast precursors at the remodelling bone site [14]. When considered together, these cells are organised into temporary anatomical structures called Basic Multicellular Units (BMU). It has been defined the BMUs as the key grouping of cells that carry out bone remodelling, a biological process that leads to structural changes and skeletal renewal [15] (**Figure 1**).

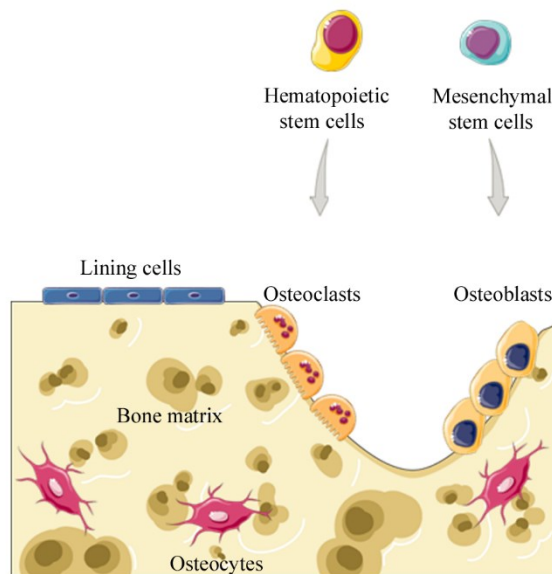


**Figure 1.** Bone remodelling. Bone tissue is subjected to bone remodelling, a life-dominant process that plays an important role in bone mass balance and mineral homeostasis. During bone remodelling osteoclasts, derived from hematopoietic stem cells, resorb old, or damaged bone. Subsequently, osteoblasts, derived from mesenchymal stem cells, are recruited to the damaged area in order to replace bone removed by osteoclasts. Instead, osteocytes derived from osteoblasts suspend their activity when buried in the bone matrix.

## 1.2. Bone remodelling

Bone remodelling consists in some sequential steps: initiation, reversal, and termination phases. During the initiation phase, osteoclast precursors are recruited and differentiated into mature osteoclasts in order to allow bone resorption. Osteoclastogenesis requires specific key factors, such as macrophage colony-stimulating factor (M-CSF or CSF-1) and receptor activator of nuclear factor- $\kappa$ B ligand (RANKL or TNFSF11). M-CSF is produced by osteoblasts and many other cell types; it is necessary for the osteoclast precursor proliferation, differentiation and fusion into osteoclasts [16]. On the other hand, RANKL binds its receptor RANK, localised on the surface of osteoclast precursors, to allow fusion, maturation, survival, and activation of osteoclasts [17,18]. Osteocytes seem to be the main source of the RANKL, which is required for osteoclast formation [19]. During bone resorption, a lot of factors that lead to recruitment and differentiation of hMSCs are released to allow bone formation in the bone marrow microenvironment [20]. The next transient phase, or reversal phase, consists in bone resorption inhibition and osteoblasts recruitment. In this context, osteoblasts can produce a protein called osteoprotegerin (OPG), which is a decoy receptor for RANKL. Thus, OPG prevents RANKL binding to RANK, inhibiting the osteoclast differentiation and activation [21]. The termination

phase represents the final step in the bone remodelling cycle, when an equal amount of resorbed bone has been replaced [22]. Osteocytes contribute to ending the remodelling process by producing sclerostin, which inhibits the bone formation induced by Wnt signalling in osteoblasts [23]. In the end, mature osteoblasts undergo apoptosis, become osteocytes or differentiate into bone lining cells [15].

A fine balance between bone resorption and bone production keeps the human skeleton in physiological conditions. Alterations to this process result in several skeletal diseases, such as osteoporosis [24], caused by excessive bone resorption, or osteopetrosis due to excessive bone formation [25].

### **1.3. Bone fracture and fracture healing**

Bone disorders are often seen on a daily basis in clinical management, with remarkable health, social and economic outcomes [26]. Loss of bone tissue affects more than 20 million people every year [27]. Bone repair after fracture is a complex process that leads to new bone formation through sequential cellular and molecular events regulated by systemic and local factors [28].

A hematoma, formed immediately after the trauma, consists of cells from peripheral and intramedullary blood, as well as bone marrow cells. An inflammatory reaction is triggered by the injury, which is required for healing. The hematoma coagulates in the spaces between and around the fracture ends, as well as within the medulla, establishing a template for callus formation [29].

Inflammatory cytokines have a negative effect on bone; however, a brief and highly regulated secretion of pro-inflammatory molecules, following the acute injury, is critical for tissue regeneration [29]. The acute inflammatory reaction peaks within the first 24h and is complete after 7 days. In the initial pro-inflammatory response, tumour necrosis factor- $\alpha$  (TNF- $\alpha$ ), interleukin-1 (IL1), IL6 and IL11 are involved. These factors recruit inflammatory cells and, at the same time, promote angiogenesis. During fracture healing, IL1 and IL6 are believed to be the most important interleukins. In the acute phase of inflammation, IL1 is produced by macrophages and induces production of IL6 in osteoblasts, promotes the production of the primary cartilaginous callus, and promotes angiogenesis at the injured site by activating either of its two receptors, IL1RI or IL1RII [29]. On the other hand, IL6 stimulates angiogenesis, vascular endothelial growth factor (VEGF) production, and the differentiation of osteoblasts and osteoclasts [30]. During the resolution of acute inflammation, macrophages are polarized from a M1 phenotype to a M2 phenotype by anti-inflammatory cytokines such as IL4, IL10, and IL13. The hBMSCs are attracted locally by cytokines, such as TNF $\alpha$  and stromal cell-

derived factor 1 (SDF1), also known as chemokine C-X-C motif chemokine ligand 12 (CXCL12) [31].

Although bone fracture repair usually restores the injured skeletal organ to its pre-injury state, approximately 10% of fractures do not heal properly [32]. In some cases, the bone regeneration process could fail in extensive bone resections and atrophic non-union [33,34]. Moreover, face rehabilitation, both functional and aesthetic, has grown in importance in maxillofacial surgery. Soft tissue asymmetry and/or bony framework abnormalities can also cause facial deformities or asymmetries. Natural proportions and harmonious face characteristics promote self-confidence and psychological well-being [35]. In clinical practice, normal conditions for affected bones can be restored using bone grafts including autograft and allograft. Autologous grafts represent the clinical gold standard in improving bone regeneration since due to histocompatibility, alongside osteoinductive and osteoconductive proprieties. However, autografts still show some disadvantages resulting from the limited amount of bone available for grafting and donor site morbidity. Conversely, allo-grafting represents an alternative approach to bone grafts with some drawbacks, such as a lack of donors, high costs, the risk of infectious agent transmission or immune reactions [33,36]. For these reasons, a more efficient clinical therapeutic strategy is needed.

To this purpose, tissue engineering has employed new osteoconductive and osteoinductive biomaterials/scaffolds, stem cells and growth factors to improve bone repair/regrowth [37]. Stem cells have been used in clinical applications for approximately 20 years, although their characteristics and potential for bone repair are yet to be fully elucidated [38]. Specifically, stem cells have been taken into consideration in several medical disciplines to repair defective tissue and organs, including bone [1].

#### **1.4. Stem cells**

Several types of stem cells have been put forward as a source of osteoblast progenitors [39]. Examples are human embryonic stem cells (hESCs), induced pluripotent stem cells (iPSCs) and human mesenchymal stem cells (hMSCs) [40].

My experimental thesis is addressed to highlight hMSCs involvement in regenerative medicine and the potential application in clinical practice. HMSCs are adherent cells positive for CD73, CD90 and CD105 markers (>95%) and negative for other specific antigens, such as CD45, CD34, CD14, CD79, and HLA class II (<2%), as defined by the International Society for Cellular Therapy (ISCT) [41]. HMSCs, first reported in bone marrow, [42] were then identified in other adult tissues (**Figure 2**) [2,43]. HMSCs derived from adipose tissue (hASCs) and bone marrow (hBMSCs) are probably the most common hMSCs used in clinical practice [44]. At

present they are one of the most studied stem cells, especially toward the healing of diseased and damaged tissues and organs.

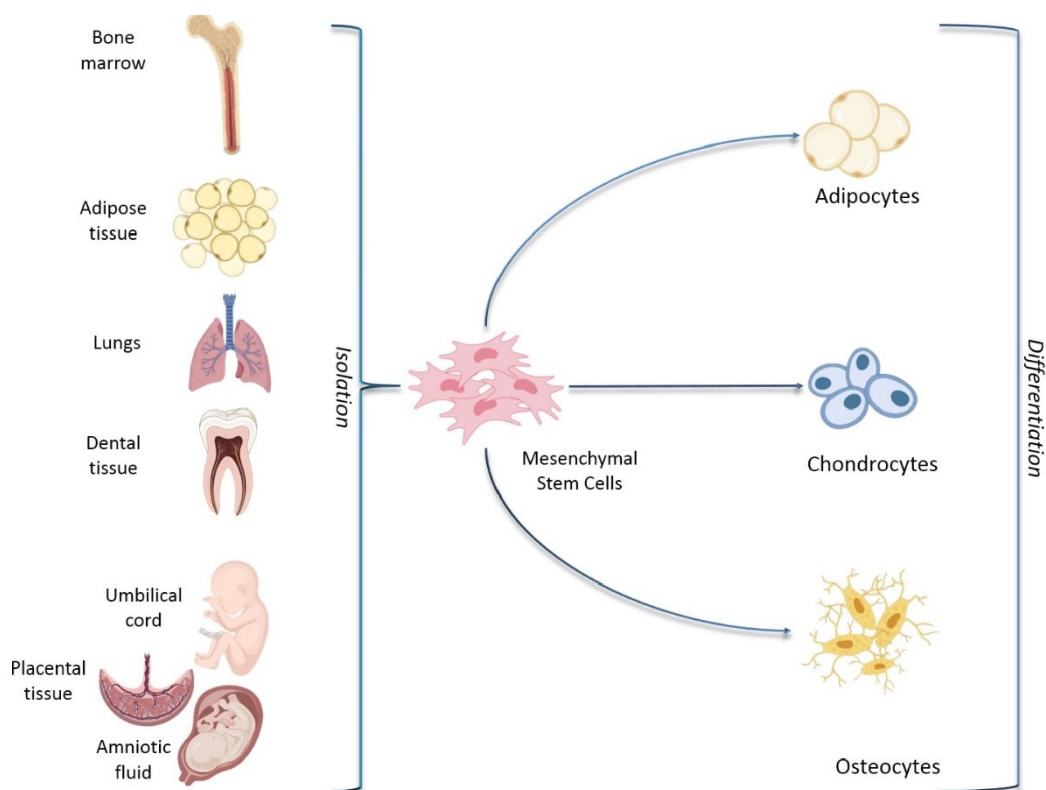


**Figure 2.** Schematic representation of adult and foetal/neonatal tissue sources of mesenchymal stem cells (MSCs) and their potential of differentiation in various cell lines. MSCs can be isolated from several tissue sources and they may differentiate into adipocytes, chondrocytes and osteocytes.

Human MSCs seem to have potent anti-inflammatory and immunomodulatory properties, in addition to their ability to form both cartilage and bone. As a result of these characteristics, hMSCs could be employed for the treatment of autoimmune disease, whereas further clinical studies are needed to produce sound evidence [45]. MSCs have the ability to release bioactive factors, which may potentially affect both local and systemic physiological processes [2,46]. The anti-inflammatory effect of MSC conditioned medium (CM) has been well investigated. The anti-inflammatory effect of MSC is at least in part mediated by soluble immunoregulatory molecules. Among the anti-inflammatory cytokines present in MSC-CM, IL13 [47,48], IL18 binding protein (IL18BP), CNTF, IL10, IL27 or IL1 receptor antagonist (IL1RA) [47] have been reported. MSC-CM has also been found to contain pro-inflammatory cytokines, such as IL1b [47], IL6 [49], IL8 and IL9 [50]. Nevertheless, it is also remarkable that MSCs inhibit



proinflammatory cytokines, such as interferon (IFN) gamma and tumour necrosis factor (TNF), while increasing anti-inflammatory IL10 release [51,52].

#### **1.4.1. hMSC osteogenic differentiation**

Human MSCs are capable of self-replication or differentiate into multiple cell lineages, such as adipocytes, osteoblasts and chondrocytes. In vitro, osteogenic differentiation cocktails typically contain at least 10 nM of dexamethasone (dex) [53], together with  $\beta$ -glycerolphosphate and ascorbic acid [54]. Recent studies provide evidence for an off-target adipocytic differentiation in standard osteogenic cultures of hBMSCs induced by dex. Previous results demonstrated that dex induces osteogenesis by inhibiting SRY-Box Transcription Factor 9 (SOX9) gene expression and not by up-regulating the expression of RUNX Family Transcription Factor 2 (RUNX2) [53]. Moreover, dex also stimulates adipogenesis by inducing the expression of peroxisome proliferator-activated receptor gamma (PPARG), the adipogenic transcription factor. However, additional studies are needed to identify which mediators lead to SOX9 downregulation [53].

Because several epigenetic factors play an important role in hMSC differentiation, a large number of studies have been conducted on i) the biological properties of hMSCs and ii) factors that might facilitate hMSC chondrogenic/osteogenic differentiation, as well as biomaterials, usually described as scaffolds, for tissue engineering [55].

#### **1.5. Biomaterials**

The ideal biomaterials for bone regeneration should not only be biocompatible, but also osteoconductive and osteoinductive. They should be able to promote the self-healing capabilities of the bone by (i) providing the main structural, compositional, and biochemical cues for the formation of new tissue; (ii) activating the host's immune cells involved in the regenerative response; (iii) improving the recruitment, proliferation, and differentiation of progenitor cells; and (iv) recovering a suitable local blood supply in order to support bone healing and remodelling.

In tissue engineering, biomaterials could be considered as a "template", providing temporary mechanical support and mass transport to promote cell adhesion, proliferation, and differentiation [56]. Ideally, a scaffold should serve as a transient structure that, over an extended period, will be degraded/reabsorbed in a controlled manner, in accordance with the regrowth rate of new bone tissue. Tissue engineering scaffolds attempt to mimic the natural extracellular matrix (ECM), at least partially, and to create a favourable microenvironment to

support tissue formation. Subsequently, the biomaterial template is correctly substituted with naturally deposited ECM and the newly formed tissue [56].

It seems that osteogenesis is not simply undertaken by bone cells from the skeleton system, rather it represents a complex physiological process involving multiple cooperating systems. The close link between the immune and skeletal systems has recently been defined using the concept of “osteimmunology”, suggesting that several molecules, which are involved in the maintenance of bone homeostasis and the regulation of inflammatory functions are shared, including receptors, signalling molecules and transcription factors [57]. Inflammation is an important factor that should be considered to develop successful biomaterial-based therapeutics. Indeed, inflammation is initially needed for wound healing while prolonged inflammation can result in delayed wound healing or, in some cases, rejection of the scaffold and additional tissue damage.

A large range of options exist for designing a specific biomaterial to be used as a matrix template, including natural/synthetic biomaterials and composites, composed of two or more material types/classes [37]. Specifically, ceramics, polymers and their composites will be considered in this study.

### **1.5.1. Ceramic Biomaterials**

Calcium phosphate (CaP)-based bioceramics, such as hydroxylapatite (HA), tricalcium phosphate (TCP), and a combination of these two, named biphasic calcium phosphate (BCP), are widely studied in orthopedics and dentistry [58]. (CaP)-based bioceramics similar to the inorganic components of natural bone, not only have intrinsic osteoinductive, [59] but also have effective osteo-immunomodulatory properties [60].

These features have been investigated by a large number of authors in literature. For example, Ishikawa et al. [61] compared three commercially ceramic-derived substitutes with different compositions: HA (Neobone<sup>®</sup>), carbonate apatite (CO3Ap, Cytrans<sup>®</sup>) and  $\beta$ -tricalcium phosphate ( $\beta$ -TCP, Cerasorb<sup>®</sup>). Their results demonstrated that CO3Ap shows limited dissolution and major stability under physiological conditions (pH 7.3) compared to other experimental groups. Cationic substitution (e.g. Sr<sup>2+</sup> or Mg<sup>2+</sup>) in CaP-based biomaterials improve the mechanical properties and change the chemical/physical properties of CaP (e.g., crystallinity, microstructure and solubility) [62]. In addition, CaP-based biomaterials can be enhanced using recombinant human bone morphogenetic proteins (rhBMPs) [63]. Montesi et al. characterized a strontium-doped HA cement (with different strontium concentrations) enriched with sodium alginate demonstrating in vitro that Sr<sup>2+</sup> has the capacity to induce osteogenic differentiation [64]. In addition, Barbanti-Brodano and his collaborators tested two

other commercial HA-derived biomaterials provided by Finceramica Faenza S.p.A., (Faenza, Italy) known as Sintlife ( $Mg^{2+}$ -doped-HA) and Engipore<sup>®</sup> (high porosity HA) in association with hBMSCs derived from adult orthopedic patients suffering from spine fusion in order to create a personalized approach to therapy for use in clinical practice. Their results suggest that Engipore biomaterials are better than Sintlife since the former induces cellular proliferation and focal adhesion kinase activation in hBMSCs [65].

Recently, HA powders doped with  $Mg^{2+}$ ,  $Sr^{2+}$ , and  $Zn^{2+}$  ions were investigated. Ion doping in the HA structure can specifically influence the phase composition and microstructure of HA/ $\beta$ -TCP composites. This fact enhances flexural strength and resistance to biofilm formation, in respect to the un-doped HA, while retaining up-regulation of various genes involving in osteogenesis, as shown by the cell analysis performed with hASCs and with two different Gram<sup>+</sup> and Gram<sup>-</sup> bacterial strains, frequent in post-surgical infections (*S. aureus* and *E. coli*) [66].

It is important to recall that HA can be synthesised in the laboratory by a chemical precipitation reaction. However, HA can be obtained naturally and economically from different natural sources [67,68]. Previous studies have found a huge potential for producing porous scaffolds from several marine sources, including marine coral [69]. Coral derived porous HA (Interpore 200<sup>®</sup>, Interpore Orthopaedics, Inc., Irvine, CA) is available in granule and block form. This biomaterial is frequently used in maxillofacial surgery for procedures to augment the splanchnocranium [35]. However, the coral reefs are exposed to catastrophic situations. According to research by the International Union for Conservation of Nature (IUCN), one third of the world's coral species are said to be at increased risk of extinction. Thus, there is a need to look for alternatives [70]. In this context, bovine bone, which is a bio-waste, is an economical alternative source of HA for hard tissue replacement in medical and dental therapy [68]. Bio-Oss<sup>®</sup> is a common bone substitute employed for bone regeneration. It consists of bovine spongy bone free of organic ingredients, in which the trabecular structure of the fine bone and the internal voids are preserved. Bio-Oss<sup>®</sup> plays a decisive role in controlling bone regeneration [71].

Despite the large number of studies and medical devices available using HA, regeneration in the case of critical-sized bone defects is still a serious concern. This is due to a lack of bioactivity relating to the classic ceramic-making process by which CaP scaffolds are obtained (i.e., powder compaction/three-dimensional forming), particularly the high temperature sintering required to give the scaffold adequate mechanical properties [72]. Problems relating to reduced HA bioactivity upon sintering are being increasingly discussed in the literature. Indeed, many studies are dedicated to the development of self-assembling or self-consolidating

ceramic-based scaffolds with adequate mechanical properties, which at the same time maintain the nanostructure [73]. Recently, it has been developed a new procedure to chemically transform rattan wood into a biomimetic hierarchically structured HA [74]. The new procedure can directly transform wood pieces into large HA scaffolds, preserving the original multiscale structure through a heterogeneous reaction under supercritical conditions directly in the three-dimensional (3D) state, without adopting any sintering process [75]. In this way, it is possible to obtain large 3D HA scaffolds with physical-chemical, morphological and mechanical features typical of natural bone [73,74].

However, bioceramics suffer from a low elasticity, a high brittleness, a poor tensile strength, a low mechanical reliability and fracture toughness, which leads to various concerns about their mechanical performance after implantation [76]. In addition, in many cases, it is difficult to form bioceramics into the desired shapes.

### **1.5.2. Polymers**

Polymer biomaterials employed for tissue regeneration can be synthetic and natural. Among the most important synthetic polymers there are poly ( $\epsilon$ -caprolactone) (PCL), polylactic acid (PLA), polyglycolide (PGA) and the copolymer of poly-(DL-lactic-co-glycolic-acid) (PLGA). PCL is an aliphatic polyester biomaterial, which was approved by the FDA since it is multiform and highly biocompatible [77]. PLA and PGA are unsuitable as biomaterials for bone tissue regrowth because of the low osteoconductivity and compressive strength. PLGA copolymers with several ratios of PLA and PGA are more soluble and have major osteoconductivity, whereas the degradation time of the latter can be controlled [78,79]. These scaffolds undergo hydrolytic degradation in vivo where in their monomeric degradation products are removed through natural pathways. They are approved by the FDA for use in tissue engineering, although their use has some disadvantages due to their degradation. This process gives rise to acid products that can alter the local microenvironment causing local change in pH [80].

Furthermore, their hydrophobic nature is not favourable for cell attachment, and the absence of functional groups results in inferior osteoinduction [80]. These limitations may be somewhat diminished in composite scaffolds with hydrophilic polymers, such as polyethylene glycol (PEG), and by coating with natural biomaterials such as collagen, the most abundant protein in the bone matrix [37,81]. Inclusion of PCL-PEG-PCL copolymer nanofibers in collagen [82] serves to combine the bio-mimic and stimulatory effects of natural polymers with the structural and mechanical stability of synthetic polymers, thus offering viable scaffold options with superior osteogenic potential. Indeed, pure collagen have not good mechanical proprieties, thus

it is usually associated also with ceramic biomaterials in bone tissue regeneration [37].

### **1.5.3. Composite Biomaterials**

Composite biomaterials derived from a combination of two or more material types/classes. Composite biomaterials composed of polymers and ceramics scaffolds have certain characteristics, such as high cytocompatibility, mechanical hardness and load-bearing capabilities that make these biomaterials suitable in tissue engineering [83].

The composite scaffolds composed of a PLLA/ $\beta$ -TCP matrix grafted with gelatin/HA represent a good candidate for bone repair [84]. Moreover, Arafat et al. analysed the proprieties of a scaffold composed of PCL/TCP with carbonated HA (CHA)-gelatin composite. This study indicated a strong increase in cellular proliferation and differentiation of porcine MSCs grown on this scaffold [85].

Some recent in vitro and in vivo studies analysed composite biomaterial formed by porous HA and collagen to evaluate the biological and mechanical effects of scaffolds [86]. Calabrese et al. analysed, both in vivo and ex vivo, the characteristics of cell-free collagen-HA scaffolds [87]. Subsequently, they evaluated implanting collagen-HA scaffold in association with hASCs to determine if bone formation could be influenced by human stem cells [88], concluding that adding hASCs can improve the bone repair process.

## **2. AIMS**

Bone injuries and abnormalities can have a highly deleterious impact on patients' quality of life. Many studies have been carried out in the effort to identify the ideal substitute for the bone regrowth. However, little is known about the biological, genetic and epigenetic effects of adding substitutes to bone. The biological parameters of cells grown on bone substitutes should be known before proposed scaffolds are clinically employed. At the same time, in vitro evaluation allow us to better understand the molecular mechanisms that lead to the formation of new bone observed after in vivo implantation.

Overall, the present project aims to evaluate the cytocompatibility, osteoconductivity and osteoinductivity proprieties of different scaffolds, which can improve bone regeneration. To this purpose, in vitro studies have been conducted through analysis described in the Materials and Methods section, using hASCs as cellular model. Specifically, metabolic activity and cytoskeleton morphology analyses allowed scaffold cytocompatibility to be evaluated. The structure of scaffolds, with cells grown on them, was analysed by scanning electron microscope. On the other hand, the study of mineral matrix deposition along with osteogenic genes expression and osteocalcin protein expression studies allowed to assess the osteoinductivity of the scaffolds under analysis.

Briefly, this scientific work is organized as follows:

- I. In the first part, investigation on two HA/Collagen composite scaffolds employed in maxillofacial surgery, i.e. Pro Osteon 200/Avitene and Bio-Oss/Avitene, have been conducted. Moreover, the immune response of hASCs grown on both Pro Osteon 200/Avitene and Bio-Oss/Avitene scaffolds has been evaluated after 21 days.
  - Coral Pro Osteon 200/Avitene has been widely used in clinical practice. Thus, the in vitro experiments were carried out up to day 40 in order to mimic the long period needed in vivo by the bone to repair itself. Patients operated for maxillomandibular malocclusion and/or asymmetry, or for aesthetic reasons, who underwent malar augmentation with Pro Osteon 200/Avitene were evaluated for the new bone formation during a 3-year period of follow-up using radiological and histological analyses.
  - Recently, bovine Bio-Oss/Avitene has been employed for zygomatic augmentation and bimaxillary osteotomy. Thus, this study provides information on its regenerative potential in vitro, up to 21 days. Radiological analysis on 30 patients after 15 days showed stable results that could guarantee adequate long-term aesthetic restoration of the zygomatic area.

In both cases, the obtained mixture composed of HA/Collagen at first result very malleable; this is an important aspect in clinical practice because the prosthesis can be shaped in view of the desired result depending on the patient's features.

- II.** In a second part, the biological proprieties of an innovative HA-derived biomaterial have been described. This scaffold, provided by Finceramica Faenza S.p.A., (Faenza, Italy), has been obtained through a new procedure of “biomorphic” transformation, which can directly transform wood pieces into large HA scaffolds, preserving the original multiscale structure through a heterogeneous reaction under supercritical conditions, directly in the 3D state, without adopting any sintering process.
- III.** Finally, in the last part of the thesis, experiments focused on the mechanisms of dexamethasone (dex)-induced osteogenesis of hBMSCs will be described. These experiments have been conducted during my abroad experience at AO Research Institute, Davos, Switzerland. The synthetic glucocorticoid dex is commonly used in protocols for trilineage differentiation of hMSCs in vitro. Previous results demonstrated that dex induces osteogenesis by inhibiting SOX9 gene expression and not by up-regulating the expression of RUNX2. Moreover, dex also stimulates adipogenesis by inducing the expression of PPAR $\gamma$ , the adipogenic transcription factor. At present, it is not clear which factor mediates SOX9 downregulation: PPAR $\gamma$  is one promising candidate. The present experiments aimed to clarify whether PPAR $\gamma$  mediates the SOX9 downregulation induced by dex, through modulation of PPAR $\gamma$  activity using the inverse agonist T0070907.



### **3. MATERIALS AND METHODS**

### **3.1. Biomaterials**

#### **3.1.1. Pro Osteon® 200/Avitene™ composite biomaterial**

The Pro Osteon 200/Avitene porous HA-derived scaffold used herein is composed of coral Granular Pro Osteon 200 (Interpore Cross Irvine, California) mixed with Avitene Microfibrillar Collagen Hemostat (Bard Warwick, Rhode Island). Avitene collagen was used in flour form. The granules of Pro Osteon 200 (5 g) were mixed with 1 g of Avitene and then 5 ml of sterile water were added [86,89]. The mixtures were separated to obtain several small disks ( $\emptyset$ , 1 cm; height, 0.2 cm). These blocks of biomaterial were left overnight to dry under UV light.

#### **3.1.2. Bio-Oss®/Avitene™ composite biomaterial**

The Bio-Oss/Avitene composite scaffold used herein is composed of bovine spongy bone substitute Bio-Oss granules 1 mm-2 mm (Geistlich Italia s.r.l., Thiene) mixed with Avitene Microfibrillar Collagen Hemostat (Bard Warwick, Rhode Island) [89]. In this study, Avitene collagen was used in flour form. The granules of Bio-Oss (3 g) were mixed with 1 g of Avitene and then 6 ml of sterile water were added (*Jaquinta et al., 2022. Accepted*). The mixtures were separated to obtain several small disks ( $\emptyset$ , 1 cm; height, 0.2 cm). These blocks of biomaterial were left overnight to dry under UV light.

#### **3.1.3. Bioceramic biomorphic hydroxlyapatite**

The biomorphic scaffold (B-HA), provided by Finceramica Faenza S.p.A., (Faenza, Italy), was obtained following the method described elsewhere [74], while being slightly modified to obtain a pure HA scaffold with no further ion doping. Briefly, cylindrical rattan wood pieces (*Calamus manna*) were pyrolyzed at 1000° C in an N<sub>2</sub> atmosphere, generating a pure carbon template. Then, the carbon template was transformed into a biomorphic HA scaffold by a sequence of gas-solid reactions in a controlled atmosphere at supercritical conditions, which concluded with a hydrothermal process carried out at 220°C. The cytocompatibility and osteoinductivity properties of B-HA were assessed compared to a commercial sintered HA scaffold (Engipore®; Finceramica Faenza, Faenza, Italy; herein after coded as S-HA) [73]. Before cell loading, each sample (diameter 8 mm, height 4 mm), was sterilized using 25 kGy  $\gamma$ -ray radiation, placed in a 24-well plate (one per well) and pre-soaked in culture medium for 72 h at 37°C.

### **3.2. Cell culture**

The characteristics of scaffolds analysed herein were evaluated using human adipose derived stem cells (hASCs). The hASCs used in this study were purchased (PT-5006, Lonza Milan,

Italy) as cryopreserved frozen cells during the first passage. The company certified that hASCs are positive for surface markers CD13, CD29, CD44, CD73, CD90, CD105 and CD166, while being negative for other markers, such as CD14, CD31 and CD45. Cells were expanded in alpha MEM (Lonza, Milan, Italy) supplemented with 10% foetal bovine serum (FBS), antibiotics and incubated at 37°C with 5% CO<sub>2</sub> in a humidified atmosphere. Primary hASC cultures were grown (i) on analysed scaffolds (ii) in osteogenic condition (OC). HASC cultures grown on biomaterials were maintained in basal medium alpha MEM (Lonza, Milan, Italy) supplemented with 10% FBS and antibiotics. Control cultures were hASCs grown in tissue culture polystyrene (TCPS) vessels, and maintained with basal medium, described above. OC was obtained using differentiation Bullekit osteogenic medium (Lonza, Milan, Italy), containing osteogenic basal medium (Lonza, Milan, Italy) and osteogenic SigleQuotes, which include dex, ascorbate, mesenchymal cell growth supplement, L-glutamine, β-glycerophosphate (Lonza, Milan, Italy) [73]. The scaffolds were placed separately in 24-well plates (Ø, 10 mm), filled with 200 µL of cell suspension containing 10<sup>4</sup> hASCs for each sample and incubated for 2 h. Cell suspension was shaken every 15 min to maximize cell-scaffold interaction. Cells were cultured at 37°C in a humidified atmosphere with 5% CO<sub>2</sub>, whereas they were re-fed with fresh medium every three days until the time of analysis.

### **3.3. Microstructural Analysis**

The scaffolds were analysed using scanning electron microscopy (SEM) [73]. Samples were washed with saline, fixed by 2.5% glutaraldehyde and with a 1% osmium solution in phosphate buffer. The specimens were coated with colloidal gold and analysed using scanning electron microscopy (SEM, model Stereoscan S-360, Cambridge UK). The open and total porosity of the studied ceramics was measured using Archimedes' method and geometrical weight-volume evaluation, respectively. The specific surface area (SSA) of the scaffold was measured using the nitrogen adsorption method, following the Brunauer–Emmett–Teller (BET) model (Sorpty 1750, Carlo Erba, Milan, Italy).

### **3.4. Cell Morphology**

In order to analyse the cytocompatibility of the scaffolds, the direct morphology of recombinant genetically engineered cells hASCs-eGFP grown on the biomaterials was evaluated by fluorescence microscopy analysis. To facilitate the observation of hASC cultures grown onto biomaterials, cells were transfected with an adenovirus vector that expresses the enhanced green fluorescence protein (eGFP) [89]. After 48 h, the efficiency of the adenovirus infection was

evaluated by measuring the emitted fluorescence by a fluorescence microscope. Cell nuclei were stained with 0.5 mg/mL DAPI.

### **3.5. Cytoskeleton Architecture**

Cytoskeletal actin filaments of hASCs were stained with tetramethyl-rhodamineisothiocyanate (TRITC) conjugated-Phalloidin (Sigma, Milan, Italy) [73]. Cells were washed with PBS 1X and fixed for 10 min at room temperature (RT) using 10% formalin. Cellular nuclei were stained with 0.5 mg/mL DAPI. Images were obtained using a TE 2000-E fluorescent microscope. Digital images were capture using ACT-1 and ACT-2 software for DXM1200F digital cameras (Nikon Instruments, Sesto Fiorentino, Italy).

### **3.6. Cell Proliferation Assay**

The proliferation rate of hASCs grown on scaffold was evaluated using the Alamar Blue assay (ThermoFisher Scientific, Milan, Italy). The assay was performed to assess cell proliferation attached and grown on biomaterials and TCPS [73]. Briefly, cells were incubated with a solution of 5% Alamar Blue in medium for 3 h at 37°C. HASCs ( $1.6 \times 10^5$  cells), serially diluted 1:2, were seeded to generate a calibration curve with scalar concentrations of hASCs, up to 5,000 cells. Afterwards, the optical density of the supernatants was measured at 570 nm and 620 nm using the spectrophotometer (Thermo Electron Corporation, model Multiskan EX, Helsinki, Finland).

### **3.7. Matrix Mineralization**

Alizarin red staining (ARS, Sigma, Milan, Italy) was performed to investigate hASC scaffold-induced mineralization, as described [73]. The medium was removed and cells were fixed with 10% formalin. Plates were rinsed three times with PBS 1X and stained with ARS (pH 4.2) for 30 min at RT. Excess dye was removed, in case of over-staining, by washing three times with PBS 1X. Cell images were captured using an inverted fluorescence microscope. The mineralized substrates were quantified using a 20% methanol and 10% acetic acid in a water solution (Sigma-Aldrich, Milan, Italy). For the quantification of matrix mineralization, the solution containing an amount of dissolved Alizarin red was read spectrophotometrically (Thermo Electron Corp., model Multiskan EX, Vantaa, Finland) at a wavelength ( $\lambda$ ) of 450 nm.

### **3.8. Alkaline phosphatase protein expression**

Alkaline phosphatase (ALP) activity was determined by a colorimetric Naphthol AS-BI phosphate-based reaction using the Alkaline Phosphatase Detection Kit (Merck Millipore

Corporation, Milan, Italy), according to manufacturer instructions [89,90]. Images were obtained by using a standard light microscope (Nikon Eclipse TE 2000-E; Nikon Instruments, Sesto Fiorentino, Italy) that was equipped with a digital camera (DXM 1200F; Nikon Instruments).

### **3.9. Osteocalcin protein expression**

More elaborate methods to demonstrate hASC osteogenic differentiation include the detection and quantification of bone-specific proteins, such as osteocalcin (OCN) [89]. To this purpose, protein extraction was performed using Cell extraction Buffer (Thermo Fischer Scientific, Milan, Italy) added to 1 Mm phenylmethylsulfonylfluoride and a protease inhibitor cocktail. Total protein concentration was determined by bicinchoninic acid assay (BCA) according to the manufacturer's instructions. The OCN protein was quantified using the Human Osteocalcin Instant ELISA (Thermo Fisher Scientific, Milan, Italy) according to the manufacturer's instructions.

### **3.10. Cytokine/Chemokine and Osteogenic gene expression**

To identify genes involved in immune response and osteogenic differentiation, activated by the scaffolds, the Real Time PCR (qPCR) Array were performed in hASCs grown on biomaterials. Specifically, total RNA was isolated through RNeasy Plus Micro Kit (Qiagen, Milan, Italy) according to the manufacturer's instructions. RNA was quantified by using a Nanodrop spectrophotometer (ND-1000; Wilmington, Delaware). Purified RNA was reverse transcribed to cDNA by using the RT<sup>2</sup> First-Strand Kit (Qiagen, Milan, Italy). Specific primers sets used in qPCR were employed to analyse the expression of differentially expressed genes (DEGs) that encode for i) human cytokines and chemokines (Qiagen, PAHS-150ZA) (*Iaquinta et al., 2022. Accepted*) and ii) human osteogenic markers (Qiagen, PAHS-026ZA) [73,89]. For data analysis, a value of  $p < 0.05$  was considered significant. The Fold Change (FC) of each gene expression was calculated by using the  $2^{-\Delta\Delta C_t}$  method, whereas housekeeping gene, used as control, was used to normalize results and  $\text{Log}_2 \text{FC} < -1$  or  $> +1$  was considered significant [73,89].

### **3.11. Statistical Analysis**

Statistical analyses of data, obtained from experiments performed in technical triplicate for each biological samples of hASCs (n=3), were carried out using Prism 8.0 (GraphPad Software, La Jolla, California). Data obtained from Alamar Blue assay were analysed with two-way

ANOVA. Data obtained from ARS quantification and OCN expression analysis were analysed using one-way ANOVA. A value of  $p < 0.05$  was considered significant.

### **3.12. *In vivo* evaluation**

The study was designed as a prospective study and approved by the ethics committee of the hospital of Verona, Verona, Italy. Shaping of the prosthesis is performed according to surgical needs, depending on the clinical evaluation of the patient. The obtained materials were very moldable; they are warmed for at least 2.5 hours and they become stiff. At the end of the main orthognathic surgical procedure, utilizing the same upper vestibular incision of the Lefort I through a subperiosteal dissection of the area between infraorbital nerve medially and the zygomatic arch laterally, a pocket is created over the zygomatic bone similar in size to the prosthesis, which are settled without any need of fixation [89,91,92].

## **4. RESULTS**

## 4.1. Pro Osteon® 200/Avitene™ composite biomaterial

### 4.1.1. SEM analysis

SEM analysis was performed to investigate the microstructure and morphology of the scaffold (Pro Osteon 200/Avitene) without hASCs (**Figure 3A**) and with cells grown on it, up to day 40 (**Figure 3B-F**). The granular HA mixed with collagen fibres creates a highly fibrous structure. The biomaterial showed a different like-bone structure, in the presence of cells, at day 40. hASCs grown on the scaffold showed a normal cell morphology exhibiting pseudopodium-like structures in tight contact with the ECM (**Figure 3F**).

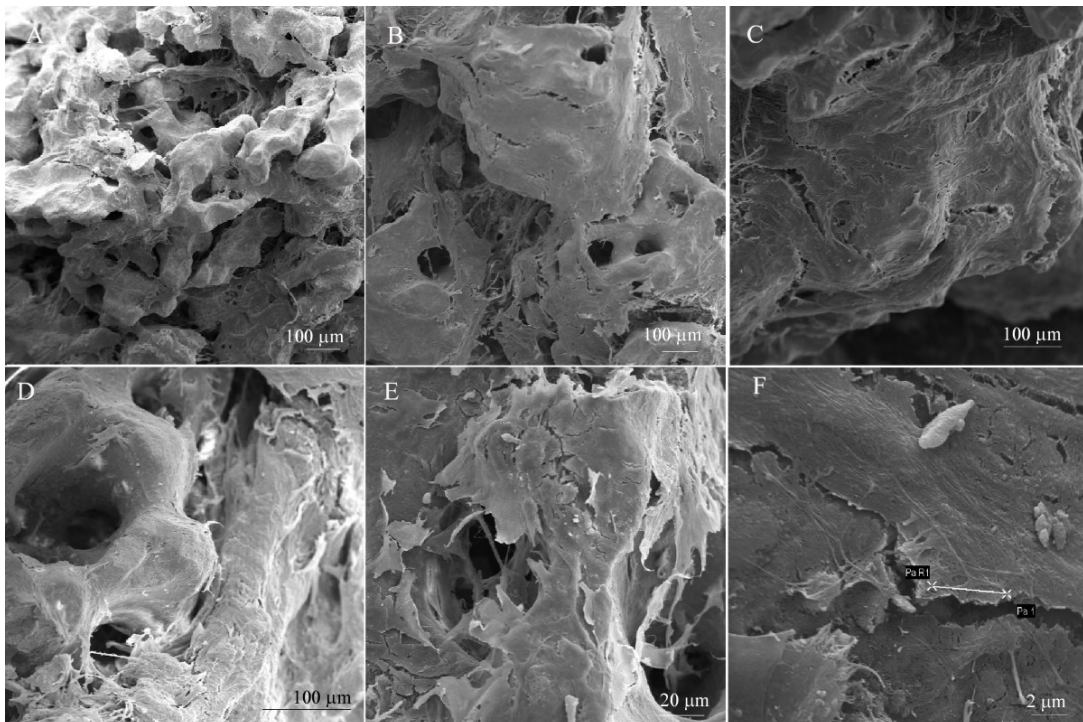


**Figure 3.** Scanning electron microscopy analysis of the Pro Osteon 200/Avitene. (A) Bovine collagen fibrils from Avitene Microfibrillar Collagen were mixed with Granular Pro Osteon 200 to generate the scaffold Pro Osteon 200/Avitene. The biomaterial shows the porous structure with several pores in the range 190 to 230 μm, Scale bar: 100 μm, ×86. (B-E) Human adipose derived stem cells (hASC) grown on HA-derived scaffold for 40 days. The structure of scaffold was observed at different magnification, Scale bar: 100 μm, ×133 (B), Scale bar: 100μm, ×214 (C), Scale bar: 100 μm, ×344 (D), Scale bar: 20 μm, ×647 (E), respectively. F, Cells, homogeneously spread on the substrate, exhibited cytoplasmic bridges, whereas their morphology did not show any sort of alteration. Scale bar: 2 μm, magnification ×6.55k.



#### 4.1.2. Scaffold is biocompatible in hASCs

hASCs grown on the biomaterial were investigated for their proliferation and cytoskeleton organization at days 14, 21, and 40. hASC-eGFP grown on biomaterial showed a normal cell morphology (**Figure 4A,B**). The biomaterial demonstrated its cytocompatibility up to day 40 in terms of cell adhesion and proliferation. The cytoskeleton architecture appeared to be well organized, whereas its integrity remains uninfluenced by the scaffold, up to day 40 (**Figure 4C,D**). Actin fibres seem to connect the cellular membranes and the cytoskeleton to the scaffold surface with no visible loss or structural displacement. Similar physiologic cytoskeleton architecture was observed by confocal microscopy at day 40 (**Figure 4D**).

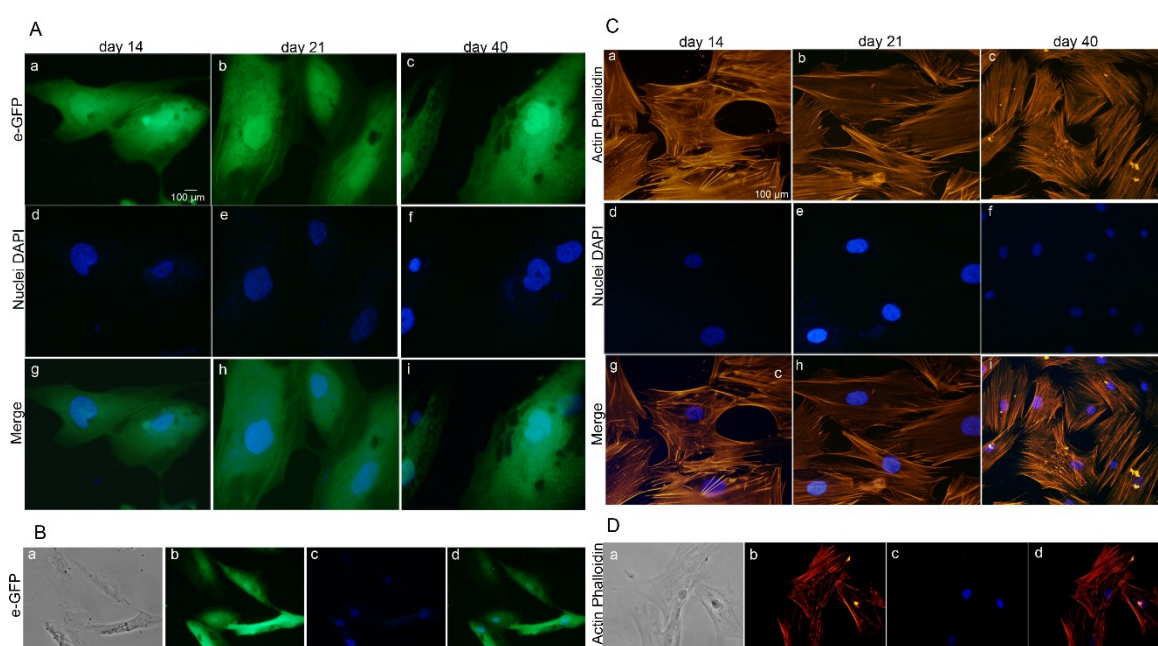


**Figure 4.** Stem cell morphology and cytoskeleton architecture. (A) Human adipose mesenchymal stem cell hASC-eGFP grown on the biomaterial at days 14, 21, and 40 are shown at magnification  $\times 40$ . (B) hASC-eGFP grown on the biomaterial at days 14, 21, and 40 are shown at magnification  $\times 20$ . (C) Cytoskeleton analysis by Phalloidintetramethyl-rhodamine-isothiocyanate (TRITC) staining of hASCs grown on the biomaterial. (D) Cytoskeleton analysis carried out by the confocal microscopy at day 40, magnification  $\times 40$ . Cellular nuclei were stained with 0.5 mg/mL DAPI.

#### 4.1.3. Scaffold induces the matrix mineralization and osteogenic expression protein in hASCs

Recently, we reported a significant increase of matrix mineralization and ALP activity in hASCs grown on the biomaterial, at day 21 [90]. In the present investigation, the osteoinductive activity of the biomaterial is highlighted by the matrix mineralization detected in hASCs grown on the scaffold at day 40. Indeed at day 40, the biomaterial favoured the matrix mineralization

better than the plastic vessel (TCPS), the control (**Figure 5A,C**,  $*p < 0.05$ ). Moreover, calcium deposits in hASCs grown on OC were higher compared with cells grown on the biomaterial or TCPS ( $**p < .0001$ ; **Figure 5A,C**). Cells grown on the biomaterial and in OC showed a significant increase of the ALP activity compared with TCPS, at day 40 (**Figure 5B**).

ELISA data show a statistically significant increase of the OCN protein expression in cells grown on biomaterial, at the three time points, i.e. 14, 21 and 40 days, compared with the control. This result is in agreement with previous data obtained at day 9 [90]. The expression of OCN in hASCs grown on the biomaterial was higher than in OC/TCPS, at day 14 ( $*p < 0.05$ ). The hybrid scaffold influences the osteogenic pathway at days 21 and 40 compared with TCPS ( $*p < 0.05$ ) (**Figure 5D**). Cells grown in OC showed higher expression levels of OCN compared with TCPS at days 14 and 21 ( $*p < 0.05$ ) (**Figure 5D**).

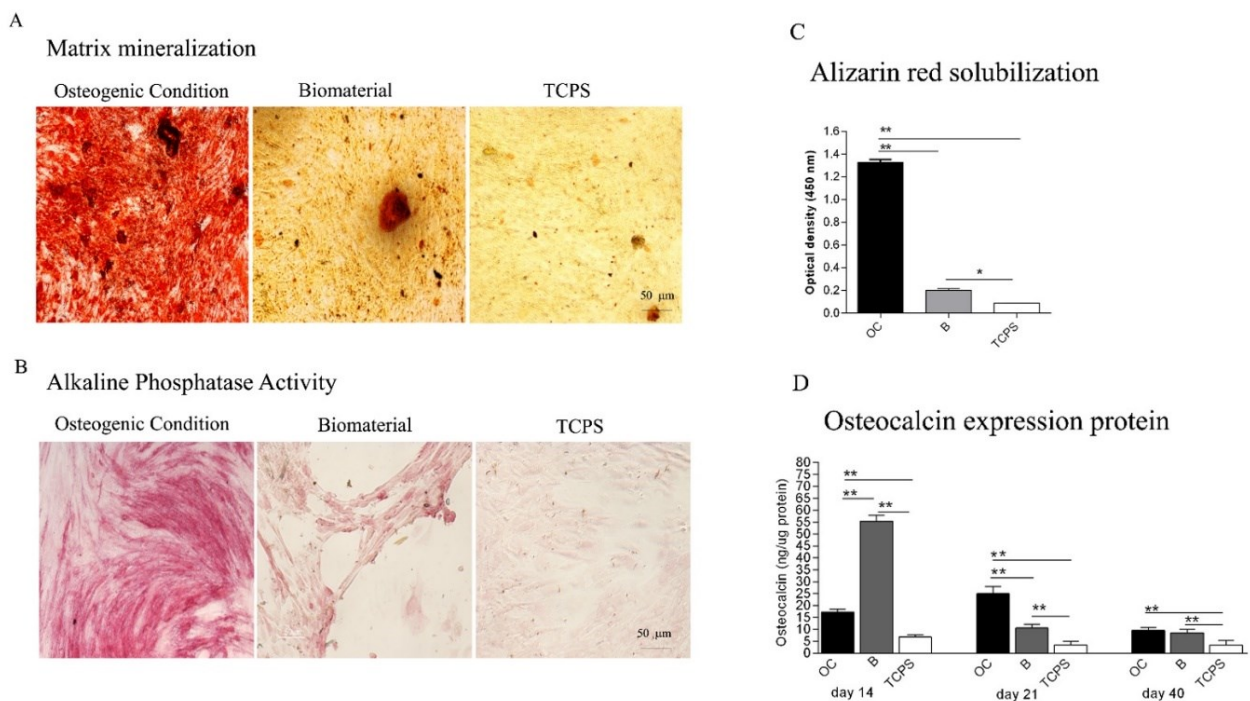


**Figure 5.** Osteogenic markers in human adipose mesenchymal stem cells (hASCs) cultured on the biomaterial. (A) ARS at day 40 is shown in the panel, in experimental conditions tested. Scale bar: 50  $\mu\text{m}$ , Magnification  $\times 4$ . (B) Alkaline phosphatase (ALP) activity at day 40. Scale bar: 50  $\mu\text{m}$ , Magnification  $\times 4$ . (C) The matrix mineralization was evaluated by ARS, whereas its quantification was carried out spectrophotometrically. (D) The temporal pattern of osteocalcin (OCN) protein levels was detected at different time points, i.e. 14, 21 and 40 days, and quantified by ELISA. Symbols indicate statistical significance ( $*p < 0.05$ ;  $**p < 0.0001$ ). Scale bar: 50  $\mu\text{m}$ , Magnification  $\times 40$ .

#### 4.1.4. Cytokine/Chemokine Gene Expression in hASCs grown on the Pro Osteon® 200/Avitene™

In hASCs grown on the Pro Osteon 200/Avitene scaffold at day 21, n=32 differentially expressed genes (DEGs, **Table 1**) including 14 up-regulated genes (**Figure 6**, red), i.e. CX3CL1, CD40LG, Interleukin 27 (IL27), IL22, Chemokine (C-C motif) ligand 1 (CCL1), CXCL13, Nodal homolog (NODAL), IL13, CXCL12, Interleukin 18 (IL18), IL15, Interleukin 7 (IL7), Transforming growth factor, beta 2 (TGFB2), CNTF were identified. On the other hand, 18 genes resulted down-regulated in hASCs grown on Pro Osteon 200/Avitene biomaterial, respect to TCPS, the control (**Figure 6**, green). Among these, we identified Interleukin 23, alpha subunit p19 (IL23A), Chemokine (C-C motif) ligand 7 (CCL7), Chemokine (C-C motif) ligand 11 (CCL11), IL6, CCL2, Chemokine (C-C motif) ligand 5 (CCL5), LIF, Interleukin 1, beta (IL1B), CXCL2, CXCL5, Tumour necrosis factor (ligand) superfamily, member 10 (TNFSF10), IL11, Chemokine (C-C motif) ligand 20 (CCL20), CXCL1, Bone morphogenetic protein 6 (BMP6), CXCL8, Interleukin 24 (IL24), IL1RN.

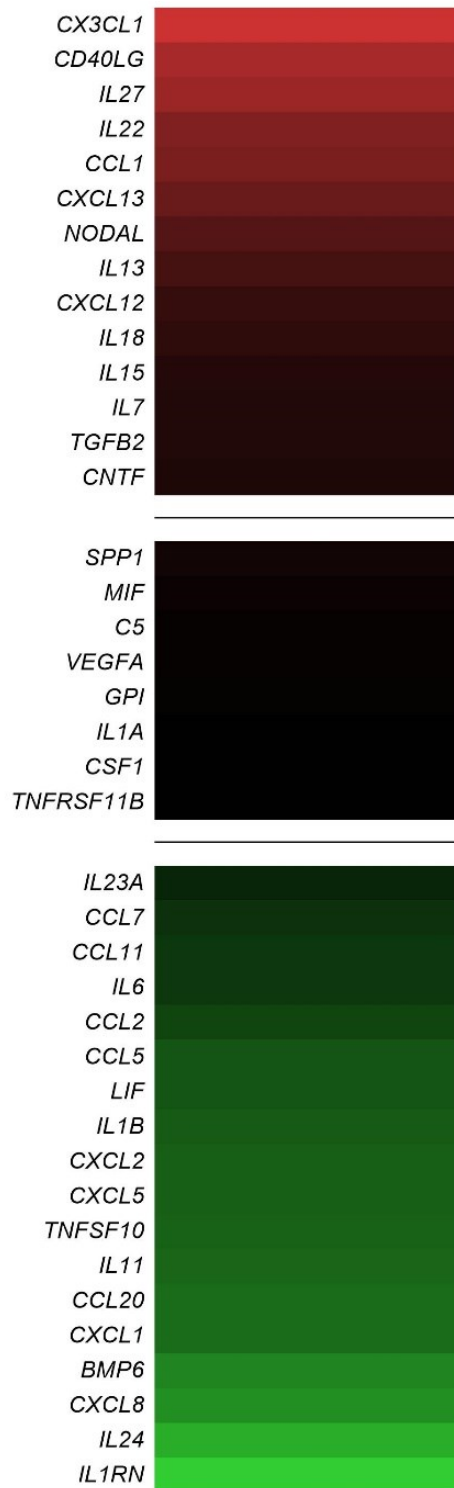


**Figure 6.** Graphical representation through heatmap of the mRNA expression. Expression of genes involved in immune response in human adipose mesenchymal stem cells (hASCs) grown on Pro Osteon 200/Avitene biomaterial compared to tissue culture polystyrene (TCPS). A value of  $p < 0.05$  was considered significant. The fold change (FC) of each gene expression was calculated using the  $2^{-\Delta\Delta C_t}$  method, whereas housekeeping genes, used as controls, were used to normalize results and  $\text{Log}_2 \text{FC} < -1$  or  $> +1$  was considered significant.

**Table 1.** List of genes involved in immune response found to be up-regulated and down-regulated in hASCs grown on Pro Osteon 200/Avitene scaffold at day 21.

Up-regulated genes			Down-regulated genes		
Number	Symbol/ Acronym	Fold-Change (Log <sub>2</sub> FC)	Number	Symbol/ Acronym	Fold-Change (Log <sub>2</sub> FC)
1	<i>CX3CL1</i>	8.27	1	<i>IL23A</i>	-1.22
2	<i>CD40LG</i>	6.70	2	<i>CCL7</i>	-1.60
3	<i>IL27</i>	6.25	3	<i>CCL11</i>	-1.84
4	<i>IL22</i>	5.20	4	<i>IL6</i>	-1.84
5	<i>CCL1</i>	4.94	5	<i>CCL2</i>	-2.25
6	<i>CXCL13</i>	4.23	6	<i>CCL5</i>	-2.74
7	<i>NODAL</i>	3.33	7	<i>LIF</i>	-2.74
8	<i>IL13</i>	2.75	8	<i>IL1B</i>	-2.94
9	<i>CXCL12</i>	2.10	9	<i>CXCL2</i>	-3.06
10	<i>IL18</i>	1.88	10	<i>CXCL5</i>	-3.06
11	<i>IL15</i>	1.40	11	<i>TNFSF10</i>	-3.18
12	<i>IL7</i>	1.35	12	<i>IL11</i>	-3.32
13	<i>TGFB2</i>	1.33	13	<i>CCL20</i>	-3.47
14	<i>CNTF</i>	1.14	14	<i>CXCL1</i>	-3.47
			15	<i>BMP6</i>	-4.32
			16	<i>CXCL8</i>	-4.64
			17	<i>IL24</i>	-5.64
			18	<i>IL1RN</i>	-6.64

*Chemokine (C-X3-C motif) ligand 1 (CX3CL1), CD40 ligand (CD40LG), Interleukin 27 (IL27), Interleukin 22 (IL22), Chemokine (C-C motif) ligand 1 (CCL1), Chemokine (C-X-C motif) ligand 13 (CXCL13), Nodal homolog (mouse, NODAL), Interleukin 13 (IL13), Chemokine (C-X-C motif) ligand 12 (CXCL12), Interleukin 15 (IL15), Interleukin 18 (IL18), Interleukin 7 (IL7), Transforming growth factor, beta 2 (TGFB2), Ciliary neurotrophic factor (CNTF), Interleukin 23, alpha subunit p19 (IL23A), Chemokine (C-C motif) ligand 7 (CCL7), Chemokine (C-X-C motif) ligand 11 (CCL11), Interleukin 6 (interferon, beta 2 IL6), Chemokine (C-C motif) ligand 2 (CCL2), Chemokine (C-C motif) ligand 5 (CCL5), Leukemia inhibitory factor (cholinergic differentiation factor, LIF), Interleukin 1, beta (IL1B), Chemokine (C-X-C motif) ligand 2 (CXCL2), Chemokine (C-X-C motif) ligand 5 (CXCL5), Tumour necrosis factor (ligand) superfamily, member 10 (TNFSF10), Interleukin 11 (IL11), Chemokine (C-C motif) ligand 20 (CCL20), Chemokine (C-X-C motif) ligand 1 (CXCL1), Bone morphogenetic protein 6 (BMP6), Chemokine (C-C motif) ligand 8 (CXCL8), Interleukin 24 (IL24), Interleukin 1 receptor antagonist (IL1RN).*

#### 4.1.5. Pro Osteon® 200/Avitene™ modulates genes implicated in skeletal development

In a previous study, few specific osteogenic genes, such as ALP, Osteonectin, Transcription factor SP7 (Osterix) and CLEC3B were analysed in a short period of time, which were reported up-regulated in hASCs grown on the scaffold at day 9 [90]. Herein, RT<sup>2</sup> Profiler PCR array was used to analyse the expression of osteogenic genes. The gene expression was evaluated in hASCs grown on Pro Osteon 200/Avitene compared with TCPS, at days 21 and 40. Among DEGs, 22 up-regulated genes (red), 7 down-regulated genes (green), and 2 genes (i.e. FGFR2 and NOG) which were up-regulated (day 21) and then down-regulated (day 40), were identified in hASCs grown on biomaterial. Among DEGs, osteogenesis-related genes, including the Bone Morphogenetic Protein 1/2 (BMP1/2), ALP, Bone Gamma-Carboxyglutamate Protein (BGLAP), transcription factor Sp7, Runt-related transcription factor 2 (RUNX2), Secreted Phosphoprotein 1 (SPP1), Collagen type I alpha 1 (COL1A1), epidermal growth factor receptor (EGFR), which play important roles in osteogenesis, were found to be up-regulated at day 21. Moreover, the transcription factor condensation SRY (sex-related Y)-type high mobility group box SOX-9 (Sox9), and BMPR1B which plays a central role in chondrocyte differentiation, were also found to be up-regulated, on hASCs grown on the scaffold, at days 21 and 40. The qPCR revealed increased expression of the receptor activator of nuclear factor kappa-B ligand (RANKL), also known as tumour necrosis factor ligand superfamily member 11 (TNFSF11) at days 21 and 40. The growth factors, such as the colony-stimulating factor 2/3 (granulocyte-macrophage) (CSF2/3), and epidermal growth factor (EGF), were also found to be up-regulated at days 21 and 40. The heatmaps, shown in **Figure 7**, provides a visualization of expression values among genes.

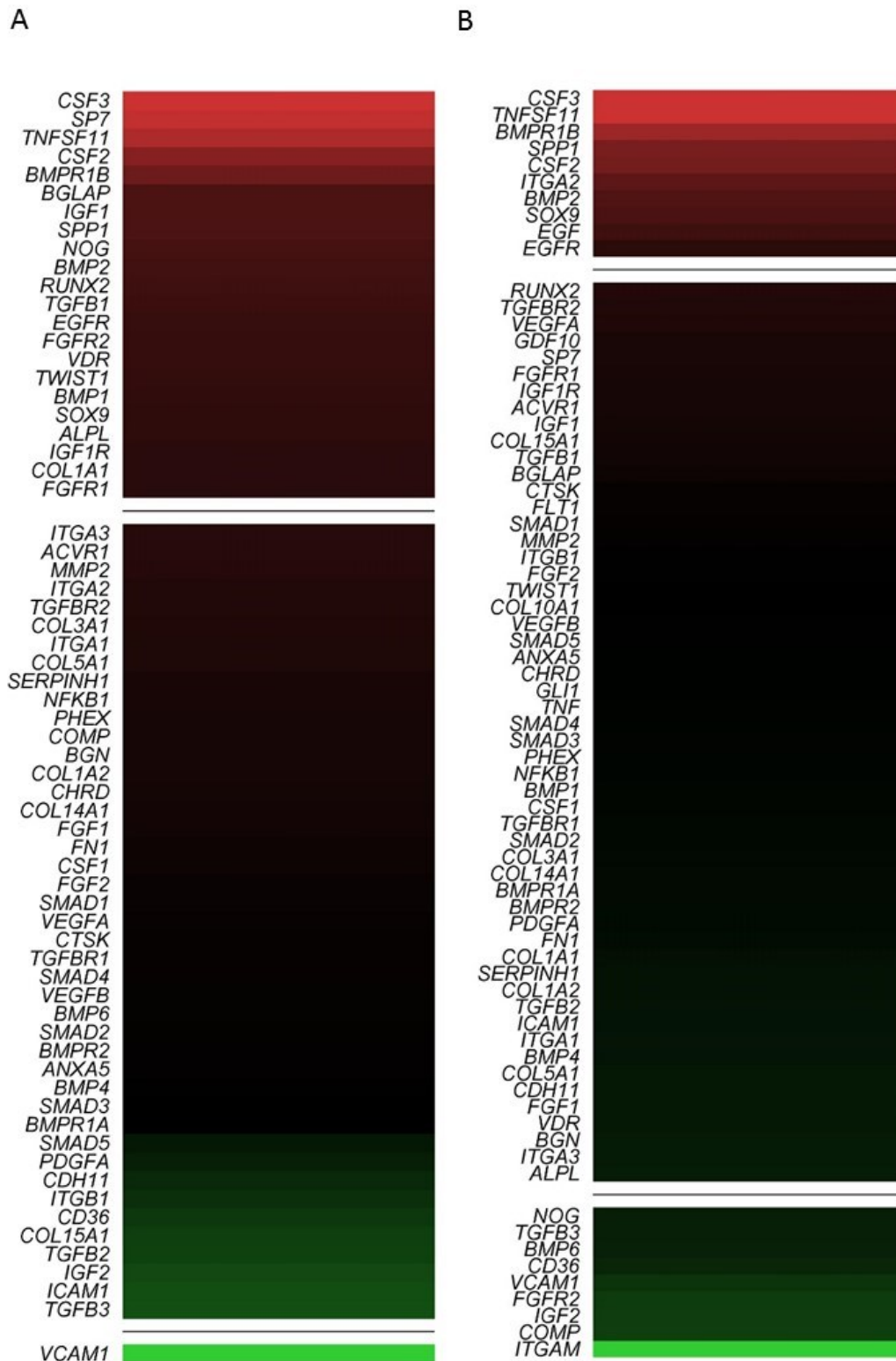


**Figure 7.** Graphical representation through heatmap of the mRNA expression in human adipose mesenchymal stem cells (hASCs) grown on Pro Osteon 200/Avitene, compared to tissue culture polystyrene (TCPS). The fold-change values of up-regulated (red) and down-regulated (green) genes in hASCs grown on Pro Osteon 200/Avitene compared with the control are reported at day 21 (A) and day 40 (B), respectively.

In hASCs grown on the biomaterial down-regulated DEGs were n=1 at day 21 and n=9 at day 40. Genes encoding for cell-ECM, adhesion molecules such as CD36 molecule thrombospondin receptor (CD36), Cartilage oligomeric matrix protein (COMP), and Integrin, alpha M complement component 3 receptor 3 subunit (ITGAM) were down-regulated at day 40. The list of up-regulated and down-regulated genes at day 21 and 40 is reported in **Table 2** and **Table 3**, respectively.

**Table 2.** List of genes involved in osteogenic differentiation found to be up-regulated and down-regulated in hASCs grown on the Pro Osteon 200/Avitene scaffold at day 21.

Up-regulated genes			Down-regulated genes		
Number	Symbol/ Acronym	Fold-Change (Log <sub>2</sub> FC)	Number	Symbol/ Acronym	Fold-Change (Log <sub>2</sub> FC)
1	<i>ALP</i>	1.15	1	<i>VCAMI</i>	-1.66
2	<i>BGLAP</i>	1.94			
3	<i>BMP1</i>	1.20			
4	<i>BMP2</i>	1.62			
5	<i>BMPR1B</i>	2.78			
6	<i>COL1A1</i>	1.05			
7	<i>CSF2</i>	3.41			
8	<i>CSF3</i>	5.18			
9	<i>EGFR</i>	1.37			
10	<i>FGFR1</i>	1.04			
11	<i>FGFR2</i>	1.35			
12	<i>IGF1</i>	1.90			
13	<i>IGF1R</i>	1.06			
14	<i>NOG</i>	1.75			
15	<i>RUNX2</i>	1.59			
16	<i>SOX9</i>	1.18			
17	<i>SP7</i>	4.89			
18	<i>SPP1</i>	1.88			
19	<i>TGFB1</i>	1.51			
20	<i>TNFSF11</i>	4.36			
21	<i>TWIST1</i>	1.27			
22	<i>VDR</i>	1.33			

*Alkaline Phosphatase (ALP), Bone Gamma-Carboxyglutamate (gla) (BGLAP), Bone Morphogenetic Proteins 1 and 2 (BMP1 and 2); Bone Morphogenetic Protein Receptor type IB (BMPR1B); Collagen type 1 alpha 1 (COL1A1); Colony Stimulating Factor 2 and 3 (CSF2 and 3); Epidermal Growth Factor receptor (EGFR); Fibroblast Growth Factor Receptor 1 and 2 (FGFR1 and 2); Insulin Growth Factor 1 (IGF1) and its Receptor (IGF1R); Noggin (NOG); Runt-related Transcription Factor 2 (RUNX2); Transcription Factor SOX9 (SOX9), Transcription Factor Sp7 (SP7), Secreted Phosphoprotein 1 (SPP1), Transforming Growth Factor Beta 1 (TGFB1); TNF Superfamily Member 11 (TNFSF11); Twist Family BHLH Transcription Factor 1 (TWIST1); Vitamin D Receptor (VDR); Vascular Cell Adhesion Molecule 1 (VCAMI).*



**Table 3.** List of genes involved in osteogenic differentiation found to be up-regulated and down-regulated in hASCs grown on the Pro Osteon 200/Avitene scaffold at day 40.

Up-regulated genes			Down-regulated genes		
Number	Symbol/ Acronym	Fold-Change (Log <sub>2</sub> FC)	Number	Symbol/ Acronym	Fold-Change (Log <sub>2</sub> FC)
1	<i>BMP2</i>	1.89	1	<i>BMP6</i>	-1.14
2	<i>BMPR1B</i>	3.73	2	<i>CD36</i>	-1.33
3	<i>CSF2</i>	2.73	3	<i>COMP</i>	-2.16
4	<i>CSF3</i>	4.88	4	<i>FGFR2</i>	-2.11
5	<i>EGF</i>	1.47	5	<i>IGF2</i>	-2.15
6	<i>EGFR</i>	1.04	6	<i>ITGAM</i>	-7.12
7	<i>ITGA2</i>	2.20	7	<i>NOG</i>	-1.05
8	<i>SOX9</i>	1.75	8	<i>TGFB3</i>	-1.07
9	<i>SPP1</i>	2.84	9	<i>VCAM1</i>	-1.83
10	<i>TNFSF11</i>	4.87			

*Bone Morphogenetic Protein 2 (BMP2); Bone Morphogenetic Protein Receptor type IB (BMPR1B); Colony Stimulating Factor 2 and 3 (CSF2 and 3); Epidermal Growth Factor (EGF); Epidermal Growth Factor Receptor (EGFR); Integrin Subunit Alpha 2 (ITGA2); Transcription Factor SOX9 (SOX9), Secreted Phosphoprotein 1 (SPP1), TNF Superfamily Member 11 (TNFSF11); Bone Morphogenetic Protein 6 (BMP6); CD36 Molecule (CD36); Cartilage Oligomeric Matrix Protein (COMP); Fibroblast Growth Factor Receptor 2 (FGFR2); Insulin-like Growth Factor 2 (IGF2); Integrin Subunit Alpha M (ITGAM); Noggin (NOG); Transforming Growth Factor, Beta 3 (TGFB3); Vascular Cell Adhesion Molecule 1 (VCAM1).*

#### 4.1.6. Bone regrowth in maxillofacial patients

The bone substitute Pro Osteon 200/Avitene, compared with other biomaterials, gave remarkable aesthetic results, in terms of naturalness and symmetry. These data allowed us to give high Visual Analogue Scale (VAS) scores to patients. A 3-year clinical study was performed to evaluate the long-term results of new bone formation in patients (n=50) who underwent malar augmentation during orthognathic surgical procedures. The imaging data collected at 1 month after surgery (T1) showed that the prosthesis maintained their granular structure, without evidence of HA granules migration into the surrounding soft tissues (**Figure 8A**). This result gives evidence of biomaterial physical stability.

The prosthesis structure was radiotransparent compared with the compact aspect of the zygomatic bone. At 24 months after surgery (T2), the prosthesis seemed to adhere staunchly to the underlying zygomatic bone in all patients (**Figure 8B**).The granular structure was still distinguishable, although less evident if compared with the previous healing period. The partial radiotransparency evolved to a radiopacity, similar to that observed in the compact part of the native bone, making it impossible to distinguish the interface between the prosthesis and bone (**Figure 8B**). At 36 months after surgery (T3), that tendency continued in agreement to the imaging data, toward progressive loss of definition of the granular architecture and an almost complete radiopacity and apparent corticalization of the bone in contact with the prosthesis. The interface between the prosthesis and bone at T3 appeared indistinguishable (**Figure 8C**).

Histological analysis on bone specimens, harvested from three patients requiring plate device removal 2 years after surgery, was carried out. The persistence of porous HA scaffold and macrophages, although without inflammatory infiltrate, was found in samples. In analysed fields, fibrous stroma was revealed in 50% of the biopsies, whereas new osteogenesis and mature bone was found in 70% of these specimens (**Figure 8D**). Immunohistochemical investigations uncovered some cathepsin K protease contained in the cytoplasm of the macrophages, thus indicating the presence of osteoclast activity localized around HA granules (**Figure 8D**). The anti-CD56 antibodies indicated a higher amount of new bone formation at the side of the biopsy sample adjacent to the native bone (deep), confirming the results of histomorphometric analyses (data not shown).

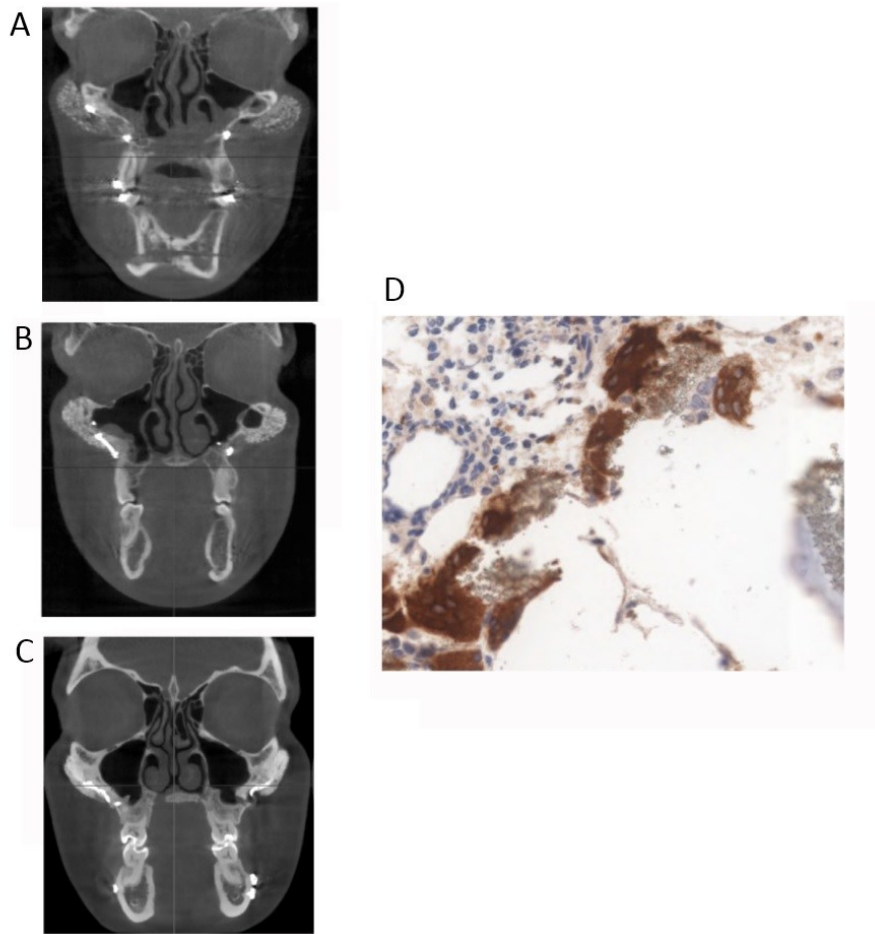


**Figure 8.** Scaffold characterization in patients: radiologic and histologic analyses. (A-C) Cone-beam tomogram, coronal slice, at T1 (1 month), T2 (24 months), and T3 (36 months) after surgery. (A) The prosthesis maintained its granular structure, whereas the granules did not migrate to the surrounding soft tissues. The structure of the prosthesis is radiotransparent compared with the compact portion of the zygomatic bone (T1). (B) Cone-beam tomogram, coronal slice, at 24 months after surgery. The prosthesis seems to adhere strongly to the underlying zygomatic bone in patients. The granular structure is still distinguishable, although less evident, whereas the partial radiotransparency evolved to a radiopacity similar to that seen in the compact part of the native bone, making it impossible to distinguish the interface between the prosthesis and bone. (C) Cone-beam tomogram, coronal slice, at 36 months after surgery. Progressive loss of definition of the granular architecture, with an almost complete radiopacity and apparent corticalization of the bone in contact with the prosthesis. The interface between the prosthesis and bone at T3 appears indistinguishable. (D) Biopsies harvested 24 months after implant placement. Bone maturation gradient can be observed proceeding from the periosteal layer toward the native bone (hematoxylin and eosin stain: magnification  $\times 10$ ). Osteoclasts surrounding HA residual granules (immunohistochemistry with cathepsin K, magnification  $\times 20$ ).

## 4.2. Bio-Oss<sup>®</sup>/Avitene<sup>™</sup> composite biomaterial

### 4.2.1. SEM analysis

SEM analysis was performed to investigate the microstructure and morphology of the scaffold (Bio-Oss/Avitene) with cells grown on it, up to day 21 (**Figure 9A-F**). The granular HA mixed with collagen fibres creates a highly fibrous structure (**Figure 9D**).

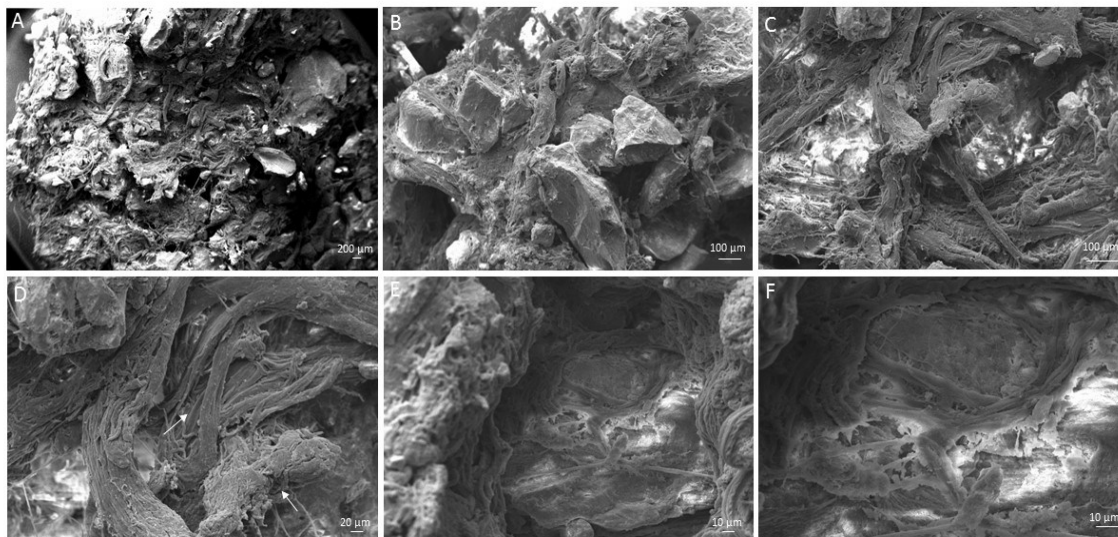


**Figure 9.** Scanning electron microscopy analysis of the Bio-Oss/Avitene. Bovine collagen fibrils from Avitene Microfibrillar Collagen Hemostat were mixed with bovine Bio-Oss to generate the final scaffold. Human adipose derived stem cells (hASCs) grown on HA/Collagen scaffold for 21 days. The structure of scaffold was observed at different magnification: Scale bar: 200  $\mu\text{m}$ ,  $\times 43$  (A), Scale bar: 100  $\mu\text{m}$ ,  $\times 200$  (B), Scale bar: 100  $\mu\text{m}$ ,  $\times 300$  (C), Scale bar: 20  $\mu\text{m}$ ,  $\times 600$  (D), Scale bar: 10  $\mu\text{m}$ ,  $\times 1.00\text{k}$  (E), Scale bar: 10  $\mu\text{m}$ ,  $\times 2.06\text{k}$  (F).

### 4.2.2. Cytocompatibility analysis of Bio-Oss<sup>®</sup>/Avitene<sup>™</sup> scaffold employing hASCs

In vitro cytocompatibility analyses, i.e., proliferation/cytoskeleton organization, tested in hASCs cultured on biomaterials, were evaluated up to day 9.

Actin filaments in the cytoskeleton appeared to be well organized, whereas its integrity remained uninfluenced by scaffolds, after 6 days (**Figure 10A**). The Bio-Oss/Avitene biomaterial was assessed in terms of cell proliferation at day 3, 6, 9. The Alamar blue assay showed increased scaffold metabolic activity in hASCs grown on the Bio-Oss/Avitene scaffold, demonstrating that the Bio-Oss/Avitene biomaterial elicited no cytotoxic effects (**Figure 10B**). The biomaterial showed the highest value in cell proliferation between day 0 and 9 ( $p < 0.05$ ). The metabolic activity measured by Alamar Blue assay demonstrated different cellular growth kinetics, which were statistically significant, at day 6 and 9, compared to cell proliferation on the TCPS control group ( $p < 0.05$ ).

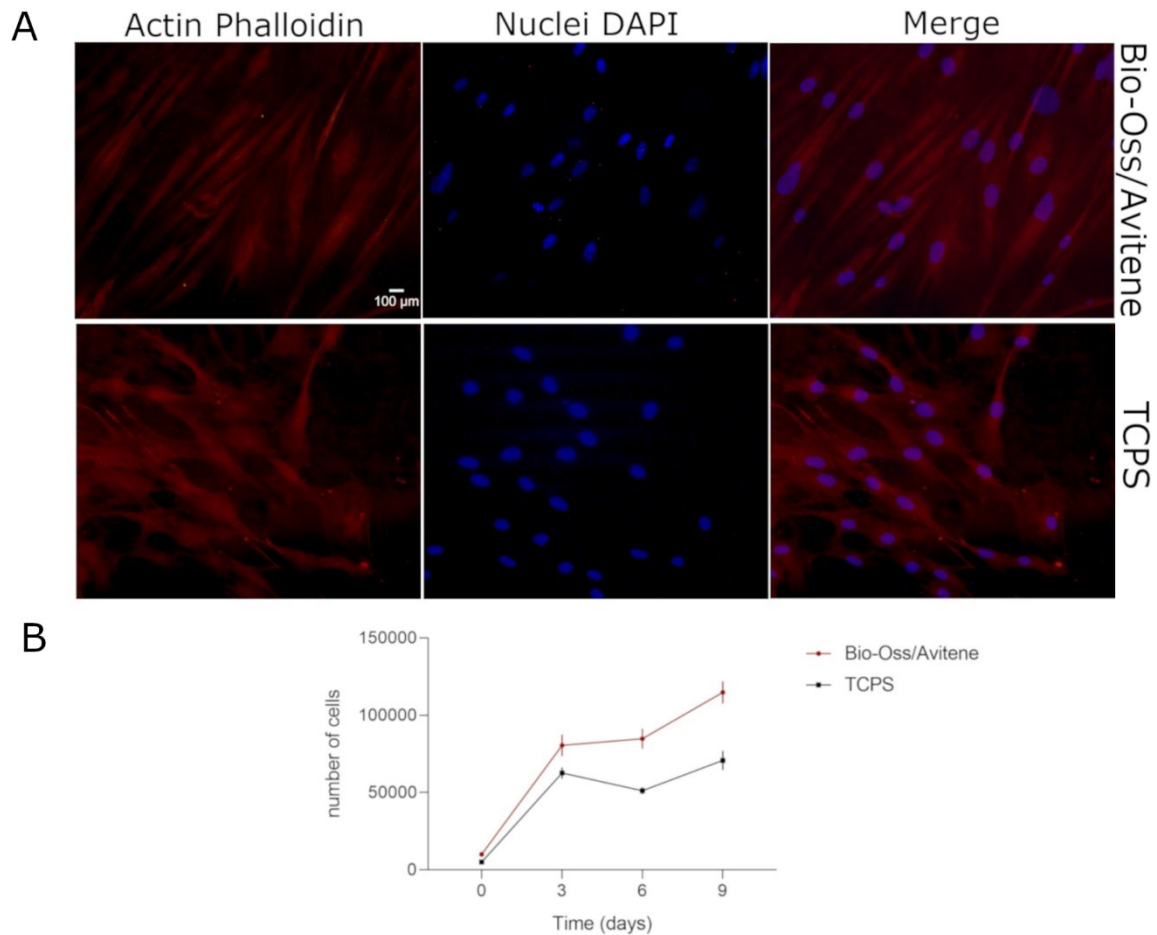


**Figure 10.** Stem cell proliferation and cytoskeleton architecture. (A) Stem cell cytoskeleton architecture. Cell nuclei were stained with 0.5 mg/mL DAPI. Cytoskeleton analysis by Phalloidin TRITC staining (magnification 20x). (B) Human adipose stem cells (hASCs) metabolic activity was evaluated by colorimetric intensity at day 3, 6 and 9 of co-culture on the Bio-Oss/Avitene and culture polystyrene (TCPS) vessels. The biomaterial showed the highest value in cell proliferation between day 0 and 9 ( $p < 0.05$ ).

#### 4.2.3. Matrix mineralization

A significant increase of matrix mineralization in hASCs grown on the biomaterial at day 21 was reported. Indeed at day 21, the biomaterial favoured the matrix mineralization better than the plastic vessel (TCPS), the control (**Figure 11A**,  $*p < 0.05$ ). Moreover, calcium deposits in hASCs grown on OC were higher compared with cells grown on the biomaterial or TCPS (**Figure 11B**,  $***p < .0001$ ).

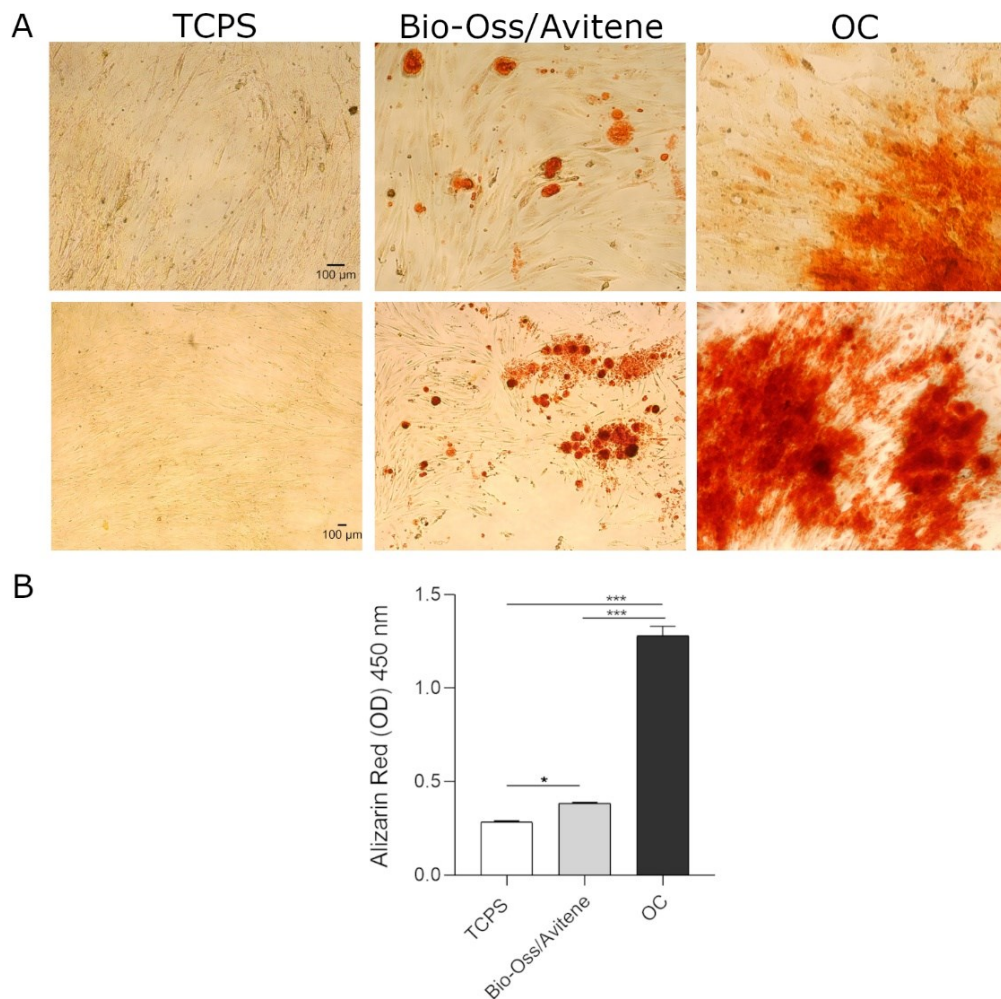


**Figure 11.** Biomaterial induced matrix mineralization. hASCs grown on scaffold were stained with ARS and imaged with bright-field microscopy at day 21 (10x magnification upper figures, 4x magnification lower figures) (A). The biomaterial induces mineral matrix deposition better than the plastic vessel (TCPS), the control (A, B). The quantification of ARS was performed by eluting ARS staining and acquiring optical density measurements. Osteogenic differentiation of hASCs grown on the biomaterial was increased than TCPS (\* $p < 0.05$ ; B). In OC, the calcium deposits were higher than in cells grown on the scaffold and in TCPS (\*\* $p < 0.0001$ ).

#### 4.2.4. Cytokine/Chemokine Gene Expression in hASCs grown on the Bio-Oss®/Avitene™

The expression profile of human genes that encode cytokines and chemokines was evaluated by qPCR Array technology. To this end, hASCs were grown on the Bio-Oss/Avitene scaffold, for 21 days. For data analysis, the Ribosomal protein, large, P0 (RPLP0) was used as housekeeping gene and  $\text{Log}_2 \text{FC} < -1$  or  $> +1$  was considered significant. Twenty-four DEGs involved in immune response (12 up-regulated and 12 down-regulated genes) were identified in hASCs grown on the Bio-Oss/Avitene biomaterial (**Figure 12A, Table 4**). The up-regulated genes which were accounted for included Chemokine (C-X3-C motif) ligand 1 (CX3CL1),

Interleukin 10 (IL10), CD40 ligand (CD40LG), Interleukin 13 (IL13), Interleukin 22 (IL22), Chemokine (C-X-C motif) ligand 13 (CXCL13), Tumour necrosis factor (ligand) superfamily, member 11 (TNFSF11), Interleukin 16 (IL16), Secreted phosphoprotein 1 (SPP1), Ciliary neurotrophic factor (CNTF), Chemokine (C-X-C motif) ligand 12 CXCL12 and Interleukin 15 (IL15). The down-regulated genes induced by Bio-Oss/Avitene biomaterial were Vascular endothelial growth factor A (VEGFA), Tumour necrosis factor receptor superfamily, member 11b (TNFRSF11B), Chemokine (C-X-C motif) ligand 5 (CXCL5), Chemokine (C-C motif) ligand 2 (CCL2), Interleukin 11 (IL11), Leukemia inhibitory factor (cholinergic differentiation factor, LIF), Chemokine (C-X-C motif) ligand 2 (CXCL2), Interleukin 1 receptor antagonist (IL1RN), Chemokine (C-X-C motif) ligand 1 (CXCL1), Interleukin 6 (interferon, beta 2 IL6) Chemokine (C-C motif) ligand 8 (CXCL8) and Colony stimulating factor 3 (granulocyte, CSF3).

#### **4.2.5. Bio-Oss®/Avitene™ modulates genes implicated in skeletal development**

DEGs (n=31) involved in osteogenic differentiation were detected in hASCs grown on the Bio-Oss/Avitene biomaterial. DEGs, including 24 up-regulated genes (red) and 7 down-regulated genes (green), were identified in hASCs grown on the Bio-Oss/Avitene biomaterial (**Figure 12B, Table 5**). These up-regulated genes included osteoblast differentiation-related genes, for instance, SPP1, SMAD family member 3 (SMAD3), Noggin (NOG), Bone morphogenetic protein 2 (BMP2), the bone morphogenetic protein receptor type II (BMP2), Bone morphogenetic protein receptor, type IA (BMP1A), the Bone gamma-carboxyglutamate (gla) protein (BGLAP), while fibroblast growth factor receptor 2 (FGFR2), resulted as up-regulated in hASCs grown on the Bio-Oss/Avitene compared to the control group (TCPS). Up-regulated transcription factors included Runt-related transcription factor 2 (RUNX2), transcription factor Sp7 (SP7) and SMAD family member 1 (SMAD1). Moreover, the transcription factor condensation SRY (sex-related Y)-type high mobility group box SOX9 (SOX9) and BMP1B, which plays a central role in chondrocyte differentiation, was also found to be up-regulated in hASCs grown on the scaffold, at day 21. Human cell adhesion analysis and ECM gene expression revealed that the following growth factors, Epidermal Growth Factor (EGF), colony-stimulating factor 2 (CSF2), (Fibroblast Growth Factor 1 (FGF1), Platelet-derived growth factor subunit A (PDGFA) were up-regulated in hASCs grown on the scaffold. In addition, genes encoding for ECM molecules, adhesion molecules, such as Fms Related Receptor Tyrosine Kinase 1 (FLT1), Integrin alpha-3 (ITGA3) and Serpin Family H Member 1 (SERPINH1) were also up-regulated. The tested genes which resulted as down-regulated included those encoding for ECM molecules, such as Col type III alpha 1 (COL3A1), Col type

V alpha 1 (COL15A1), Twist Family BHLH Transcription Factor 1 (TWIST), VEGFA, Cartilage Oligomeric Matrix Protein (COMP), Intercellular adhesion molecule 1 (ICAM1) and CSF3.

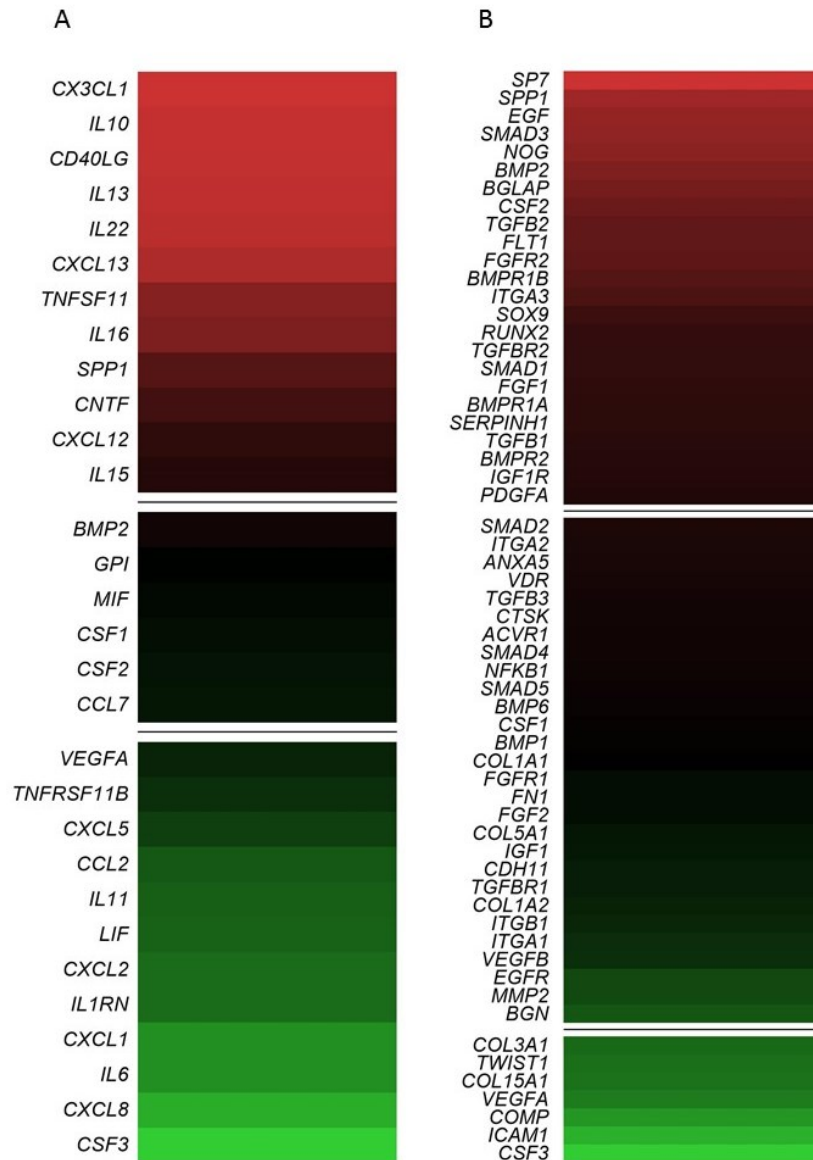


**Figure 12.** Gene expression involved in immune response and in osteogenic differentiation in human adipose mesenchymal stem cells grown on Bio-Oss/Avitene biomaterial. (A) Analysis of genes involved in the immune response. In hASC cultures, CX3CL1, IL10, CD40LG, IL13, IL22, CXCL13 TNFSF11, IL16, SPP1, CNTF, CXCL12 and IL15 resulted up-regulated (red). Moreover, VEGFA, TNFRSF11B, CXCL5, CCL2, IL11, LIF, CXCL2, IL1RN CXCL1, IL6, CXCL8 and CSF3 tested down-regulated (green) at day 21. (B) PCR array analysis genes involved in osteogenic differentiation. The genes SP7, SPP1, EGF, SMAD3, NOG, BMP2, BGLAP, CSF2, TGFB2, FLT1, FGFR2, BMPR1B, ITGA3, SOX9, RUNX2, TGFBR2, SMAD1, FGF1, BMPR1A, SERPINH1, TGFB1, BMPR2, IGF1R and PDGFA were up-regulated compared to TCPS (red) while COL3A1, TWIST1, COL15A1, VEGFA, COMP, ICAM1, CSF3 resulted as down-regulated after 21 days. A value of p-value <0.05 was considered significant. The fold change (FC) of each gene expression was calculated using the  $2^{-\Delta\Delta Ct}$  method, whereas housekeeping genes, used as controls, were used to normalize results and Log<sub>2</sub> FC < -1 or > +1 was considered significant.



**Table 4.** List of genes involved in immune response found to be up-regulated and down-regulated in hASCs grown on the Bio-Oss/Avitene scaffold at day 21.

Up-regulated genes			Down-regulated genes		
Number	Symbol/ Acronym	Fold-Change (Log <sub>2</sub> FC)	Number	Symbol/ Acronym	Fold-Change (Log <sub>2</sub> FC)
1	<i>CX3CL1</i>	8.56	1	<i>VEGFA</i>	-1.15
2	<i>IL10</i>	8.16	2	<i>TNFRSF11B</i>	-1.51
3	<i>CD40LG</i>	8.14	3	<i>CXCL5</i>	-2.06
4	<i>IL13</i>	7.99	4	<i>CCL2</i>	-2.84
5	<i>IL22</i>	7.74	5	<i>IL11</i>	-3.06
6	<i>CXCL13</i>	7.23	6	<i>LIF</i>	-3.18
7	<i>TNFSF11</i>	5.58	7	<i>CXCL2</i>	-3.47
8	<i>IL16</i>	5.26	8	<i>IL1RN</i>	-3.47
9	<i>SPP1</i>	3.57	9	<i>CXCL1</i>	-4.64
10	<i>CNTF</i>	2.73	10	<i>IL6</i>	-4.64
11	<i>CXCL12</i>	1.89	11	<i>CXCL8</i>	-5.64
12	<i>IL15</i>	1.47	12	<i>CSF3</i>	-6.64

*Chemokine (C-X3-C motif) ligand 1 (CX3CL1), Interleukin 10 (IL10), CD40 ligand (CD40LG), Interleukin 13 (IL13), Interleukin 22 (IL22), Chemokine (C-X-C motif) ligand 13 (CXCL13), Tumour necrosis factor (ligand) superfamily, member 11 (TNFSF11), Interleukin 16 (IL16), Secreted phosphoprotein 1 (SPP1), Ciliary neurotrophic factor (CNTF), Chemokine (C-X-C motif) ligand 12 (CXCL12), Interleukin 15 (IL15), Vascular endothelial growth factor A (VEGFA), Tumour necrosis factor receptor superfamily, member 11b (TNFRSF11B), Chemokine (C-X-C motif) ligand 5 (CXCL5), Chemokine (C-C motif) ligand 2 (CCL2), Interleukin 11 (IL11), Leukemia inhibitory factor (cholinergic differentiation factor, LIF), Chemokine (C-X-C motif) ligand 2 (CXCL2), Interleukin 1 receptor antagonist (IL1RN), Chemokine (C-X-C motif) ligand 1 (CXCL1), Interleukin 6 (interferon, beta 2 IL6) Chemokine (C-C motif) ligand 8 (CXCL8), Colony stimulating factor 3 (granulocyte, CSF3).*

**Table 5.** List of genes involved in osteogenic differentiation found to be up-regulated and down-regulated in hASCs grown on the Bio-Oss/Avitene scaffold at day 21

Up-regulated genes			Down-regulated genes		
Number	Symbol/ Acronym	Fold-Change (Log <sub>2</sub> FC)	Number	Symbol/ Acronym	Fold-Change (Log <sub>2</sub> FC)
1	SP7	7.14	1	COL3A1	-1.09
2	SPP1	5.52	2	TWIST1	-1.15
3	EGF	5.12	3	COL15A1	-1.18
4	SMAD3	4.99	4	VEGFA	-1.29
5	NOG	4.80	5	COMP	-1.56
6	BMP2	4.41	6	ICAM1	-1.84
7	BGLAP	4.05	7	CSF3	-2.12
8	CSF2	3.67			
9	TGFB2	3.41			
10	FLT1	3.37			
11	FGFR2	3.23			
12	BMPR1B	2.99			
13	ITGA3	2.64			
14	SOX9	2.08			
15	RUNX2	1.77			
16	TGFBR2	1.74			
17	SMAD1	1.72			
18	FGF1	1.59			
19	BMPR1A	1.57			
20	SERPINH1	1.52			
21	TGFB1	1.42			
22	BMPR2	1.30			
23	IGF1R	1.23			
24	PDGFA	1.10			

*Sp7 transcription factor (SP7), Secreted phosphoprotein 1 (SPP1), Epidermal growth factor (EGF), SMAD family member 3 (SMAD3), Noggin (NOG), Bone morphogenetic protein 2 (BMP2), Bone gamma-carboxyglutamate (gla) protein (BGLAP), Colony stimulating factor 2 (CSF2), Transforming growth factor, beta 3 (TGFB2), Fms-related tyrosine kinase 1 (FLT1), Fibroblast growth factor receptor 2 (FGFR2), Bone morphogenetic protein receptor, type IB (BMPR1B), Integrin, alpha 3 (ITGA3), SRY (sex determining region Y)-box 9 (SOX9), Runt-related transcription factor 2 (RUNX2), Transforming growth factor, beta receptor II (TGFBR2), SMAD family member 1 (SMAD1), Fibroblast growth factor 1 (FGF1), Bone morphogenetic protein receptor, type IA (BMPR1A), Serpin peptidase inhibitor, clade H (heat shock protein 47), member 1 (SERPINH1), Transforming growth factor, beta 1 (TGFB1), Bone morphogenetic protein receptor, type II (BMPR2), Insulin-like growth factor 1 receptor (IGF1R), Platelet-derived growth factor alpha polypeptide (PDGFA), Collagen, type III, alpha 1 (COL3A1), Twist homolog 1 (TWIST1), Collagen, type XV, alpha 1 (COL15A1), Vascular endothelial growth factor A (VEGFA), Cartilage oligomeric matrix protein (COMP), Intercellular adhesion molecule 1 (ICAM1) and Colony stimulating factor 3 (CSF3).*

#### 4.2.6. *In vivo* evaluation

A combination of bony biomaterial (Bio-Oss) and Microfibrillar Collagen (Avitene) can be successfully used to mold prostheses for aesthetic cheek bone augmentation during orthognathic surgery in patients with flat or inadequate projection or asymmetry of the zygomatic area. The bone substitute Bio-Oss/Avitene gave remarkable aesthetic results in terms of naturalness and symmetry. The mean dimension of the prostheses calculated on 30 patients' Cone Beam Computed Tomography (CBCT) was 6.8 x 27.9 x 16.0 mm with a mean volume of 1,793 mm<sup>3</sup> (**Figure 13**).

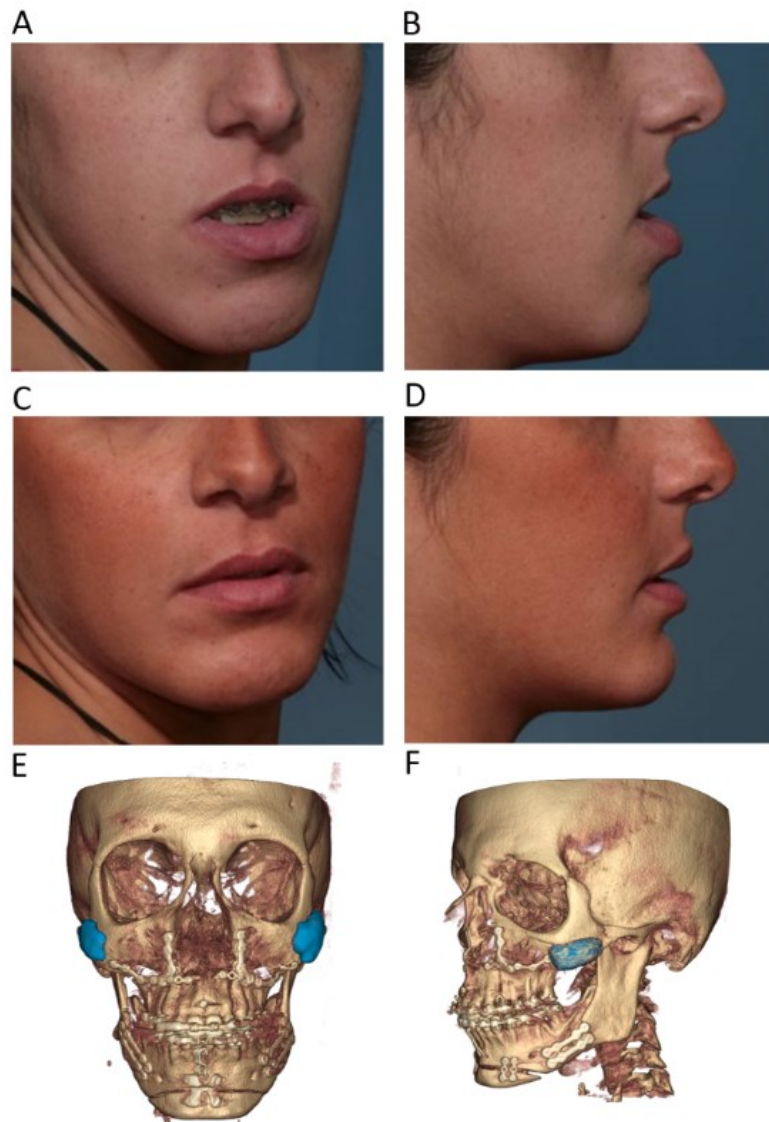


**Figure 13.** In vivo evaluation of Bio-Oss/Avitene biomaterial. (A, B) Patient 1 clinical evaluation before implant. (C, D) Patient 1 post-operative assessment 15 days after the procedure. (E, F) Placement of the implants in the subperiosteal pockets. Cone-beam CT scan showing final position of the prosthesis in the malar area.

### 4.3. Biomorphic hydroxyapatite

#### 4.3.1. Microstructural Analysis

Biomorphic scaffold (B-HA) shows lamellar, closely interconnected HA nanocrystals ( $\sim 200 \times 20$  nm) with a hexagonal shape (**Figure 14A**). The absence of any high temperature sintering process prevented grain growth in B-HA, thus resulting in a higher specific surface area (i.e., B-HA:  $12.5 \text{ m}^2/\text{g}$ ; S-HA:  $4.8 \text{ m}^2/\text{g}$ ), without evidence of intergranular boundary layers in strong contrast to the typical microstructure of sintered ceramic bodies. Both scaffolds showed a porosity extent of  $\sim 60$  vol. %. Conversely, S-HA shows a typical sintered HA microstructure, with coalesced rounded  $\sim 1\text{--}2 \mu\text{m}$  sized grains and diffuse intergranular porosity (**Figure 14B**).

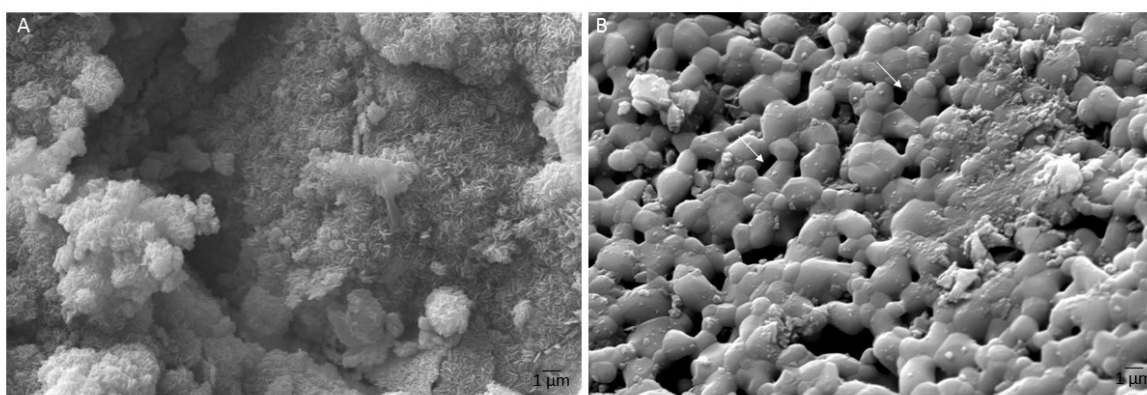
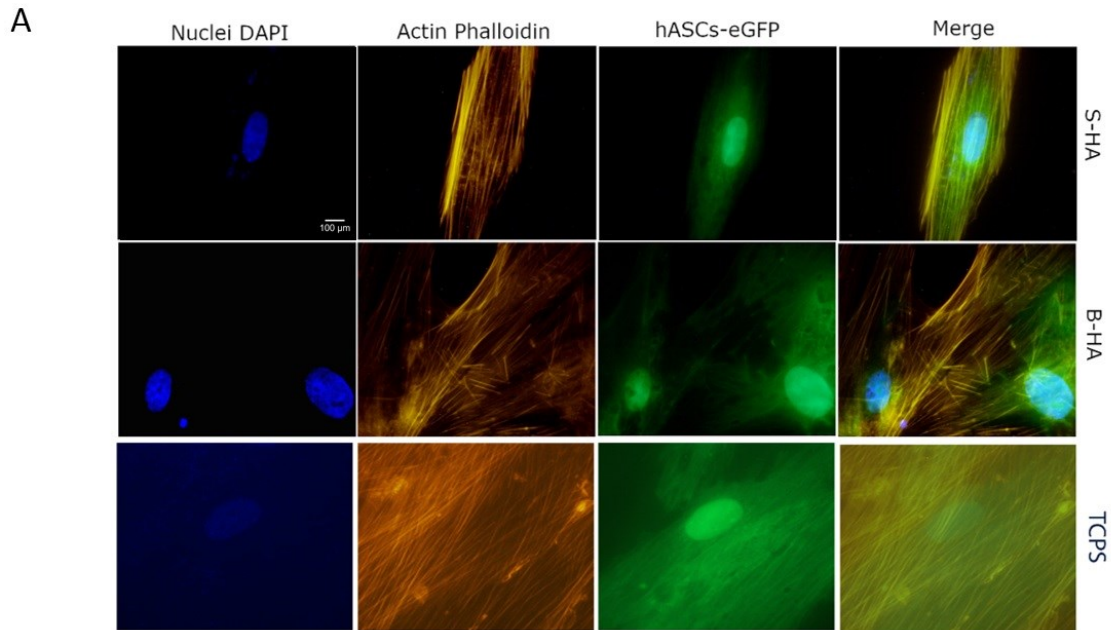


**Figure 14.** Scanning electron microscopy (SEM) analysis of B-HA and S-HA. (A) B-HA structure is characterized by nanometric particles forming thin lamellae with a microstructure composed of nano-size building blocks and multi-scale porosity, Scale bar:  $1 \mu\text{m}$ ,  $\times 10,210\text{K}$ . (B) SEM S-HA images show its porous structure, Scale bar:  $1 \mu\text{m}$ ,  $\times 11,57\text{K}$ .

#### 4.3.2. Cytocompatibility analysis of biomorphic HA scaffold employing hASCs

In vitro cytocompatibility analyses, i.e. proliferation and cytoskeleton organization, assayed in hASCs cultured on biomaterials were evaluated up to day 14. B-HA and sintered S-HA biomaterials demonstrated cytocompatibility in terms of cell growth and proliferation. Actin fibres of the cytoskeleton appeared to be well organized, whereas its integrity remains uninfluenced by scaffolds (**Figure 15A**). The Alamar Blue assay showed an increased scaffold metabolic activity during the analysis in hASCs grown on B-HA and S-HA scaffold. The metabolic activity measured by Alamar Blue assay demonstrated that B-HA and S-HA biomaterials did not elicit cytotoxic effects, although different cellular growth kinetics, which are statistically significant at day 14 compared to day 7 ( $p < 0.05$ ), were induced. Moreover,

the B-HA scaffold had a substantial overall effect on cell proliferation compared to S-HA and TCPS ( $p < 0.05$ ) (**Figure 15B**).



**B**

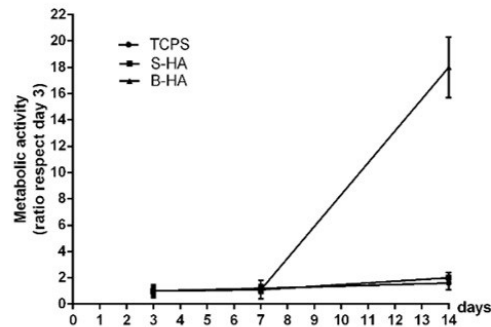


**Figure 15.** Stem cell proliferation and cytoskeleton architecture. (A) Cytoskeleton analysis by Phalloidin TRITC staining of hASCs-eGFP grown on biomaterials B-HA and S-HA (magnification 40x). Actin filaments do not show alteration in the structural organization, confirming the compatibility of the assayed biomaterials, at day 14. Cellular nuclei were stained with 0.5 mg/ml DAPI. (B) hASC metabolic activity measured by colorimetric intensity at day 3, 7, and 14 of co-culture on B-HA, S-HA and TCPS. 3D biomorphic biomaterials exhibited the highest value in cell proliferation between day 7 and day 14 ( $p < 0.05$ ). Statistically differences are significant for B-HA, S-HA and TCPS at day 7 and day 14 ( $p < 0.05$ ).

### 4.3.3. Matrix mineralization and osteocalcin expression protein in hASCs

In order to test the osteogenic differentiation induced by biomorphic material B-HA, hASCs were grown on scaffolds for two weeks. Mineral matrix deposition was evaluated by ARS at day 14 in hASCs cultured on B-HA and SHA biomaterials, in osteogenic condition (OC) and in plastic vessels (TCPS) (**Figure 16A**).

ARS staining showed that stem cells formed a small number of calcified nodules (**Figure 16A**). When co-culture processing was performed for a further two weeks, several calcified nodules were observed (**Figure 16A**). The B-HA scaffold favoured matrix mineralization better than TCPS, the control group (\*\*  $p < 0.01$ ). Calcium deposits quantified in hASCs grown on the B-HA material were higher compared to stem cells grown on the S-HA biomaterial (\*\*  $p < 0.01$ ). Cells grown in OC showed a significant increase in calcium deposits compared to S-HA, TCPS (\*\*  $p < 0.01$ ) and B-HA (\*  $p < 0.05$ ), (**Figure 16B**). OCN is the most important non-collagenous protein involved in bone matrix organization and deposition. ELISA data show a statistically significant increasing level of OCN protein expression in cells grown on B-HA biomaterial, compared to the other experimental groups, represented by S-HA and OC (\* $p < 0.05$ ) and TCPS (\*\* $p < 0.01$ ) at day 14 (**Figure 16C**). These improved cellular responses for hASCs grown on B-HA material demonstrate the inductive effect exerted by B-HA compared to S-HA scaffold.

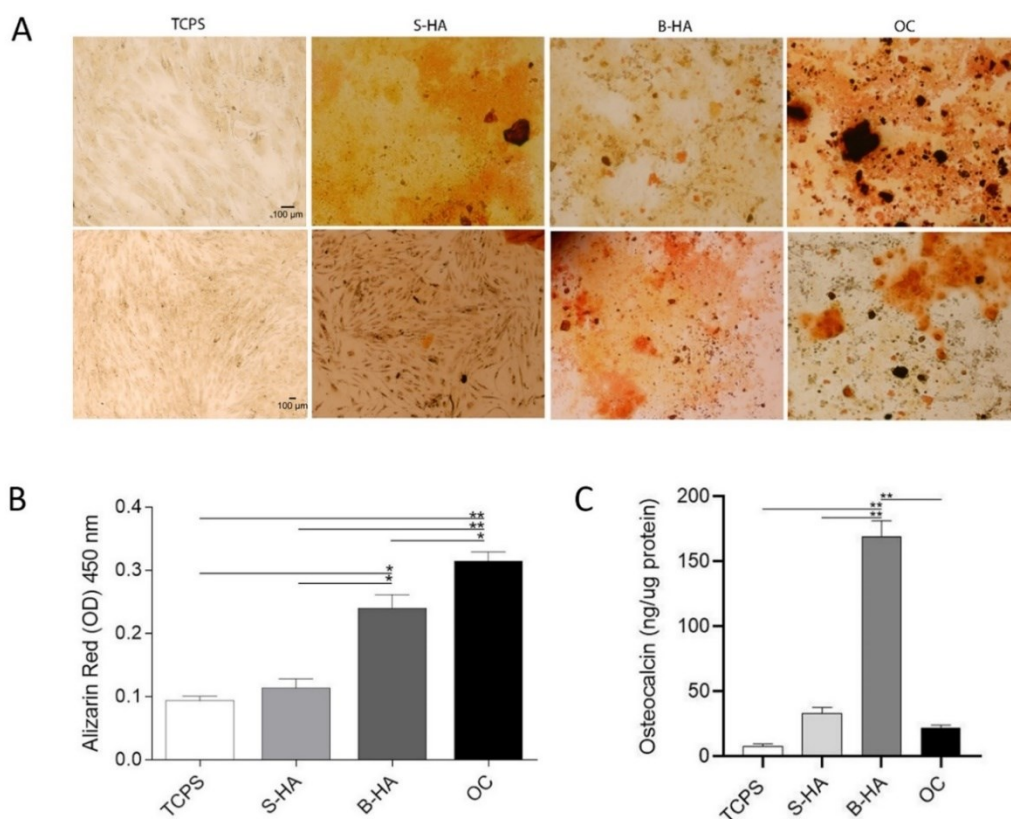


**Figure 16.** Osteogenic markers in hASCs cultured on Biomorphic (B-HA) and Engipore (S-HA) biomaterials. (A) ARS at day 14 is shown in the panel, in experimental conditions tested, 10x magnification upper figures, 4x magnification lower figures. (B) The matrix mineralization was evaluated by ARS, whereas its quantification was carried out spectrophotometrically. \* $p < 0.05$ ; \*\* $p < 0.01$ , ANOVA test. Matrix mineralization data was reported as optical density. (C) The osteocalcin (OCN) protein levels detected at day 14 were quantified by ELISA test. OCN protein was reported as ng of Osteocalcin/ $1\mu\text{g}$  of total protein, \*\* $p < 0.01$  ANOVA test.

The matrix mineralization was also evaluated at day 21 showing that the B-HA scaffold favoured matrix mineralization better than TCPS (\* $p < 0.05$ ) (**Figure 17**).

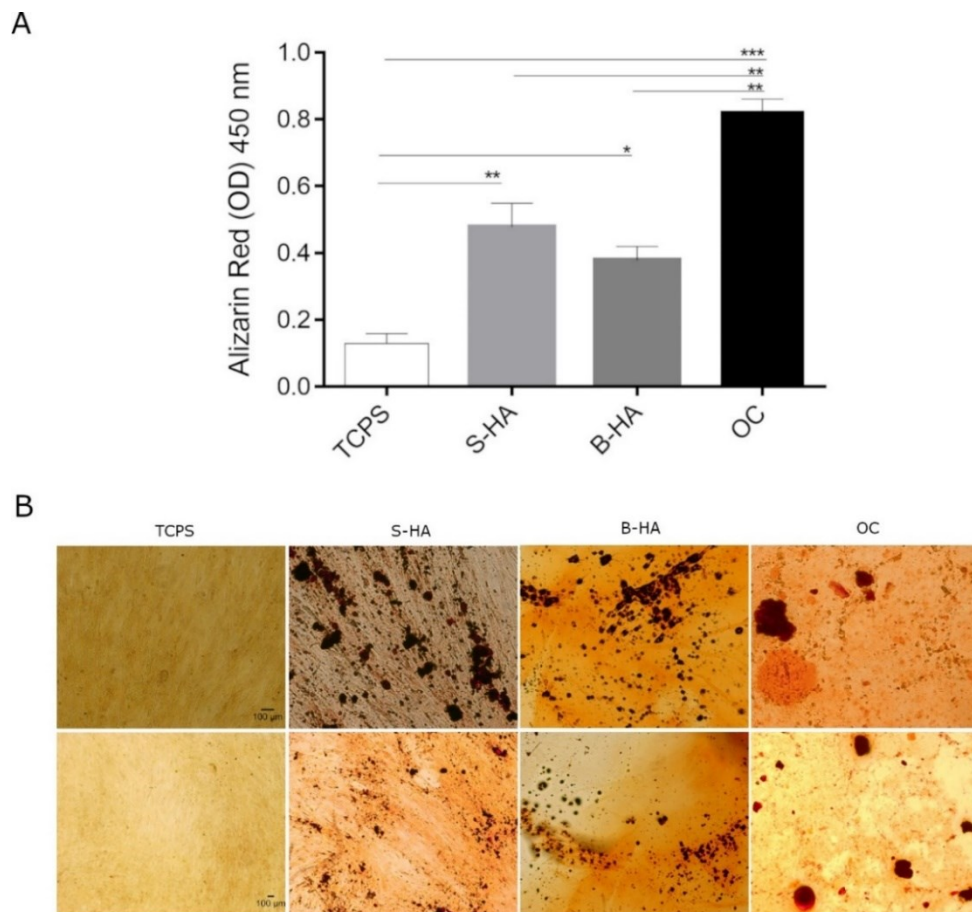


**Figure 17.** Matrix mineralization in hASCs cultured on B-HA and S-HA biomaterials at day 21. (A) The matrix mineralization was evaluated by Alizarin red staining at day 21, whereas its quantification was carried out spectrophotometrically. Matrix mineralization data was reported as optical density. \* $p < 0.05$ ; \*\* $p < 0.01$ ; \*\*\*  $p < 0.001$  (ANOVA test was used). (B) Alizarin red staining is shown in the panel, in experimental conditions tested (10x magnification upper figures, 4x magnification lower figures).

#### 4.3.4. Osteogenic Gene Expression in hASCs

The expression profile of human osteogenic genes was evaluated by qPCR Array technology. To this end, hASCs were grown on both B-HA and S-HA scaffolds for 14 days. Quantitative qPCR Array results were compared to the control group using hASCs grown on TCPS. A value of  $p < 0.05$  was considered significant. In hASCs grown on B-HA, 17 DEGs were detected up-regulated at day 14 (**Table 6**), i.e. ALPL, BGLAP, CHRD, COL10A1, CSF3, EGF, FGFR2, GLI1, ITGA3, MMP10, MMP8, MMP9, SMAD3, SOX9, SP7, TGFB3 and TNFSF11.

**Table 6.** List of genes found to be up-regulated in hASCs grown on the B-HA scaffold at day 14.

Up-regulated genes		
Number	Symbol/ Acronym	Fold-Change (Log <sub>2</sub> FC)
1	<i>ALPL</i>	7.72
2	<i>BGLAP</i>	6.94
3	<i>CHRD</i>	9.46
4	<i>COL10A1</i>	7.72
5	<i>CSF3</i>	11.18
6	<i>EGF</i>	11.21
7	<i>FGFR2</i>	9.83
8	<i>GLI1</i>	12.85
9	<i>ITGA3</i>	6.97
10	<i>MMP10</i>	16.46
11	<i>MMP8</i>	14.08
12	<i>MMP9</i>	10.49
13	<i>SMAD3</i>	10.65
14	<i>SOX9</i>	7.50
15	<i>SP7</i>	14.29
16	<i>TGFB3</i>	6.95
17	<i>TNFSF11</i>	13.78

*Alkaline phosphatase (ALPL), Bone gamma-carboxyglutamate (gla) protein (BGLAP), Chordin (CHRD), Collagen, type X, alpha 1 (COL10A1), Colony stimulating factor 3 (CSF3), Epidermal growth factor (EGF), Fibroblast growth factor receptor 2 (FGFR2), GLI family zinc finger 1 (GLI1), Integrin, alpha 3 (ITGA3), Matrix metalloproteinase 10 (MMP10), Matrix metalloproteinase 8 (MMP8), Matrix metalloproteinase 9 (MMP9), SMAD family member 3 (SMAD3), SRY (sex determining region Y)-box 9 (SOX9), Sp7 transcription factor (SP7), Transforming growth factor, beta 3 (TGFB3), Tumour necrosis factor (ligand) superfamily, member 11 (TNFSF11).*



26 DEGs were identified in hASCs grown on S-HA biomaterial, 10 up-regulated genes and 16 downregulated genes were identified (**Table 7**). Among these genes were accounted BMP2, COL2A1, CSF2, EGF, GLI1, MMP10, MMP8, SP7, SPP1, TNFSF11, which were up-regulated, while 16 tested genes resulted down-regulated at day 14, i.e. BGLAP, BGN, BMP6, COL1A1, COL1A2, COL3A1, COL5A1, FGF1, FN1, IGF1, ITGA2, ITGA3, ITGB1, MMP2, TGFB3 and VCAM1.

**Table 7.** List of genes found to be up-regulated and down-regulated in hASCs grown on the S-HA scaffold at day 14

Up-regulated genes			Down-regulated genes		
Number	Symbol/ Acronym	Fold-Change (Log <sub>2</sub> FC)	Number	Symbol/ Acronym	Fold-Change (Log <sub>2</sub> FC)
1	<i>BMP2</i>	1.90	1	<i>BGLAP</i>	-2.18
2	<i>COL2A1</i>	1.01	2	<i>BGN</i>	-2.18
3	<i>CSF2</i>	5.30	3	<i>BMP6</i>	-3.64
4	<i>EGF</i>	2.01	4	<i>COL1A1</i>	-2.12
5	<i>GLI1</i>	2.75	5	<i>COL1A2</i>	-1.60
6	<i>MMP10</i>	5.59	6	<i>COL3A1</i>	-1.06
7	<i>MMP8</i>	3.10	7	<i>COL5A1</i>	-2.00
8	<i>SP7</i>	3.08	8	<i>FGF1</i>	-1.47
9	<i>SPP1</i>	2.33	9	<i>FN1</i>	-2.06
10	<i>TNFSF11</i>	4.02	10	<i>IGF1</i>	-2.12
			11	<i>ITGA2</i>	-1.36
			12	<i>ITGA3</i>	-1.89
			13	<i>ITGB1</i>	-1.06
			14	<i>MMP2</i>	-1.09
			15	<i>TGFB3</i>	-1.06
			16	<i>VCAM1</i>	-1.03

*Bone morphogenetic protein 2 (BMP2), Collagen, type II, alpha 1 (COL2A1), Colony stimulating factor 2 (CSF2), Epidermal growth factor (EGF), GLI family zinc finger 1 (GLI1), Matrix metalloproteinase 10 (MMP10), Matrix metalloproteinase 8 (MMP8), Sp7 transcription factor (SP7), Secreted phosphoprotein 1 (SPP1), Tumour necrosis factor (ligand) superfamily, member 11 (TNFSF11), Bone gamma-carboxyglutamate (gla) protein (BGLAP), Biglycan (BGN), Bone morphogenetic protein 6 (BMP6), Collagen, type I, alpha 1 (COL1A1), Collagen, type I, alpha 2 (COL1A2), Collagen, type III, alpha 1 (COL3A1), Collagen, type V, alpha 1 (COL5A1), Fibroblast growth factor 1 (FGF1), Fibronectin 1 (FN1), Intercellular adhesion molecule 1 (ICAM1), Insulin-like growth factor 1 (IGF1), Integrin, alpha 1 (ITGA1), Integrin, alpha 2 (ITGA2), Integrin, alpha 3 (ITGA3), Integrin, beta 1 (ITGB1), Matrix metalloproteinase 2 (MMP2), Transforming growth factor, beta 3 (TGFB3), Vascular cell adhesion molecule 1 (VCAM1).*

It appears that both biomaterials stimulate the over-expression of specific osteoblastic genes, such as Sp7 and GLI1 with different fold change values. DEGs modulated by the two scaffolds also include growth factors such as EGF and ECM molecules, including MMP8 and MMP10,

and factors implicated in osteoclastic differentiation, such as TNFSF11. B-HA induced the up-regulation of these common genes, with a higher fold change compared to S-HA material. BGLAP, ITGA3 and TGFB3 tested up- and down-regulated in hASCs grown on B-HA and S-HA, respectively.

## **5. DISCUSSION**

### **5.1. Pro Osteon 200/Avitene and Bio-Oss®/Avitene™ composite biomaterials**

In tissue engineering, biomaterials could be considered as a “template”, providing temporary mechanical support and mass transport to promote cell adhesion, proliferation, and differentiation [56]. Ideally, a scaffold should serve as a transient structure that, over an extended period, will be degraded/reabsorbed in a controlled manner, in accordance with the regrowth rate of new bone tissue. Tissue engineering scaffolds attempt to mimic the natural ECM, at least partially, and to create a favourable microenvironment to support tissue formation. Subsequently, the biomaterial template will be correctly substituted with naturally deposited ECM and the newly formed tissue [56]. The mineral content of bone is predominantly HA, while the organic matrix is composed mainly of type I collagen (~90%). Biomechanically, the inorganic mineral HA endows bone with its rigid structural framework, while collagen confers bone with its elastic properties [93]. To mimic the natural bone composition, prevailing scaffolds for bone tissue engineering are HA/Collagen composites.

In this study, in vitro cellular model consisting of primary hASCs was employed to evaluate two composites HA-derived scaffolds, i.e. coral (0.5 mm-1 mm) and bovine (1 mm-2 mm) granules combined with bovine collagen Avitene, named Pro Osteon 200/Avitene and Bio-Oss/Avitene, respectively. A cohort of maxillofacial patients was evaluated for their cytocompatibility proprieties and bone regrowth. To this end, collagen and HA were joined with sterile water to form collagen–apatite slurry. In vivo, Shaping was performed according to surgical needs, depending on the clinical evaluation of the patient. The handmade bone substitutes were made in vitro according to clinical procedures. Subsequently, their cytocompatibility, immunomodulatory and osteoinductivity proprieties were analysed.

Coral derived porous HA is frequently used in maxillofacial surgery for procedures to augment the splanchnocranium [91]. In a previous study [90], hASCs from adults were employed as an in vitro model to evaluate the cytocompatibility, osteoconductivity, osteoinductivity, and osteogenic properties of Pro Osteon 200/Avitene, until 21 days. In the present study, in order to mimic the long period needed in vivo by the bone to regrowth and repair itself, the experiments were carried out up to day 40. Patients operated for maxillomandibular malocclusion and/or asymmetry, or for aesthetic reasons, who underwent malar augmentation with porous Pro Osteon 200/Avitene prostheses, were evaluated for the new bone formation during a 3-year period of follow-up using radiological and histological analyses [89].

However, because the coral reefs are exposed to catastrophic situations, there is a need to look for alternatives [70]. In this context, bovine bone, which is considered a biowaste, is an alternative source of HA for hard tissue replacement in medical and dental therapy [68].

Bio-Oss is a common bone substitute employed for bone regeneration. It consists of bovine spongy bone free of organic ingredients, in which the trabecular structure of the fine bone and the internal voids are preserved. Numerous studies have shown that this physical microstructure of Bio-Oss plays a decisive role in controlling bone regeneration [71]. In this study, Bio-Oss granules were used in combination with collagen Avitene and the in vitro analysis were performed until day 21 (Jaquinta et al., 2022. *Accepted*). Patients operated for maxillomandibular malocclusion and/or asymmetry, or for aesthetic reasons, who underwent malar augmentation with porous Bio-Oss/Avitene prostheses, were evaluated for the new bone formation after 15 days.

Analysis of proliferation conducted with hASCs suggest that both Pro Osteon 200/Avitene and Bio-Oss/Avitene scaffolds meet the requirements for in vitro cytocompatibility, offering a good microenvironment for hASCs adhesion and proliferation. Cytoskeleton architecture seemed to be well organized. Indeed, the actin filaments were distributed uniformly in hASCs grown on the Pro Osteon 200/Avitene and Bio-Oss/Avitene biomaterials.

Inflammation is an important factor that should be considered to develop successful biomaterial-based therapeutics. Indeed, inflammation is initially needed for wound healing while prolonged inflammation can result in delayed wound healing or, in some cases, rejection of the scaffold and additional tissue damage. Epigenetic studies were carried out at day 21 by analysing the main genes involved in the immune response to hASCs grown on the Pro Osteon 200/Avitene and Bio-Oss/Avitene biomaterials, compared to hASCs grown on plastic vessel TCPS, used as control. Cytokines are small signalling proteins secreted by immune cells and many different cell types to stimulate immune response, inflammation and other processes. Historically, cytokines were functionally separated into two families: lymphokines/interleukins and chemokines. All cytokines released by immune cells were called lymphokines/interleukins, whereas chemotactic cytokines were called chemokines. In **Table 8**, were indicated the common genes involved in immune response found to be dysregulated in hASCs grown on both scaffolds at day 21.

**Table 8.** List of common genes involved in immune response found to be dysregulated in hASCs grown on both scaffolds at day 21.

Up-regulated genes				Down-regulated genes			
Number	Symbol/ Acronym	Fold-Change (Log <sub>2</sub> FC)		Number	Symbol/ Acronym	Fold-Change (Log <sub>2</sub> FC)	
		PA	BA			PA	BA
1	<i>CX3CL1</i>	8.27	8.56	1	<i>IL6</i>	-1.84	-4.64
2	<i>CD40LG</i>	6.70	8.14	2	<i>CCL2</i>	-2.25	-2.84
3	<i>IL22</i>	5.20	7.74	3	<i>LIF</i>	-2.74	-3.18
4	<i>CXCL13</i>	4.23	7.23	4	<i>CXCL2</i>	-3.06	-3.47
5	<i>IL13</i>	2.75	7.99	5	<i>CXCL5</i>	-3.06	-2.06
6	<i>CXCL12</i>	2.10	1.89	6	<i>IL11</i>	-3.32	-3.06
7	<i>IL15</i>	1.40	1.47	7	<i>CXCL1</i>	-3.47	-4.64
8	<i>CNTF</i>	1.14	2.73	8	<i>CXCL8</i>	-4.64	-5.64
				9	<i>IL1RN</i>	-6.64	-3.47

*Chemokine (C-X3-C motif) ligand 1 (CX3CL1), CD40 ligand (CD40LG), Interleukin 22 (IL22), Chemokine (C-X-C motif) ligand 13 (CXCL13), Nodal homolog (mouse, NODAL), Interleukin 13 (IL13), Chemokine (C-X-C motif) ligand 12 (CXCL12), Interleukin 15 (IL15), Interleukin 7 (IL7), Ciliary neurotrophic factor (CNTF), Interleukin 6 (interferon, beta 2 IL6), Chemokine (C-C motif) ligand 2 (CCL2), Leukemia inhibitory factor (cholinergic differentiation factor, LIF), Chemokine (C-X-C motif) ligand 2 (CXCL2), Chemokine (C-X-C motif) ligand 5 (CXCL5), Interleukin 11 (IL11), Chemokine (C-X-C motif) ligand 1 (CXCL1), Chemokine (C-C motif) ligand 8 (CXCL8), Interleukin 1 receptor antagonist (IL1RN).*

PA: Pro Osteon 200/Avitene; BA: Bio-Oss/Avitene.

Among up-regulated genes, 8 common DEGs were identified. These include anti-inflammatory cytokine, such as IL-13 and IL-22 in hASCs grown on both the Pro Osteon 200/Avitene and Bio-Oss/Avitene biomaterials. IL-22 is involved in human MSC proliferation/migration in inflammatory environments [94]. This biomaterial also induced CD40L up-regulation, which facilitates B-cell activation to promote early bone healing [95]. Protein XC chemokine ligand-13 (CXCL13) and its receptors were involved in the process of BMSCs migration. For example, CXCL13, alongside chemokine CXCR5, regulated the B-cell chemotaxis and the recruitment of BMSCs during fracture healing [96,97]. CNTF resulted as over-expressed in hASCs grown on both the Pro Osteon 200/Avitene and Bio-Oss/Avitene biomaterial, after day 21. Finally, CXCL12, also known as SDF1, tested up-regulated in hASCs grown on the scaffolds; this chemokine is responsible of recruitment of MSCs [31].

On the other hand, 9 DEGs were identified down-regulated by Pro Osteon 200/Avitene and Bio-Oss/Avitene biomaterials after day 21. Neutrophils play a critical initial role in controlling infections, firstly by phagocytosing the microorganisms and secondly, by releasing mediators

that draw other leukocytes into the injured tissue. It is therefore important to understand how these cells are recruited. Chemokine CXCL1 and many others are potent chemo-attractants, which neutrophils respond to [98]. In this study, CXCL1 resulted as down-regulated in hASCs grown on the Pro Osteon 200/Avitene and Bio-Oss/Avitene biomaterials, compared to the control. CXCL8 (also known as Interleukin 8) binds to CXCR1 as well as CXCR2, specifically [99,100]. CXCL8 also tested as down-expressed in hASCs grown on the Pro Osteon 200/Avitene and Bio-Oss/Avitene biomaterials. CXCL8, a multifunctional pro-inflammatory chemokine that was initially classified as a neutrophil chemoattractant, has recently been found to be a key contributor in tumourigenesis [101]. Indeed, CXCL8 is up-regulated in several human cancers. This suggests interplay between the tumour and its microenvironment, rendering tumour progression by enhancing angiogenesis, tumour genetic diversity, survival, proliferation, immune escape, metastasis and multidrug resistance [101]. In addition, chemokine CCL2 tested as down-regulated in hASCs grown on the Pro Osteon 200/Avitene and Bio-Oss/Avitene. CCL2 can affect bone metabolism. Osseous inflammation studies have shown selective expression of this chemokine by osteoblasts, which are strictly correlated to monocyte recruitment at osteolytic inflammatory lesion sites. In vivo, CCL2 is one of the main chemokines induced in osteoblasts in response to bacterial infections.

After acute injury, pro-inflammatory cytokines IL6 and IL11 are involved in the initial proinflammatory response. After 21 days, hASCs grown on both biomaterials studied herein, i.e. Pro Osteon 200/Avitene and Bio-Oss/Avitene, show a decreased expression of IL6 and IL11 (**Figure 18**), which are considered the most important interleukins involved in immune response in fracture healing.

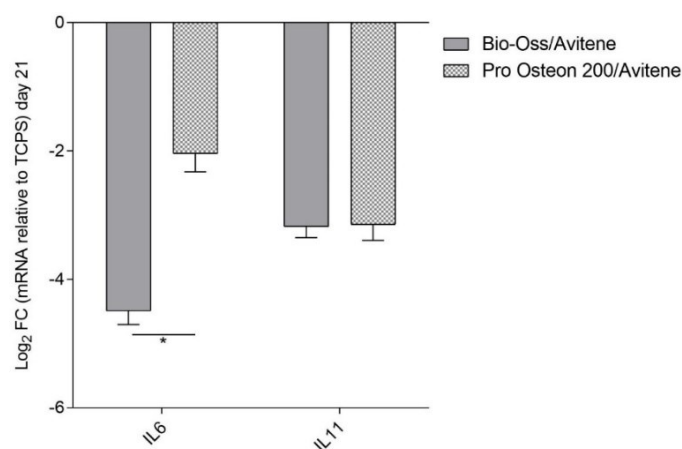


**Figure 18.** IL6 and IL11 gene expression in hASCs grown on Pro Osteon 200/Avitene and Bio-Oss/Avitene at day 21 (\*p<0.05).

IL6 stimulates angiogenesis, VEGF production [30]. In agreement, VEGFA resulted down-regulated in hASCs grown on the Bio-Oss/Avitene scaffolds. In order to confer angiogenic properties to the scaffold material, VEGF is frequently used [102].

Interestingly, SPP1 gene, which codifies for OPN, was up-regulated by the Bio-Oss/Avitene biomaterial. OPN is considered to play an important role in bone regrowth [89]. Some studies indicate OPN as a cell adhesive, signalling, migratory and survival stimulus for various mesenchymal, epithelial and inflammatory cells, in addition to being a potent regulator of osseous and ectopic calcification. Based on these reports, a general picture of OPN as an important inflammation and biomineralization regulator is emerging [103]. Recently, Mahon et al., observed increased expression of BMP2, ALP and OPN in MSCs in the presence of recombinant anti-inflammatory cytokine IL-10 [60], demonstrating a direct pro-osteogenic role for this cytokine, which resulted as up-regulated by the Bio-Oss/Avitene biomaterial in the present study. Current strategies being explored include incorporating anti-inflammatory cytokines, including IL-10, into scaffolds [104].

The close link between the immune and skeletal systems has recently been defined using the concept of “osteimmunology”, suggesting that several molecules which are involved in the maintenance of bone homeostasis and the regulation of inflammatory functions are shared, including receptors, signalling molecules and transcription factors [57]. DEGs (n= 14) involved in osteogenic pathways resulted dyregulated in hASCs grown on both scaffolds under analysis, respect to the control TCPS at day 21 ( $p<0.05$ ) (**Table 9**).



**Table 9.** List of common genes found to be dysregulated in hASCs grown on the scaffolds at day 21.

Common dysregulated genes			
Number	Symbol/Acronym	Fold-Change (Log2 FC)	
		PA	BA
1	<i>BGLAP</i>	1.94	4.05
2	<i>BMP2</i>	1.62	4.41
3	<i>BMPR1B</i>	2.78	2.99
4	<i>CSF2</i>	3.41	3.67
5	<i>CSF3</i>	5.18	-2.12
6	<i>FGFR2</i>	1.35	3.23
7	<i>IGF1R</i>	1.06	1.23
8	<i>NOG</i>	1.75	4.80
9	<i>RUNX2</i>	1.59	1.77
10	<i>SOX9</i>	1.18	2.08
11	<i>SP7</i>	4.89	7.14
12	<i>SPP1</i>	1.88	5.52
13	<i>TGFB1</i>	1.51	1.42
14	<i>TWIST1</i>	1.27	-1.15

*Bone gamma-carboxyglutamate (gla) protein (BGLAP), Bone morphogenetic protein 2 (BMP2), Bone morphogenetic protein receptor, type 1B (BMPR1B), Colony stimulating factor 2 (CSF2), Colony stimulating factor 3 (CSF3), Fibroblast growth factor receptor 2 (FGFR2), Insulin-like growth factor 1 receptor (IGF1R), Noggin (NOG), SRY (sex determining region Y)-box 9 (SOX9), Runt-related transcription factor 2 (RUNX2), Sp7 transcription factor (SP7), Secreted phosphoprotein 1 (SPP1), Transforming growth factor, beta 1 (TGFB1), Twist homolog 1 (TWIST1).*

PA: Pro Osteon 200/Avitene; BA: Bio-Oss/Avitene.

It is important to notice that among these, four essential transcription factors resulted dysregulated by both biomaterials at day 21 (**Figure 19**).

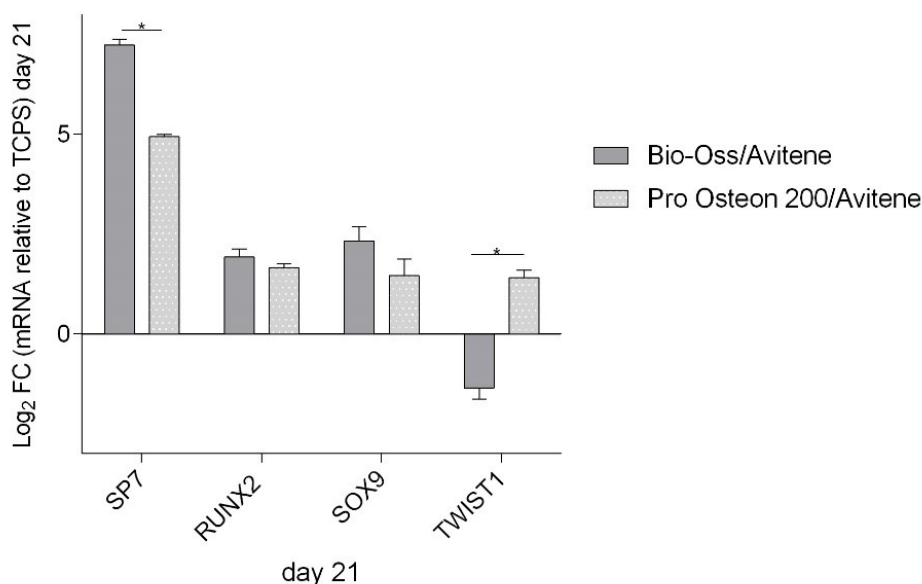


**Figure 19.** Expression of most important transcription factors (TFs) resulted dysregulated in hASCs grown on Pro Osteon 200/Avitene and Bio-Oss/Avitene biomaterials at day 21 (\*p<0.05).

During osteoblast differentiation, RUNX2 is weakly expressed in uncommitted MSCs, and its expression is up-regulated in pre-osteoblasts, where it reaches the maximal level in immature osteoblasts, while decrease in mature osteoblasts [105]. SP7, also known as Osterix (Osx), is an osteoblast-specific transcription factor [106]. It plays a role in the latter stages of osteogenesis and maturation, controlling maturation in functional osteoblasts and further differentiation to osteocytes. Deletion of *Osx* in mice leads to neonatal lethality due to a failure in general bone formation, severe rib cage malformation and a lack of expression of osteoblast genes, such as *SPP1* [106]. As a result, during osteogenic lineage specification, RUNX2 promotes mesenchymal progenitor differentiation thus, initiating osteogenesis, and OSX supports the maturation of functional osteoblasts. SOX9 is a transcription factor which plays a key role in chondrogenesis, by controlling type II collagen and aggrecan expression, as well as supporting chondrocyte survival and hypertrophy [107].

RUNX2/SOX9 ratio it has been proposed as *in vitro* screening method for osteogenicity of human MSCs [108]. It has been reported that RUNX2/SOX9 ratios decrease on day 14 and 21 compared to days 2 and 7 in hBMSCs induced to osteogenic differentiation [108]. In this study,

an increase of RUNX2 and SOX9 expression respect to TCPS was identified; not statistical difference between hASCs grown on biomaterials was shown in terms of RUNX2/SOX9 ratio (**Figure 20**).

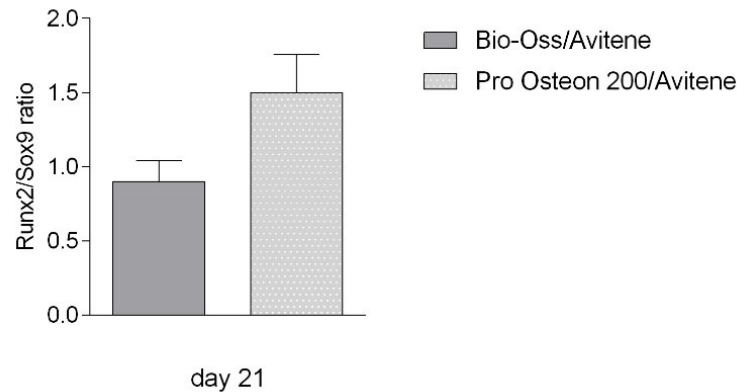


**Figure 20.** RUNX2/SOX9 ratio based on expression fold change to TCPS, day 21. RUNX2/SOX9 ratio it has been proposed as in vitro screening method for osteogenicity of human MSCs.

TWIST1 plays key roles in the control of mesenchymal cell lineage allocation during skeletal development as supported by several in vivo studies [109,110]. Twist1 is expressed in vivo by osteoprogenitor cells but not by mature osteoblasts [110]. Several studies have indicated that TWIST1 also plays a role in skull vault and craniofacial development [110,111]. The lack of one TWIST allele in mice caused misexpression of FGFR2 in the sagittal suture [110]. In humans, haplo-insufficiency of TWIST1 is associated with the autosomal dominant Saethre-Chotzen syndrome [112], characterized by a varied pattern of craniofacial defects including craniosynostosis, indicating that TWIST1 is an important transcription factor controlling osteoblastogenesis. TWIST1 shRNA silencing increased the osteogenic potential of hASCs in vitro and their skeletal regenerative ability when applied in vivo [113].

BMP2, belonging to the BMPs family, is a potent osteoinductive cytokine from the transforming growth factor beta (TGF- $\beta$ ) family, and it is currently the most commonly used protein-based bone graft substitute [114]. BMP2 is induced and up-regulated by both scaffolds analysed herein at day 21. Accumulating studies proved that BMP2 is involved in bone formation, bone remodelling, bone development, and osteoblast differentiation [115]. Among DEGs modulated by the biomaterials, BMPRI1B was identified. BMPRI1B appears primarily expressed in mesenchymal precartilaginous condensations, in differentiated osteoblasts and

chondrocytes [116]. In hBMSCs, the knockdown of BMPR1B by siRNA inhibited the osteogenic differentiation [117].

MSC recruitment is a crucial process in the development, maintenance and repair of tissues throughout the body. In this context, TGF $\beta$ 1 is a potent chemokine, which is essential for MSC recruitment in bone, as it couples the remodelling cycle. Dysregulation of TGF $\beta$  signalling has been linked to a number of skeletal pathologies [118].

Both SPP1 and BGLAP resulted up-regulated in hASCs grown on the scaffolds respect to TCPS, the control group ( $p < 0.05$ ). Interestingly, Bio-Oss/Avitene induce their up-regulation with higher value of FC (**Table 9**). As reported above, OPN is considered to play an important role in bone regrowth [103,119]. BGLAP gene encodes for OCN, a highly abundant bone protein secreted by osteoblasts which regulates bone remodelling and energy metabolism. OCN expression analysis in hASCs grown on Pro Osteon 200/Avitene show a statistically significant increase of the OCN in cells grown on biomaterial, at the three time points (14, 21 and 40 days), compared with the control. In the same way, Pro Osteon 200/Avitene modulated ALP expression at both mRNA and protein level. Further analysis on OPN and ALP protein expression are needed for long-term evaluation of Bio-Oss/Avitene biomaterial.

The results of this work demonstrated that both Bio-Oss/Avitene and Pro Osteon 200/Avitene composite biomaterials induced hASC osteogenic differentiation, stimulating the production of anti-inflammatory cytokines compared to 2D plastic-cultured hASCs (TCPS).

In recent years, the application of 3D cell culture techniques has received incremental interest with evidence showing significant differences between the cellular phenotype and biological response of cells cultured in monolayers respect to 3D culture. The latter facilitates greater cell-cell contacts and interactions of cells with the ECM by allowing cells to adapt to their native morphology, an aspect that might influence intercellular signalling activity [120]. Approaches used to provide cells with a 3D environment include 3D multicellular spheroids [121,122], which show superior secretion profiles compared to similar number of MSCs in monolayer culture, or 3D cell sheet [2,123].

Thus, further studies should be carried out in order to understand the cellular and molecular aspects of hASCs grown on Bio-Oss/Avitene and Pro Osteon 200/Avitene composite biomaterials respect to other scaffolds with similar chemical-physical characteristics and 3D cell culture, which might provide a cellular environment more consistent with that in vivo.

## 5.2. Biomorphic hydroxylapatite scaffold

Previous *in vivo* studies, carried out on skeletally mature adult New Zealand White disease-free rabbits, have highlighted the osteogenic and osteoconductive character of biomorphic HA scaffolds inherited from the original wood template structure and show extensive bone formation and penetration inside the channel-like pores of the scaffold [124]. Indeed, a more recent study has reported the *in vivo* osteoinductive ability shown by biomorphic HA scaffold, which was attested by the formation of mature bone tissue in ectopic sites 12 weeks after subcutaneous implantation in rabbits [74]. *In vivo* data are a clear indication of the relevance of biomimetic physical/chemical, morphological and mechanical features of biomorphic HA scaffold, which stimulates bone tissue regeneration. This scaffold has been obtained through a new procedure of “biomorphic” transformation, which can directly transform wood pieces into large HA scaffolds, preserving the original multiscale structure through a heterogeneous reaction under supercritical conditions, directly in the 3D state, without adopting any sintering process.

However, genes and cellular signalling pathways, which drive biomorphic HA osteoinductivity in human MSCs, are not known. The aim of this investigation is address to analyse molecular/cellular pathways and osteogenic genes induced in hASCs grown on biomorphic B-HA. When taken together, analysis conducted with hASCs suggest that both scaffolds meet the requirements for *in vitro* cytocompatibility, offering surface properties with good microenvironments for stem cell adhesion and proliferation. In the examined hASCs grown on the biomorphic B-HA scaffold, the actin filaments were distributed uniformly and occupied most of the cell cytoplasm at day 14. The hASCs grown on S-HA also showed good cellular metabolic activity and well-organized cytoskeleton confirming its cytocompatibility.

The *in vitro* osteoinductive ability of both the B-HA and S-HA scaffolds was assessed by an analysis of i) calcium deposits and ii) OCN protein expression. The hASCs grown on both B-HA and S-HA scaffolds, at day 14, accumulated calcium in the ECM, thus demonstrating osteoinductive properties in both scaffolds ( $p < 0.05$ ). The B-HA scaffold favoured matrix mineralization better than TCPS, also at day 21 ( $p < 0.05$ ). Furthermore, ELISA data show a statistically significant increase of OCN in B-HA compared to controls, represented by S-HA and TCPS, at day 14, in agreement with the up-modulation of BGLAP gene expression. In contrast, this gene tested down-expressed in hASCs grown on S-HA (**Table 10**). As previously described, OCN, together with OPN, are known to be major non-collagenous proteins (NCPs) that play key roles in both the biological and mechanical functions of bone [125]. Indeed, OCN is produced during bone formation, late in the mineralization process, as it is involved in organizing ECM, coordinating cell–matrix and mineral–matrix interactions, particularly

controlling either directly and/or indirectly bone mass, mineral size and orientation [125]. These improved osteogenic markers, expressed by hASCs grown on the B-HA scaffold, demonstrate a higher osteoinductive ability for B-HA compared to S-HA scaffold. In addition, a PCR array was performed in order to analyse the expression of genes involved in the osteogenic pathway. S-HA biomaterial influences the differentiation of hASCs by up-regulating osteogenic genes. Indeed, S-HA biomaterial, at day 14, induced the up-regulation of 10 genes including BMP2, COL2A1, SPP1 and SP7, which play important roles in the ossification process. In agreement, previous studies have reported that sintered HA induced the expression of osteogenic genes, including SPP1, in hASCs [66], as well as high proliferation and focal adhesion kinase activation were observed in hBMSCs [65]. In this study, the novel biomimetic scaffold modulated the ossification differentiation genes including the chondrogenic transcription factor and genes involved in the osteoclast pathway, at day 14. Among the DEGs, gene expression analysis showed significant early up-regulation of the osteogenic markers ALPL, BGLAP, CHRD, FGFR2, SMAD3, and TGFB3 in hASCs grown on B-HA.

Animal models have indicated that the BMP-antagonist chordin (CHRD) and Noggin promote inductive and trophic activities in rostral organizing centers during early development of the mammalian head [126]. SMAD3 is an intracellular molecule that transmit signals from plasma membrane receptors to the nucleus. SMAD3 operates down-stream of growth factors, such as TGFB [127]. It is worth noting that TGFB3 tested up-regulated in hASCs grown on B-HA, whereas it was down-regulated in cells grown on the S-HA scaffold. TGFB3 loaded on a 3D scaffold enhanced the chondrogenic differentiation of hASCs during 28-days of culture [128]. Interestingly, it has been reported that TGFB3 promotes osteogenic differentiation [129] and it is used for cartilage repair, tissue regeneration and wound healing in vivo [128,130]. TGFB3 promotes the proliferation and early differentiation of MSCs into osteoblasts, chondrocytes, adipocytes and tendon cells [131]. Moreover, it is also involved in the recruitment of endogenous MSCs to initiate bone tissue regeneration [132]. Furthermore, it stimulates endochondral ossification [133] and completes bone remodelling [134].

In this investigation, B-HA modulated EGF, GLI1, MMP8-10, SP7 and TNFSF11 gene expression with higher fold change values compared to S-HA material (**Table 10**). The intracellular stimulation of EGF gene expression is much more active with B-HA scaffolds than S-HA (11.21 vs. 2.01 Log<sub>2</sub> FC). EGF has been reported as playing an enhancer role on osteogenic differentiation since it increases ECM mineralization [135]. GLI1 gene expression is also up-regulated by B-HA, compared to S-HA. GLI1, together with to GLI2 and GLI3, is involved in the signalling-mediated specification of the osteoblast lineage. GLI1 induces an early stage of osteoblast differentiation, at least to some extent, in a Runx2-independent manner

[136]. Chi et al., reported that the Hedgehog signalling pathway can promote osteogenic differentiation in BMSCs via the activation of key molecules Smoothed (Smo) and GLI1 Family Zinc Finger 1 [137]. B-HA modulated matrix metalloproteinases (MMP) expression genes more actively than S-HA in hASCs (**Table 10**). MMPs are members of a family of zinc-dependent proteinases, which are able to cleave many non-ECM and ECM components, such as collagens and proteoglycans. They have a role in normal development and tissue damage in various pathophysiological conditions involving wound healing and tissue remodelling [138]. MMP8 has been reported as being expressed by osteoblastic progenitors, differentiated osteoblasts, osteocytes and chondrocytes [139]. In the present study, ITGA3 was up- and down-regulated in hASCs grown on B-HA and S-HA, respectively (**Table 10**). In this context, it is important to recall that at the cellular level, the integrins are significant mechano-transducers involved in both matrix deposition and organization. SP7, an important transcriptional factor that controls the proliferation and differentiation of MSCs in mature bone cells, tested as over-expressed in hASCs grown on both S-HA and B-HA scaffolds. In this context, it is worth recalling that SP7 controls the expression of proteins involved in terminal osteoblast differentiation [140]. Osteoclast differentiation, mediated by TNFSF11/RANKL gene, was greatly up-regulated (13.78 Log<sub>2</sub> FC) by B-HA compared to S-HA (4.02 Log<sub>2</sub> FC) (**Table 10**). RANKL is a homotrimeric transmembrane protein secreted by osteoblasts as well as immune and tumour cells, which stimulate the differentiation of osteoclasts in the bone and the release immature progenitor cells into the circulation.

**Table 10.** List of gene differentially modulated in hASCs grown on the S-HA and B-HA scaffolds at day 14.

<b>Common differentially modulated genes</b>			
Number	Symbol/Acronym	Fold-Change (Log <sub>2</sub> FC)	
		S-HA	B-HA
1	<i>BGLAP</i>	-2.18	+6.94
2	<i>EGF</i>	+2.01	+11.21
3	<i>GLI1</i>	+2.75	+12.85
4	<i>ITGA3</i>	-1.89	+6.97
5	<i>MMP10</i>	+5.59	+16.46
6	<i>MMP8</i>	+3.10	+14.08
7	<i>SP7</i>	+3.08	+14.29
8	<i>TGFB3</i>	-1.06	+6.95
9	<i>TNFSF11</i>	+4.02	+13.78

*Bone gamma-carboxyglutamate (gla) protein (BGLAP), Epidermal growth factor (EGF), GLI family zinc finger 1 (GLI1), Integrin alpha 3 (ITGA3), Matrix metalloproteinase 10 (MMP10), Matrix metalloproteinase 8 (MMP8), Sp7 transcription factor (SP7), Transforming growth factor, beta 3 (TGFB3), Tumour necrosis factor (ligand) superfamily, member 11 (TNFSF11).*

*S-HA: Sintered HA; B-HA: biomorphic HA*

The high expression of various genes or transcription factors implicated in skeletal development, e.g. SP7, induced by B-HA compared to S-HA can be ascribed to the different physical-chemical features of the two HA-derived scaffolds. Despite having the same composition, B-HA is characterized by nano-size lamellar particles resembling the structure of the mineral phase in natural bone tissue. Due to such a fine nanostructure, in comparison with the micron-size particles making up the sintered S-HA structure, B-HA shows a much higher specific surface area and can also exchange Ca and P ions which are relevant as chemical signals for stem cells favouring osteogenic gene expression, as previously shown with a Mg, Sr-doped biomorphic HA based scaffold [74]. Furthermore, in comparison with S-HA, characterized by wide open, but random and non-aligned porosity, B-HA shows a hierarchically organized structure at increasing size scales, following the complex structure of the rattan wood used as a template and closely mimicking the osteon structure of bone. Therefore, hASCs cultured on the B-HA scaffold could also receive topological information from its 3D architecture, which



closely reproduces the physiological bone environment from the nano- to the macro-scale and is relevant in instructing cells on new bone formation and organization [141].

Overall, these new data indicate that B-HA improves the osteogenic, osteoclastic and chondrogenic gene expression, promoting bone regrowth. However, as the osteogenesis process is the result of a very complex sequence of biochemical reactions, induced by both the chemistry and the structure of the scaffold, a more detailed investigation with different time points is required in order to have a global understanding of the molecular events related to osteogenesis [75]. The HA derived from rattan wood, studied herein, could be considered as a good alternative source of HA for hard tissue replacement. The enhanced osteoinductive ability of B-HA, compared to S-HA scaffold, confirms that the use of biomimetic scaffolds can support metabolic processes yielding tissue regeneration without the aid of additional growth factors, bioactive molecules and cells. These results could have a significant impact on translational processes, because it would be possible to avoid regulatory complexes, linked to the use of osteogenic molecules and human stem cells. This scaffold may significantly reduce the time required for the translation “from the bench to the patient”, whereas decreasing subsequent healthcare costs.

## **6. CONCLUSIONS**

In order to develop new biomaterials, an in-depth understanding of a number of important issues is mandatory. The hybrid scaffolds Pro Osteon/Avitene and Bio-Oss/Avitene, investigated herein, seems to be excellent biomaterials for driving bone regrowth and remodelling. Analysis conducted with hASCs suggest that both Pro Osteon 200/Avitene and Bio-Oss/Avitene scaffolds meet the requirements for in vitro cytocompatibility, offering a good microenvironment for hASCs adhesion, proliferation and osteogenic differentiation. Inflammation is an important factor that should be considered to develop successful biomaterial-based therapeutics. Indeed, inflammation is initially needed for wound healing while prolonged inflammation can result in delayed wound healing or, in some cases, rejection of the scaffold and additional tissue damage. In this context, the two hybrid scaffolds under analysis displayed no significant negative effects on inflammation, stimulating the production of anti-inflammatory cytokines at day 21. However, further analysis will be needed to better define the pathway involved in the immune response. In both cases, the obtained mixture composed of HA and collagen at first result very malleable; in the context of personalized medicine, this is an important aspect because the prosthesis can be shaped in view of the desired result depending on the patient's features. In conclusion, the study carried out on the Pro Osteon 200/Avitene and Bio-Oss/Avitene scaffolds indicates that both the scaffolds are suitable materials for use in maxillofacial surgery.

In order to identify a new source of HA employing as scaffold, in this study HA derived from rattan wood has been investigated. The creation of a 3D ceramic scaffold retaining nanostructure was possible thanks to the use of a new fabrication process transforming a natural wood into a ceramic scaffold, without using high temperature sintering thus preventing the growth of HA crystals and the loss of bioactivity. The over-expression of osteogenic genes in hASCs allow us to better understand the molecular mechanisms that lead to the formation of new bone observed before in the animal model. The unique features of biomorphic HA are relevant in enhancing the capacity to modulate various osteogenic genes, transcription factors and genes related to osteoclast differentiation in hASCs, indicating that the use of scaffolds associating biomimetic composition and nanostructure, enabling higher surface activity, is a promising route towards the development of new bio-devices with superior performance in the regeneration of bone tissue.

## **7. Research activity at AO RESEARCH INSTITUTE**

## **7.1. INTRODUCTION**

The regeneration of bone fractures, resulting from trauma, osteoporosis or tumours, is a major problem in our super-aging society [37]. Glucocorticoids are powerful immunomodulatory and anti-inflammatory drugs, widely prescribed for the treatment of idiopathic disorders with a strong inflammatory component, e.g. chronic obstructive pulmonary disease, rheumatoid arthritis, inflammatory bowel disease, and autoimmune disorders [142]. The long-term use of such drugs, however, comes at the expense of serious side effects, such as osteoporosis [143] or osteonecrosis [144], including osteonecrosis of the jaws (ONJ) [145,146]. Glucocorticoids exert important effects on bone and are crucial for human osteoblast differentiation, along with the formation of the extracellular matrix [147].

As previously reported, the synthetic glucocorticoid dexamethasone (dex) is commonly used for in vitro trilineage differentiation of hBMSCs, thus it presents pro-osteogenic as well as pro-adipogenic and pro-chondrogenic effects. The osteogenic medium used for hBMSCs osteogenic differentiation contains usually 10 nM of dex, together with ascorbic acid and glycerol-2-phosphate [55,148]. Despite clear induction of osteogenesis by glucocorticoids in vitro, they are still considered to be negative regulators of osteogenesis [149]. Previous studies provide evidence for an off-target adipocytic differentiation in standard osteogenic cultures of hBMSCs induced by dex. Dex induces osteogenesis by SOX9 gene expression inhibition and not by up-regulating the expression of RUNX2. Moreover, dex also stimulates adipogenesis by inducing the expression of PPARG, the adipogenic transcription factor [53]. At present, it is not clear which factor mediates SOX9 downregulation: PPARG is one promising candidate (**Figure 1**).

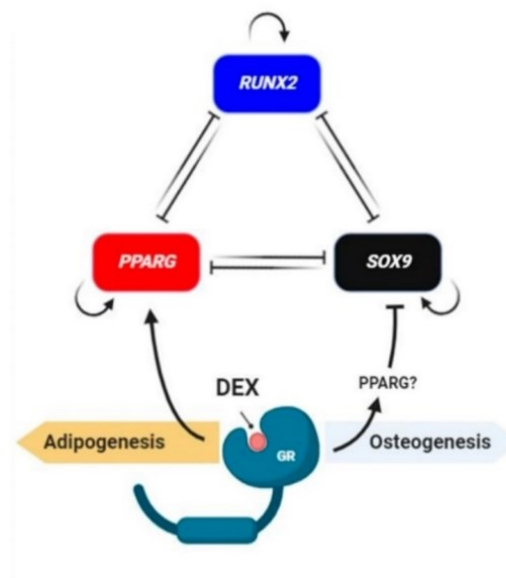


**Figure 1.** Theoretical model of RUNX2-SOX9-PPARG interaction. The basic model, proposed by MacArthur [150], was modified to account for the influence of dex-activated glucocorticoid receptor gene expression [53].

Recent studies have shown that repressive PPAR $\gamma$  modulators promote bone formation [151]. T0070907 was identified as inverse agonist of PPAR $\gamma$ ; this molecule could display a profile opposite of an agonist, increasing the binding affinity of corepressors and decreasing the binding affinity of coactivators, or weaken the affinity for coactivators or coregulators, resulting in transcriptional repression [152].

Thus, the present experiment aimed to clarify whether PPAR $\gamma$  mediates the SOX9 downregulation induced by dex, through modulation of PPAR $\gamma$  activity using T0070907.

## **7.2. MATERIALS AND METHODS**



### 7.2.1. Cell culture

The bone marrow mesenchymal stem cells used for this experiment were obtained from different donors with full ethical approval and after written informed consent [53,153]. After isolation and initial expansion, the cells were cryopreserved in 92% FBS BMSCs and were seeded at a density of  $1.5 \times 10^4$  cells/cm<sup>2</sup> in 24-well plates (TPP, Trasadingen, Switzerland) and treated with different concentrations of dex (Dexamethasone-Cyclodextrin complex, water-soluble formulation, cat. D2915 Sigma-Aldrich) and PPARG antagonist (T0070907, cat. T8703 Sigma-Aldrich). The 20 experimental groups were realized as reported in **Table 1**.

**Table 1.** List of experimental groups realized using different concentrations of dex and T0070907.

Number	Experimental groups	Dex (nM)	T0070907 (nM)
1	Control	-	-
2		-	10
3		-	100
4		-	1000
5	DMSO Control	-	-
6	Osteo	-	-
7		-	10
8		-	100
9		-	1000
10	Osteo DMSO control	-	-
11	Osteo 10	10	-
12		10	10
13		10	100
14		10	1000
15	Osteo 10 DMSO control	10	-
16	Osteo 100	100	-
17		100	10
18		100	100
19		100	1000
20	Osteo 100 DMSO control	100	-

*Control: DMEM basal medium+10% FBS, and penicillin/streptomycin*

*Osteo: DMEM basal medium+10% FBS, and penicillin/streptomycin+ascorbic acid+glycerol-2-phosphate*

### 7.2.2. RNA extraction, reverse transcription and Real Time PCR

Total RNA was isolated using TRIreagent (Molecular Research Center Inc., Cincinnati, OH, USA) after 7 days of treatments. Afterward, reverse transcription (RT) was performed with TaqMan Reverse Transcription reagents (Applied Biosystems, Foster City, CA, USA). In order to understand how T0070907 regulates PPARG, SOX9 and RUNX2 expression, the levels of these transcription factors (TFs) were analysed through Real Time PCR (qPCR; QuantStudio 7

Flex Real-Time PCR system, Applied Biosystems), n=4 donors. Moreover, the expression of PPARG target genes, i.e., ADIPOQ, IL8, IL6 was evaluated (n=3 donors). Relative gene expression was calculated as  $2^{-\Delta Ct}$  using RPLP0 as a reference gene. Primer details are reported in **Table 2**.

**Table 2.** Details of primers used for *PPARG*, *SOX9*, *RUNX2*, *ADIPOQ*, *IL8*, *IL6* and *RPLP0* gene expression analysis through Real Time PCR.

<b><i>RPLP0</i></b> *	Forward primer: 5'-TGGGCAAGAACACCATGATG-3' Reverse primer: 5'-CGGATATGAGGCAGCAGTTTC-3' Probe: 5'-AGGGCACCTGGAAAACAACCCAGC-3'
<b><i>RUNX2</i></b> *	Forward primer: 5'-AGCAAGGTTCAACGATCTGAGAT-3' Reverse primer: 5'-TTTGTGAAGACGGTTATGGTCAA-3' Probe: 5'-TGAAACTCTTGCCTCGTCCACTCCG-3'
<b><i>PPARG</i></b> **	TaqMan Gene Expression Assay Hs00234592_m1
<b><i>SOX9</i></b> **	TaqMan Gene Expression Assay Hs00165814_m1
<b><i>ADIPOQ</i></b> **	TaqMan Gene Expression Assay Hs00605917_m1
<b><i>IL6</i></b> **	TaqMan Gene Expression Assay Hs00174131_m1
<b><i>CXCL8 (IL8)</i></b> **	TaqMan Gene Expression Assay Hs00174103_m1

\* Custom sequences (synthesized from MicroSynth, Balgach, Switzerland). Reporter dye: 6-carboxyfluorescein (FAM); quencher: 6-carboxy-N, N, N', N'-tetramethylrhodamine (TAMRA).

\*\* Commercially available assays (Thermo Fisher) Reporter dye: FAM; quencher: non-fluorescent quencher, minor groove binder (NFQ-MGB).

### 7.2.3. Alizarin Red Staining and Quantification

Cells at day 21 (n=2 donor) were fixed in 4% neutral buffered formalin and stained with a 40 mM, pH 4.2 solution of Alizarin Red S (ARS, Sigma-Aldrich). After extensive washing to remove unbound staining, mosaic pictures were created with an Evos2 microscope (ThermoFisher). Subsequently, ARS was eluted from cultures, using the cetylpyridinium chloride method and quantification was performed by measuring absorbance at 540 nm.

## **7.3. RESULTS**

### 7.3.1. Gene expression level of PPARG, SOX9 and RUNX2 transcription factors

To determine if osteogenic and adipogenic pathways are controlled separately by dex and how the different TFs interact with each other, the gene expression analysis of PPARG, SOX9 and RUNX2 were performed at day 7 (**Figure 2**). As expected, PPARG gene was up-regulated in the presence of dex 10 nM and 100 nM compared to experimental groups without dex. Moreover, PPARG showed no differences in term of gene expression among the experimental groups with different concentration of T0070907. The reason might be the inhibitory activity on PPARG at post-transcriptional level. SOX9 expression resulted down-regulated in cells cultured in osteogenic medium with 10 nM and 100 nM of dex compared to cells cultured in undifferentiated control medium and osteogenic medium without dex, confirming previous observations [53]. In cells cultured in osteogenic medium without dex, a statistically significant decrease of SOX9 expression level in a T0070907 dose-dependent manner was observed (**Figure 2**). In undifferentiated control medium, RUNX2 expression decreased in hBMSCs treated with 1000 nM of T0070907, in comparison to control 0 nM and 100 nM of T0070907 ( $p < 0.05$ ). Finally, a decrease in RUNX2 expression levels has been detected in hBMSCs grown in osteogenic medium without dex in presence of 1000 nM of T0070907, when compared to 10 nM of T0070907 ( $p < 0.05$ ).

The RUNX2/SOX9 ratio ( $2^{-\Delta Ct}$  ratio), that is a strong marker of osteogenesis [108], revealed that hBMSCs osteogenesis is enhanced in the presence of dex, in particular in cells treated with 10 nM dex and 1000 nM of T0070907 (**Figure 2**).

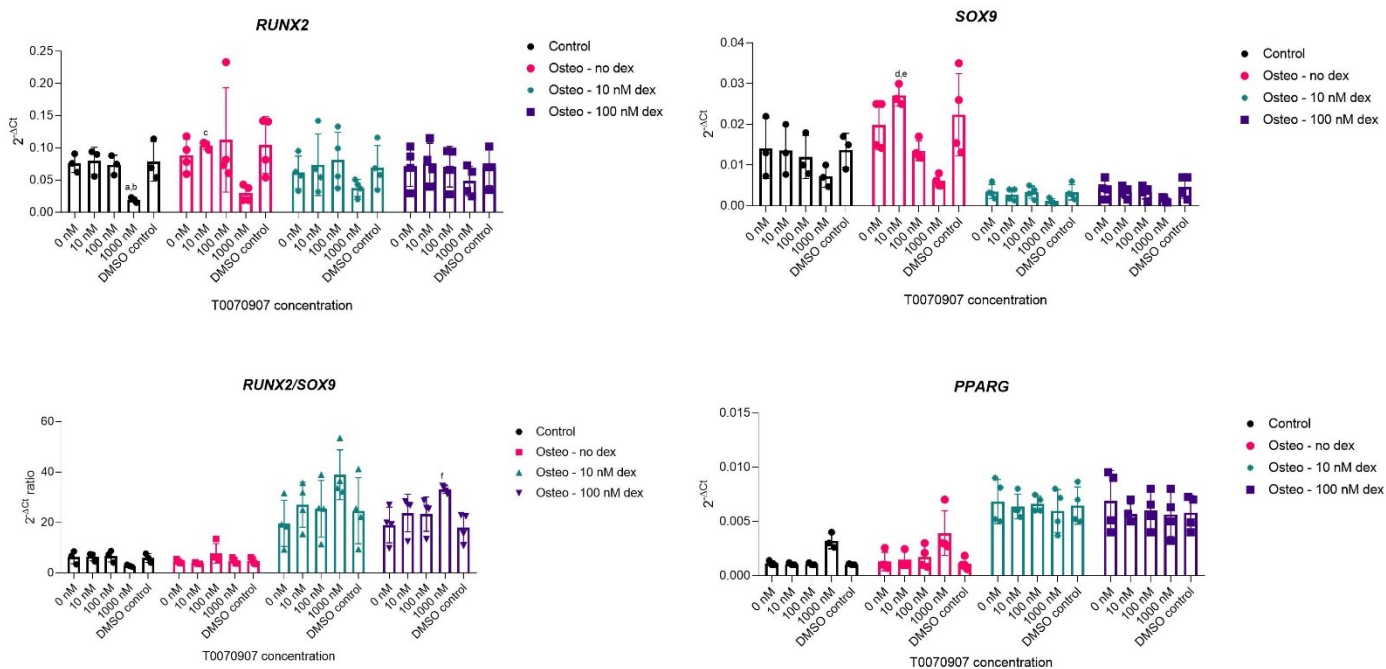


**Figure 2.** Expression of genes encoding for transcription factors with a known influence on osteogenic or adipogenic differentiation. Summary of results from a two-way ANOVA with the Tukey post-hoc test. *RUNX2*. a.  $p < 0.05$ ; Control 0 nM T0070907 vs. Control 1000 nM T0070907. b.  $p < 0.05$ ; Control 10 nM T0070907 vs. Control 1000 nM T0070907. c.  $p < 0.05$ ; Osteo-no dex 10 nM T0070907 vs. Osteo-no dex 1000 nM T0070907. *SOX9*. d.  $p < 0.001$ ; Osteo-no dex 10 nM T0070907 vs. Osteo-no dex 100 nM T0070907. e.  $p < 0.05$ ; Osteo-no dex 10 nM T0070907 vs. Osteo-no dex 1000 nM T0070907. *RUNX2/SOX9* ratio. f.  $p < 0.05$ ; Osteo-100 nM dex 1000 nM T0070907 vs. Osteo-100 nM dex DMSO control.

### 7.3.2. Gene expression level of PPARG target genes

As reported above, T0070907 can increase the binding affinity of corepressors and decrease the binding affinity of coactivators of PPARG. Thus, after 7 days of treatment, the expression of i) ADIPOQ, an adipocyte marker, and ii) CXCL8 (IL8) and IL6, which are NF- $\kappa$ B target genes and represent two of the major mediators of the inflammatory response, have been analysed (**Figure 3**). ADIPOQ expression level resulted up-regulated in the presence of dex 10 nM and 100 nM, compared to experimental groups without dex. ADIPOQ also decreased in cells treated with T0070907 in comparison to the controls. Interestingly, although not significantly, cells treated with 1000 nM T0070907 showed a strong increase of IL8 mRNA expression, both in presence and in absence of dex. Finally, we observed high expression levels of IL6 in cells grown in undifferentiated control medium and osteogenic medium without dex in comparison

to cells cultured in presence of dex 10 nM and 100 nM, while T0070907 did not influence IL6 expression.

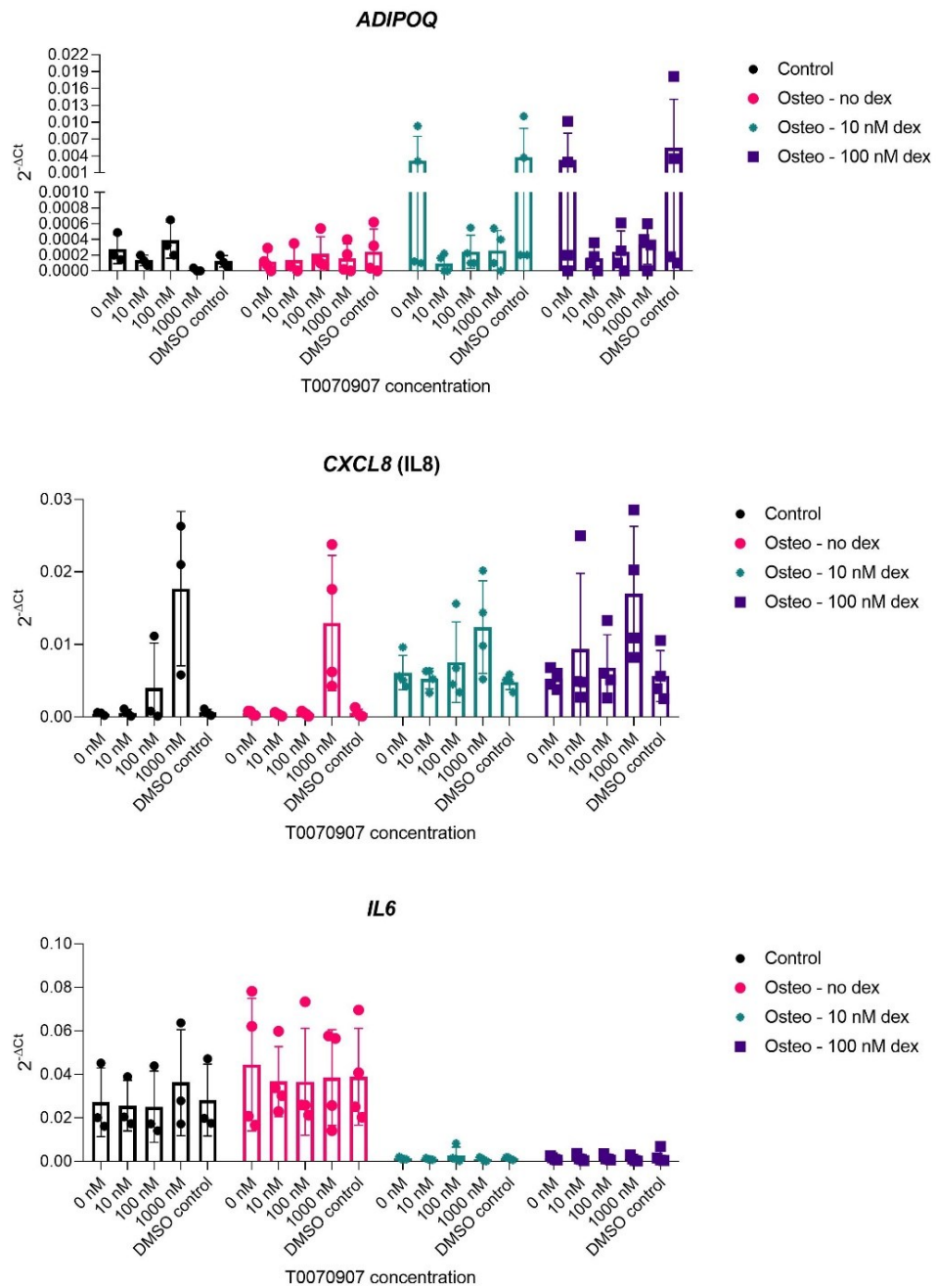


**Figure 3.** Expression of PPAR $\gamma$  target genes. Statistical analysis was performed using two-way ANOVA with the Tukey post-hoc test.

### 7.3.3. Matrix mineralization

In order to evaluate cell mineralization, cells were stained with ARS at day 21. The morphology of the cells was observed after 21 days of treatment (**Figure 4A**). Results showed increased calcium deposition in cells cultured in osteogenic medium with and without dex respect to the control, as expected (**Figure 4B**).

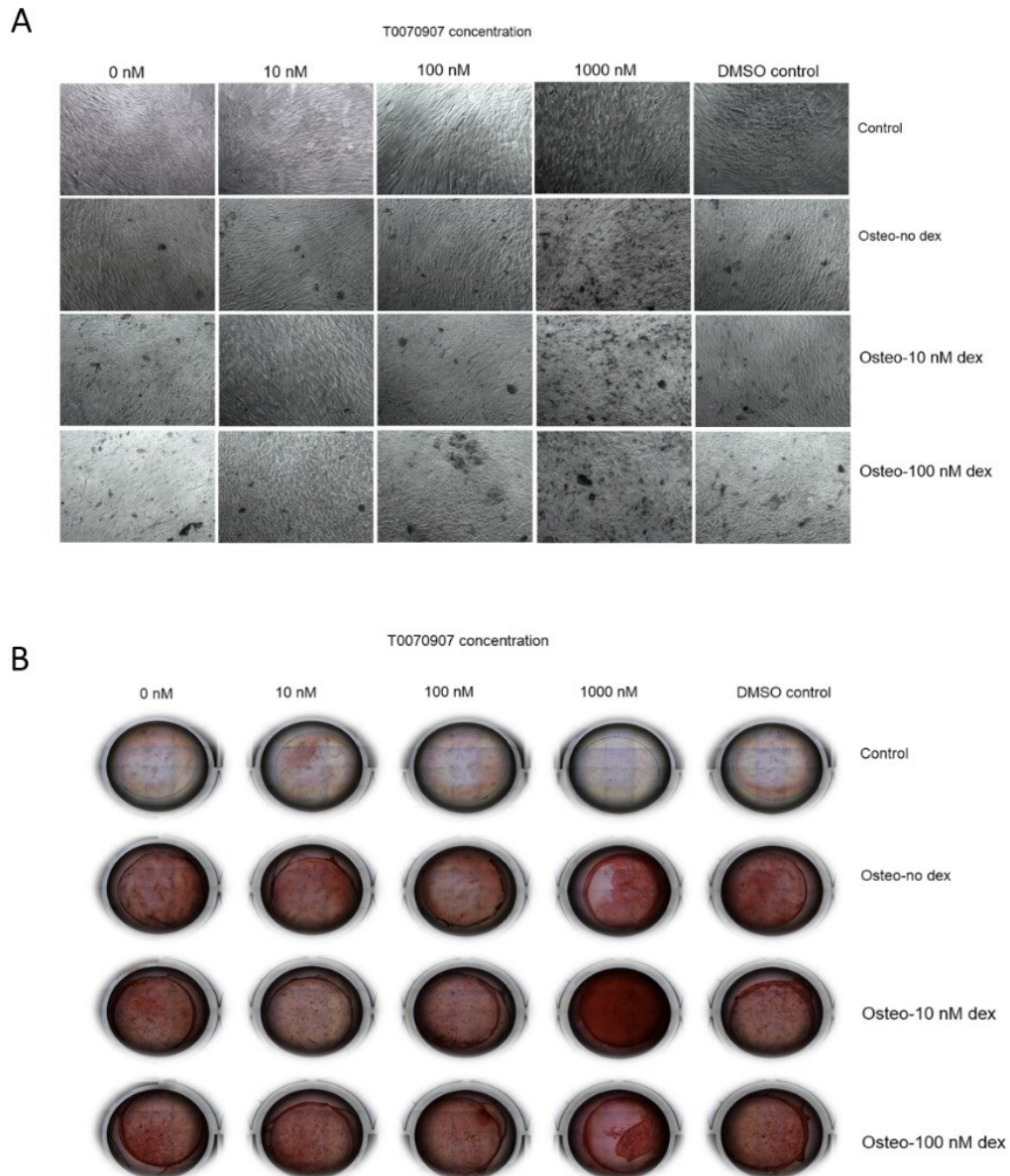


**Figure 4.** (A) The morphology of the cells was observed after 21 days of treatment. (B) Cells were stained with ARS at day 21 in order to evaluate cell mineralization. Images represent mosaics of pictures, transmitted light, and brightfield images. The diameter of Thermanox coverslips, which were fully pictured, was 22 mm.

ARS quantification revealed an increase of calcium deposition in cells treated with dex 10 nM and 1000 nM of T0070907 (**Figure 5A**). The RUNX2/SOX9 ratio at day 7 was shown to positively correlate with ARS at day 21 (**Figure 5B**).

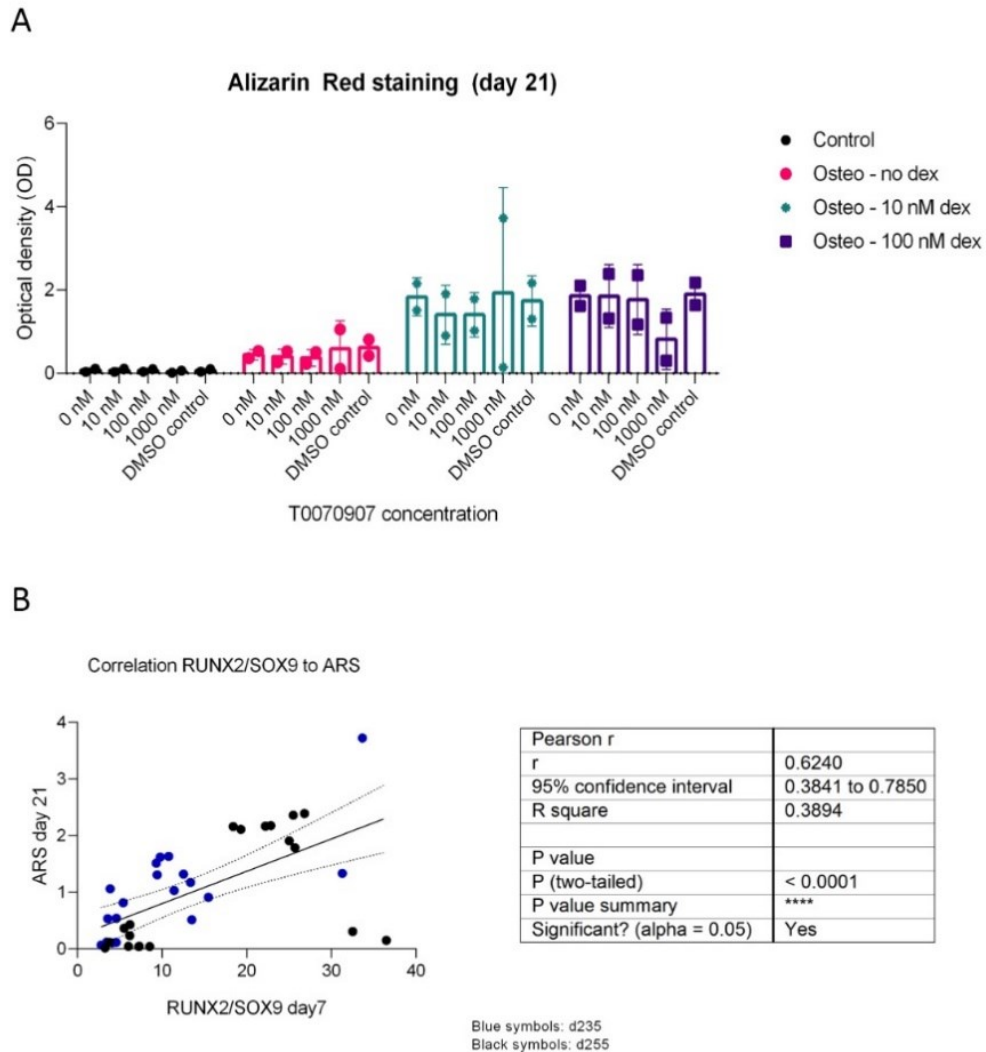


**Figure 5.** ARS staining quantification and RUNX2/SOX9 ratio correlation to ARS. (A) ARS staining quantification was performed via elution of the stain from the cultures and the subsequent spectrophotometric determination of optical density. Statistical analysis was performed using a two-way ANOVA with the Tukey post-hoc test. (B) RUNX2/SOX9 ratio correlation to ARS. Pearson's correlation was calculated to correlate the RUNX2/SOX9 ratio ( $2^{-\Delta Ct}$  ratio) at day 7 with amount of Alizarin Red staining at day 21, expressed as a fold-change in comparison to the undifferentiated control. The  $R^2$  value obtained (0.3894) suggests other factors were involved in process, which influenced the linear correlation. The dashed line represents the line of best fit, of which the equation is reported. The dotted lines represent the 95% confidence interval.



## **7.4. DISCUSSION**

The common protocols for inducing osteogenic differentiation in hMSCs are based on the use of dex. Even though dex has a pro-osteogenic effect, the evidence from the clinical use of glucocorticoids is that it negatively affects bone tissue and vasculature health, with serious consequence for the patient in the long term. Dex promotes hBMSC osteogenic differentiation enhancing RUNX2/SOX9 ratio after 7 days [53]. The RUNX2/SOX9 ratio, rather than RUNX2 alone, is a better predictor of the mineralization potential of hBMSCs due to changes in SOX9 expression [108]. Dex induces PPARG gene expression and inhibits SOX9 expression, and both effects seem to be mediated by a transactivation pathway [53].

Therefore, in order to understand whether PPARG could mediate the SOX9 downregulation induced by dex, an inverse agonist of PPARG (T0070907) has been used in this work [152]. The initial hypothesis was that PPARG activation mediates SOX9 inhibition. Unexpectedly, it has been observed that PPARG inhibition decreased SOX9 expression. Afterwards, in order to elucidate the mechanism by which T0070907 inhibits PPARG and clarify if the treatment was effective, the expression of well-established PPARG target genes, i.e. ADIPOQ, IL8 AND IL6, was analysed. ADIPOQ is a target of PPARG transactivation pathway. The obtained results confirm that T0070907 blocks the transactivation activity of PPARG downregulating ADIPOQ. The IL6 and IL8 expression is inhibited by PPARG activity through the transrepression pathway. The obtained results indicated that T0070907 also blocks the transrepression activity of PPARG showing the upregulation of IL8 expression. Therefore, T0070907 effectively inhibits both transactivation and transrepression activities of PPARG. However, PPARG seems not to mediate SOX9 downregulation induced by dex. Further investigations are needed to understand the reason of SOX9 down-regulation in the presence of dex and T0070907. Further analysis could be carried out using a siRNA to effectively knock down overall PPARG gene expression, also analysing PPARG and SOX9 protein expression.

### *Acknowledgements*

I wish to thank Prof. Fernanda Martini and Prof. Mauro Tognon for their supervision during the PhD programme, and Elisa Mazzoni for the support. My gratitude extends to Prof. Antonio D'Agostino and Prof. Lorenzo Trevisiol (University of Verona, Verona, Italy) for their collaboration in performing maxillofacial surgery and companies to provide the biomaterials. I also thank Prof. Martin Stoddart, Dr. Elena Della Bella and the research team of AO Research Institute, Switzerland, for making it possible to realize part of the results of this work.

## **8. REFERENCES**

1. Abdel Meguid, E.; Ke, Y.; Ji, J.; El-Hashash, A.H.K. Stem Cells Applications in Bone and Tooth Repair and Regeneration: New Insights, Tools, and Hopes. *J. Cell. Physiol.* **2018**, *233*, 1825–1835, doi:10.1002/jcp.25940.
2. Iaquinta, M.R.; Mazzoni, E.; Bononi, I.; Rotondo, J.C.; Mazziotta, C.; Montesi, M.; Sprio, S.; Tampieri, A.; Tognon, M.; Martini, F. Adult Stem Cells for Bone Regeneration and Repair. *Front. Cell Dev. Biol.* **2019**, *7*, 268, doi:10.3389/fcell.2019.00268.
3. Farbod, K.; Nejadnik, M.R.; Jansen, J.A.; Leeuwenburgh, S.C.G. Interactions between Inorganic and Organic Phases in Bone Tissue as a Source of Inspiration for Design of Novel Nanocomposites. *Tissue Eng. Part B Rev.* **2014**, *20*, 173–188, doi:10.1089/ten.TEB.2013.0221.
4. Schönherr, E.; Hausser, H.J. Extracellular Matrix and Cytokines: A Functional Unit. *Dev. Immunol.* **2000**, *7*, 89–101.
5. Fujisawa, R.; Tamura, M. Acidic Bone Matrix Proteins and Their Roles in Calcification. *Front. Biosci. Landmark Ed.* **2012**, *17*, 1891–1903.
6. Palmer, L.C.; Newcomb, C.J.; Kaltz, S.R.; Spoerke, E.D.; Stupp, S.I. Biomimetic Systems for Hydroxyapatite Mineralization Inspired by Bone and Enamel. *Chem. Rev.* **2008**, *108*, 4754–4783, doi:10.1021/cr8004422.
7. Weatherholt, A.M.; Fuchs, R.K.; Warden, S.J. Specialized Connective Tissue: Bone, the Structural Framework of the Upper Extremity. *J. Hand Ther. Off. J. Am. Soc. Hand Ther.* **2012**, *25*, 123–131; quiz 132, doi:10.1016/j.jht.2011.08.003.
8. Eliaz, N.; Metoki, N. Calcium Phosphate Bioceramics: A Review of Their History, Structure, Properties, Coating Technologies and Biomedical Applications. *Mater. Basel Switz.* **2017**, *10*, doi:10.3390/ma10040334.
9. Kartsogiannis, V.; Ng, K.W. Cell Lines and Primary Cell Cultures in the Study of Bone Cell Biology. *Mol. Cell. Endocrinol.* **2004**, *228*, 79–102, doi:10.1016/j.mce.2003.06.002.
10. Charles, J.F.; Aliprantis, A.O. Osteoclasts: More than ‘Bone Eaters.’ *Trends Mol. Med.* **2014**, *20*, 449–459, doi:10.1016/j.molmed.2014.06.001.
11. Sims, N.A.; Civitelli, R. Cell-Cell Signaling: Broadening Our View of the Basic Multicellular Unit. *Calcif. Tissue Int.* **2014**, *94*, 2–3, doi:10.1007/s00223-013-9766-y.
12. Su, P.; Tian, Y.; Yang, C.; Ma, X.; Wang, X.; Pei, J.; Qian, A. Mesenchymal Stem Cell Migration during Bone Formation and Bone Diseases Therapy. *Int. J. Mol. Sci.* **2018**, *19*, doi:10.3390/ijms19082343.
13. Miller, S.C.; de Saint-Georges, L.; Bowman, B.M.; Jee, W.S. Bone Lining Cells: Structure and Function. *Scanning Microsc.* **1989**, *3*, 953–960; discussion 960-961.
14. Lerner, U.H.; Kindstedt, E.; Lundberg, P. The Critical Interplay between Bone Resorbing and Bone Forming Cells. *J. Clin. Periodontol.* **2019**, doi:10.1111/jcpe.13051.

15. Sims, N.A.; Martin, T.J. Coupling Signals between the Osteoclast and Osteoblast: How Are Messages Transmitted between These Temporary Visitors to the Bone Surface? *Front. Endocrinol.* **2015**, *6*, doi:10.3389/fendo.2015.00041.
16. Jiao, H.; Xiao, E.; Graves, D.T. Diabetes and Its Effect on Bone and Fracture Healing. *Curr. Osteoporos. Rep.* **2015**, *13*, 327–335, doi:10.1007/s11914-015-0286-8.
17. Levaot, N.; Ottolenghi, A.; Mann, M.; Guterman-Ram, G.; Kam, Z.; Geiger, B. Osteoclast Fusion Is Initiated by a Small Subset of RANKL-Stimulated Monocyte Progenitors, Which Can Fuse to RANKL-Unstimulated Progenitors. *Bone* **2015**, *79*, 21–28, doi:10.1016/j.bone.2015.05.021.
18. Jimi, E.; Akiyama, S.; Tsurukai, T.; Okahashi, N.; Kobayashi, K.; Udagawa, N.; Nishihara, T.; Takahashi, N.; Suda, T. Osteoclast Differentiation Factor Acts as a Multifunctional Regulator in Murine Osteoclast Differentiation and Function. *J. Immunol. Baltim. Md 1950* **1999**, *163*, 434–442.
19. Xiong, J.; Piemontese, M.; Onal, M.; Campbell, J.; Goellner, J.J.; Dusevich, V.; Bonewald, L.; Manolagas, S.C.; O'Brien, C.A. Osteocytes, Not Osteoblasts or Lining Cells, Are the Main Source of the RANKL Required for Osteoclast Formation in Remodeling Bone. *PloS One* **2015**, *10*, e0138189, doi:10.1371/journal.pone.0138189.
20. Crane, J.L.; Cao, X. Bone Marrow Mesenchymal Stem Cells and TGF- $\beta$  Signaling in Bone Remodeling. *J. Clin. Invest.* **2014**, *124*, 466–472, doi:10.1172/JCI70050.
21. Boyce, B.F. Advances in Osteoclast Biology Reveal Potential New Drug Targets and New Roles for Osteoclasts. *J. Bone Miner. Res. Off. J. Am. Soc. Bone Miner. Res.* **2013**, *28*, 711–722, doi:10.1002/jbmr.1885.
22. Raggatt, L.J.; Partridge, N.C. Cellular and Molecular Mechanisms of Bone Remodeling. *J. Biol. Chem.* **2010**, *285*, 25103–25108, doi:10.1074/jbc.R109.041087.
23. van Bezooijen, R.L.; Papapoulos, S.E.; Löwik, C.W.G.M. Bone Morphogenetic Proteins and Their Antagonists: The Sclerostin Paradigm. *J. Endocrinol. Invest.* **2005**, *28*, 15–17.
24. McClung, M.R. Romosozumab for the Treatment of Osteoporosis. *Osteoporos. Sarcopenia* **2018**, *4*, 11–15, doi:10.1016/j.afos.2018.03.002.
25. Sobacchi, C.; Schulz, A.; Coxon, F.P.; Villa, A.; Helfrich, M.H. Osteopetrosis: Genetics, Treatment and New Insights into Osteoclast Function. *Nat. Rev. Endocrinol.* **2013**, *9*, 522–536, doi:10.1038/nrendo.2013.137.
26. Figliomeni, A.; Signorini, V.; Mazzantini, M. One Year in Review 2018: Progress in Osteoporosis Treatment. *Clin. Exp. Rheumatol.* **2018**, *36*, 948–958.
27. Habibovic, P. \* Strategic Directions in Osteoinduction and Biomimetics. *Tissue Eng. Part A* **2017**, *23*, 1295–1296, doi:10.1089/ten.TEA.2017.0430.
28. Arvidson, K.; Abdallah, B.M.; Applegate, L.A.; Baldini, N.; Cenni, E.; Gomez-Barrena, E.; Granchi, D.; Kassem, M.; Konttinen, Y.T.; Mustafa, K.; et al. Bone Regeneration and Stem Cells. *J. Cell. Mol. Med.* **2011**, *15*, 718–746, doi:10.1111/j.1582-4934.2010.01224.x.

29. Marsell, R.; Einhorn, T.A. The Biology of Fracture Healing. *Injury* **2011**, *42*, 551–555, doi:10.1016/j.injury.2011.03.031.
30. Yang, X.; Ricciardi, B.F.; Hernandez-Soria, A.; Shi, Y.; Camacho, N.P.; Bostrom, M.P.G. Callus Mineralization and Maturation Are Delayed during Fracture Healing in Interleukin-6 Knockout Mice. *Bone* **2007**, *41*, 928–936, doi:10.1016/j.bone.2007.07.022.
31. Maruyama, M.; Rhee, C.; Utsunomiya, T.; Zhang, N.; Ueno, M.; Yao, Z.; Goodman, S.B. Modulation of the Inflammatory Response and Bone Healing. *Front. Endocrinol.* **2020**, *11*.
32. Einhorn, T.A.; Gerstenfeld, L.C. Fracture Healing: Mechanisms and Interventions. *Nat. Rev. Rheumatol.* **2015**, *11*, 45–54, doi:10.1038/nrrheum.2014.164.
33. Ferracini, R.; Martínez Herreros, I.; Russo, A.; Casalini, T.; Rossi, F.; Perale, G. Scaffolds as Structural Tools for Bone-Targeted Drug Delivery. *Pharmaceutics* **2018**, *10*, doi:10.3390/pharmaceutics10030122.
34. Gao, C.; Deng, Y.; Feng, P.; Mao, Z.; Li, P.; Yang, B.; Deng, J.; Cao, Y.; Shuai, C.; Peng, S. Current Progress in Bioactive Ceramic Scaffolds for Bone Repair and Regeneration. *Int. J. Mol. Sci.* **2014**, *15*, 4714–4732, doi:10.3390/ijms15034714.
35. D’Agostino, A.; Trevisiol, L.; Favero, V.; Gunson, M.J.; Pedica, F.; Nocini, P.F.; Arnett, G.W. Hydroxyapatite/Collagen Composite Is a Reliable Material for Malar Augmentation. *J. Oral Maxillofac. Surg. Off. J. Am. Assoc. Oral Maxillofac. Surg.* **2016**, *74*, 1238.e1-1238.e15, doi:10.1016/j.joms.2016.01.052.
36. Ho-Shui-Ling, A.; Bolander, J.; Rustom, L.E.; Johnson, A.W.; Luyten, F.P.; Picart, C. Bone Regeneration Strategies: Engineered Scaffolds, Bioactive Molecules and Stem Cells Current Stage and Future Perspectives. *Biomaterials* **2018**, *180*, 143–162, doi:10.1016/j.biomaterials.2018.07.017.
37. Iaquinta, M.; Mazzoni, E.; Manfrini, M.; D’Agostino, A.; Trevisiol, L.; Nocini, R.; Trombelli, L.; Barbanti-Brodano, G.; Martini, F.; Tognon, M. Innovative Biomaterials for Bone Regrowth. *Int. J. Mol. Sci.* **2019**, *20*, 618, doi:10.3390/ijms20030618.
38. Jin, Y.-Z.; Lee, J.H. Mesenchymal Stem Cell Therapy for Bone Regeneration. *Clin. Orthop. Surg.* **2018**, *10*, 271–278, doi:10.4055/cios.2018.10.3.271.
39. Mushahary, D.; Spittler, A.; Kasper, C.; Weber, V.; Charwat, V. Isolation, Cultivation, and Characterization of Human Mesenchymal Stem Cells. *Cytom. Part J. Int. Soc. Anal. Cytol.* **2018**, *93*, 19–31, doi:10.1002/cyto.a.23242.
40. Perez, J.R.; Kouroupis, D.; Li, D.J.; Best, T.M.; Kaplan, L.; Correa, D. Tissue Engineering and Cell-Based Therapies for Fractures and Bone Defects. *Front. Bioeng. Biotechnol.* **2018**, *6*, 105, doi:10.3389/fbioe.2018.00105.
41. Dominici, M.; Le Blanc, K.; Mueller, I.; Slaper-Cortenbach, I.; Marini, F.; Krause, D.; Deans, R.; Keating, A.; Prockop, D.; Horwitz, E. Minimal Criteria for Defining Multipotent Mesenchymal Stromal Cells. The International Society for Cellular Therapy Position Statement. *Cytotherapy* **2006**, *8*, 315–317, doi:10.1080/14653240600855905.
42. Drela, K.; Stanaszek, L.; Nowakowski, A.; Kuczynska, Z.; Lukomska, B. Experimental Strategies of Mesenchymal Stem Cell Propagation: Adverse Events and Potential Risk

- of Functional Changes. *Stem Cells Int.* **2019**, *2019*, 7012692, doi:10.1155/2019/7012692.
43. Mazziotta, C.; Lanzillotti, C.; Iaquina, M.R.; Taraballi, F.; Torreggiani, E.; Rotondo, J.C.; Otòn-Gonzalez, L.; Mazzoni, E.; Frontini, F.; Bononi, I.; et al. MicroRNAs Modulate Signaling Pathways in Osteogenic Differentiation of Mesenchymal Stem Cells. *Int. J. Mol. Sci.* **2021**, *22*, 2362, doi:10.3390/ijms22052362.
  44. Fitzsimmons, R.E.B.; Mazurek, M.S.; Soos, A.; Simmons, C.A. Mesenchymal Stromal/Stem Cells in Regenerative Medicine and Tissue Engineering. *Stem Cells Int.* **2018**, *2018*, 8031718, doi:10.1155/2018/8031718.
  45. Ansboro, S.; Roelofs, A.J.; De Bari, C. Mesenchymal Stem Cells for the Management of Rheumatoid Arthritis: Immune Modulation, Repair or Both? *Curr. Opin. Rheumatol.* **2017**, *29*, 201–207, doi:10.1097/BOR.0000000000000370.
  46. Gnecci, M.; Zhang, Z.; Ni, A.; Dzau, V.J. Paracrine Mechanisms in Adult Stem Cell Signaling and Therapy. *Circ. Res.* **2008**, *103*, 1204–1219, doi:10.1161/CIRCRESAHA.108.176826.
  47. Zagoura, D.S.; Roubelakis, M.G.; Bitsika, V.; Trohatou, O.; Pappa, K.I.; Kapelouzou, A.; Antsaklis, A.; Anagnou, N.P. Therapeutic Potential of a Distinct Population of Human Amniotic Fluid Mesenchymal Stem Cells and Their Secreted Molecules in Mice with Acute Hepatic Failure. *Gut* **2012**, *61*, 894–906, doi:10.1136/gutjnl-2011-300908.
  48. Bermudez, M.A.; Sendon-Lago, J.; Seoane, S.; Eiro, N.; Gonzalez, F.; Saa, J.; Vizoso, F.; Perez-Fernandez, R. Anti-Inflammatory Effect of Conditioned Medium from Human Uterine Cervical Stem Cells in Uveitis. *Exp. Eye Res.* **2016**, *149*, 84–92, doi:10.1016/j.exer.2016.06.022.
  49. Cantinieaux, D.; Quertainmont, R.; Blacher, S.; Rossi, L.; Wanet, T.; Noël, A.; Brook, G.; Schoenen, J.; Franzen, R. Conditioned Medium from Bone Marrow-Derived Mesenchymal Stem Cells Improves Recovery after Spinal Cord Injury in Rats: An Original Strategy to Avoid Cell Transplantation. *PloS One* **2013**, *8*, e69515, doi:10.1371/journal.pone.0069515.
  50. Lee, M.J.; Kim, J.; Lee, K.I.; Shin, J.M.; Chae, J.I.; Chung, H.M. Enhancement of Wound Healing by Secretory Factors of Endothelial Precursor Cells Derived from Human Embryonic Stem Cells. *Cytotherapy* **2011**, *13*, 165–178, doi:10.3109/14653249.2010.512632.
  51. Caplan, A.I. Adult Mesenchymal Stem Cells for Tissue Engineering versus Regenerative Medicine. *J. Cell. Physiol.* **2007**, *213*, 341–347, doi:10.1002/jcp.21200.
  52. Yi, T.; Song, S.U. Immunomodulatory Properties of Mesenchymal Stem Cells and Their Therapeutic Applications. *Arch. Pharm. Res.* **2012**, *35*, 213–221, doi:10.1007/s12272-012-0202-z.
  53. Della Bella, E.; Buetti-Dinh, A.; Licandro, G.; Ahmad, P.; Basoli, V.; Alini, M.; Stoddart, M.J. Dexamethasone Induces Changes in Osteogenic Differentiation of Human Mesenchymal Stromal Cells via SOX9 and PPARG, but Not RUNX2. *Int. J. Mol. Sci.* **2021**, *22*, 4785, doi:10.3390/ijms22094785.



54. Manfrini, M.; Di Bona, C.; Canella, A.; Lucarelli, E.; Pellati, A.; D'Agostino, A.; Barbanti-Bròdano, G.; Tognon, M. Mesenchymal Stem Cells from Patients to Assay Bone Graft Substitutes. *J. Cell. Physiol.* **2013**, *228*, 1229–1237, doi:10.1002/jcp.24276.
55. Iaquinta, M.R.; Lanzillotti, C.; Mazziotta, C.; Bononi, I.; Frontini, F.; Mazzoni, E.; Oton-Gonzalez, L.; Rotondo, J.C.; Torreggiani, E.; Tognon, M.; et al. The Role of MicroRNAs in the Osteogenic and Chondrogenic Differentiation of Mesenchymal Stem Cells and Bone Pathologies. *Theranostics* **2021**, *11*, 6573–6591, doi:10.7150/thno.55664.
56. Chen, F.-M.; Liu, X. Advancing Biomaterials of Human Origin for Tissue Engineering. *Prog. Polym. Sci.* **2016**, *53*, 86–168, doi:10.1016/j.progpolymsci.2015.02.004.
57. Chen, Z.; Klein, T.; Murray, R.Z.; Crawford, R.; Chang, J.; Wu, C.; Xiao, Y. Osteoimmunomodulation for the Development of Advanced Bone Biomaterials. *Mater. Today* **2016**, *19*, 304–321, doi:10.1016/j.mattod.2015.11.004.
58. Duta, L.; Dorcioman, G.; Grumezescu, V. A Review on Biphasic Calcium Phosphate Materials Derived from Fish Discards. *Nanomater. Basel Switz.* **2021**, *11*, 2856, doi:10.3390/nano11112856.
59. He, Y.; Tian, M.; Li, X.; Hou, J.; Chen, S.; Yang, G.; Liu, X.; Zhou, S. A Hierarchical-Structured Mineralized Nanofiber Scaffold with Osteoimmunomodulatory and Osteoinductive Functions for Enhanced Alveolar Bone Regeneration. *Adv. Healthc. Mater.* **2022**, *11*, e2102236, doi:10.1002/adhm.202102236.
60. Mahon, O.R.; Browe, D.C.; Gonzalez-Fernandez, T.; Pitacco, P.; Whelan, I.T.; Von Euw, S.; Hobbs, C.; Nicolosi, V.; Cunningham, K.T.; Mills, K.H.G.; et al. Nano-Particle Mediated M2 Macrophage Polarization Enhances Bone Formation and MSC Osteogenesis in an IL-10 Dependent Manner. *Biomaterials* **2020**, *239*, 119833, doi:10.1016/j.biomaterials.2020.119833.
61. Ishikawa, K.; Miyamoto, Y.; Tsuchiya, A.; Hayashi, K.; Tsuru, K.; Ohe, G. Physical and Histological Comparison of Hydroxyapatite, Carbonate Apatite, and  $\beta$ -Tricalcium Phosphate Bone Substitutes. *Mater. Basel Switz.* **2018**, *11*, E1993, doi:10.3390/ma11101993.
62. Tarafder, S.; Davies, N.M.; Bandyopadhyay, A.; Bose, S. 3D Printed Tricalcium Phosphate Scaffolds: Effect of SrO and MgO Doping on in Vivo Osteogenesis in a Rat Distal Femoral Defect Model. *Biomater. Sci.* **2013**, *1*, 1250–1259, doi:10.1039/C3BM60132C.
63. Sun, H.; Yang, H.-L. Calcium Phosphate Scaffolds Combined with Bone Morphogenetic Proteins or Mesenchymal Stem Cells in Bone Tissue Engineering. *Chin. Med. J. (Engl.)* **2015**, *128*, 1121–1127, doi:10.4103/0366-6999.155121.
64. Montesi, M.; Panseri, S.; Dapporto, M.; Tampieri, A.; Sprio, S. Sr-Substituted Bone Cements Direct Mesenchymal Stem Cells, Osteoblasts and Osteoclasts Fate. *PloS One* **2017**, *12*, e0172100, doi:10.1371/journal.pone.0172100.
65. Barbanti Brodano, G.; Mazzoni, E.; Tognon, M.; Griffoni, C.; Manfrini, M. Human Mesenchymal Stem Cells and Biomaterials Interaction: A Promising Synergy to Improve Spine Fusion. *Eur. Spine J. Off. Publ. Eur. Spine Soc. Eur. Spinal Deform. Soc. Eur. Sect. Cerv. Spine Res. Soc.* **2012**, *21 Suppl 1*, S3-9, doi:10.1007/s00586-012-2233-z.

66. Sprio, S.; Dapporto, M.; Preti, L.; Mazzoni, E.; Iaquina, M.R.; Martini, F.; Tognon, M.; Pugno, N.M.; Restivo, E.; Visai, L.; et al. Enhancement of the Biological and Mechanical Performances of Sintered Hydroxyapatite by Multiple Ions Doping. *Front. Mater.* **2020**, *7*, 224, doi:10.3389/fmats.2020.00224.
67. LeGeros, R.Z. Properties of Osteoconductive Biomaterials: Calcium Phosphates. *Clin. Orthop. Relat. Res.* **2002**, *395*, 81–98.
68. Odusote, J.K.; Danyuo, Y.; Baruwa, A.D.; Azeez, A.A. Synthesis and Characterization of Hydroxyapatite from Bovine Bone for Production of Dental Implants. *J. Appl. Biomater. Funct. Mater.* **2019**, *17*, 228080001983682, doi:10.1177/2280800019836829.
69. Xu, Y.; Ye, J.; Zhou, D.; Su, L. Research Progress on Applications of Calcium Derived from Marine Organisms. *Sci. Rep.* **2020**, *10*, 18425, doi:10.1038/s41598-020-75575-8.
70. Yahia, L.H.; Bayade, G.; Cirotteau, Y. Natural Coral as a Biomaterial Revisited. *Am. J. Biomed. Sci. Res.* **2021**, *13*, 667.
71. Gong, J.; Yang, L.; He, Q.; Jiao, T. In Vitro Evaluation of the Biological Compatibility and Antibacterial Activity of a Bone Substitute Material Consisting of Silver-Doped Hydroxyapatite and Bio-Oss®. *J. Biomed. Mater. Res. B Appl. Biomater.* **2018**, *106*, 410–420, doi:10.1002/jbm.b.33843.
72. de Siqueira, L.; de Paula, C.G.; Gouveia, R.F.; Motisuke, M.; de Sousa Trichês, E. Evaluation of the Sintering Temperature on the Mechanical Behavior of  $\beta$ -Tricalcium Phosphate/Calcium Silicate Scaffolds Obtained by Gelcasting Method. *J. Mech. Behav. Biomed. Mater.* **2019**, *90*, 635–643, doi:10.1016/j.jmbbm.2018.11.014.
73. Iaquina, M.R.; Torreggiani, E.; Mazziotta, C.; Ruffini, A.; Sprio, S.; Tampieri, A.; Tognon, M.; Martini, F.; Mazzoni, E. In Vitro Osteoinductivity Assay of Hydroxylapatite Scaffolds, Obtained with Biomorphic Transformation Processes, Assessed Using Human Adipose Stem Cell Cultures. *Int. J. Mol. Sci.* **2021**, *22*, 7092, doi:10.3390/ijms22137092.
74. Tampieri, A.; Ruffini, A.; Ballardini, A.; Montesi, M.; Panseri, S.; Salamanna, F.; Fini, M.; Sprio, S. Heterogeneous Chemistry in the 3-D State: An Original Approach to Generate Bioactive, Mechanically-Competent Bone Scaffolds. *Biomater. Sci.* **2018**, *7*, 307–321, doi:10.1039/c8bm01145a.
75. Bigoni, D.; Cavuoto, R.; Misseroni, D.; Paggi, M.; Ruffini, A.; Sprio, S.; Tampieri, A. Ceramics with the Signature of Wood: A Mechanical Insight. *Mater. Today Bio* **2020**, *5*, 100032, doi:10.1016/j.mtbio.2019.100032.
76. Dorozhkin, S.V. Biocomposites and Hybrid Biomaterials Based on Calcium Orthophosphates. *Biomater* **2011**, *1*, 3–56, doi:10.4161/biom.1.1.16782.
77. Gunatillake, P.A.; Adhikari, R. Biodegradable Synthetic Polymers for Tissue Engineering. *Eur. Cell. Mater.* **2003**, *5*, 1–16; discussion 16, doi:10.22203/ecm.v005a01.
78. Remya, K.R.; Joseph, J.; Mani, S.; John, A.; Varma, H.K.; Ramesh, P. Nanohydroxyapatite Incorporated Electrospun Polycaprolactone/Polycaprolactone-Polyethyleneglycol-Polycaprolactone Blend Scaffold for Bone Tissue Engineering Applications. *J. Biomed. Nanotechnol.* **2013**, *9*, 1483–1494, doi:10.1166/jbn.2013.1640.

79. Gentile, P.; Chiono, V.; Carmagnola, I.; Hatton, P.V. An Overview of Poly(Lactic-Co-Glycolic) Acid (PLGA)-Based Biomaterials for Bone Tissue Engineering. *Int. J. Mol. Sci.* **2014**, *15*, 3640–3659, doi:10.3390/ijms15033640.
80. Thirivikraman, G.; Athirasala, A.; Twohig, C.; Boda, S.K.; Bertassoni, L.E. Biomaterials for Craniofacial Bone Regeneration. *Dent. Clin. North Am.* **2017**, *61*, 835–856, doi:10.1016/j.cden.2017.06.003.
81. Wang, T.; Yang, X.; Qi, X.; Jiang, C. Osteoinduction and Proliferation of Bone-Marrow Stromal Cells in Three-Dimensional Poly ( $\epsilon$ -Caprolactone)/ Hydroxyapatite/Collagen Scaffolds. *J. Transl. Med.* **2015**, *13*, 152, doi:10.1186/s12967-015-0499-8.
82. Fu, S.; Ni, P.; Wang, B.; Chu, B.; Zheng, L.; Luo, F.; Luo, J.; Qian, Z. Injectable and Thermo-Sensitive PEG-PCL-PEG Copolymer/Collagen/n-HA Hydrogel Composite for Guided Bone Regeneration. *Biomaterials* **2012**, *33*, 4801–4809, doi:10.1016/j.biomaterials.2012.03.040.
83. Niemeyer, P.; Krause, U.; Fellenberg, J.; Kasten, P.; Seckinger, A.; Ho, A.D.; Simank, H.-G. Evaluation of Mineralized Collagen and Alpha-Tricalcium Phosphate as Scaffolds for Tissue Engineering of Bone Using Human Mesenchymal Stem Cells. *Cells Tissues Organs* **2004**, *177*, 68–78, doi:10.1159/000079182.
84. Wang, J.-L.; Chen, Q.; Du, B.-B.; Cao, L.; Lin, H.; Fan, Z.-Y.; Dong, J. Enhanced Bone Regeneration Composite Scaffolds of PLLA/ $\beta$ -TCP Matrix Grafted with Gelatin and HAp. *Mater. Sci. Eng. C Mater. Biol. Appl.* **2018**, *87*, 60–69, doi:10.1016/j.msec.2018.02.011.
85. Arafat, M.T.; Lam, C.X.F.; Ekaputra, A.K.; Wong, S.Y.; Li, X.; Gibson, I. Biomimetic Composite Coating on Rapid Prototyped Scaffolds for Bone Tissue Engineering. *Acta Biomater.* **2011**, *7*, 809–820, doi:10.1016/j.actbio.2010.09.010.
86. Mazzoni, E.; Mazziotta, C.; Iaquinta, M.R.; Lanzillotti, C.; Fortini, F.; D'Agostino, A.; Trevisiol, L.; Nocini, R.; Barbanti-Brodano, G.; Mescola, A.; et al. Enhanced Osteogenic Differentiation of Human Bone Marrow-Derived Mesenchymal Stem Cells by a Hybrid Hydroxylapatite/Collagen Scaffold. *Front. Cell Dev. Biol.* **2020**, *8*, 610570, doi:10.3389/fcell.2020.610570.
87. Calabrese, G.; Giuffrida, R.; Forte, S.; Salvatorelli, L.; Fabbi, C.; Figallo, E.; Gulisano, M.; Parenti, R.; Magro, G.; Colarossi, C.; et al. Bone Augmentation after Ectopic Implantation of a Cell-Free Collagen-Hydroxyapatite Scaffold in the Mouse. *Sci. Rep.* **2016**, *6*, 36399, doi:10.1038/srep36399.
88. Calabrese, G.; Giuffrida, R.; Forte, S.; Fabbi, C.; Figallo, E.; Salvatorelli, L.; Memeo, L.; Parenti, R.; Gulisano, M.; Gulino, R. Human Adipose-Derived Mesenchymal Stem Cells Seeded into a Collagen-Hydroxyapatite Scaffold Promote Bone Augmentation after Implantation in the Mouse. *Sci. Rep.* **2017**, *7*, 7110, doi:10.1038/s41598-017-07672-0.
89. Mazzoni, E.; D'Agostino, A.; Iaquinta, M.R.; Bononi, I.; Trevisiol, L.; Rotondo, J.C.; Patergnani, S.; Giorgi, C.; Gunson, M.J.; Arnett, G.W.; et al. Hydroxylapatite-Collagen Hybrid Scaffold Induces Human Adipose-Derived Mesenchymal Stem Cells to Osteogenic Differentiation in Vitro and Bone Regrowth in Patients. *Stem Cells Transl. Med.* **2020**, *9*, 377–388, doi:10.1002/sctm.19-0170.

90. Mazzoni, E.; D'Agostino, A.; Manfrini, M.; Maniero, S.; Puozzo, A.; Bassi, E.; Marsico, S.; Fortini, C.; Trevisiol, L.; Patergnani, S.; et al. Human Adipose Stem Cells Induced to Osteogenic Differentiation by an Innovative Collagen/Hydroxylapatite Hybrid Scaffold. *FASEB J.* **2017**, *31*, 4555–4565, doi:10.1096/fj.201601384R.
91. D'Agostino, A.; Trevisiol, L.; Favero, V.; Gunson, M.J.; Pedica, F.; Nocini, P.F.; Arnett, G.W. Hydroxyapatite/Collagen Composite Is a Reliable Material for Malar Augmentation. *J. Oral Maxillofac. Surg. Off. J. Am. Assoc. Oral Maxillofac. Surg.* **2016**, *74*, 1238.e1-1238.e15, doi:10.1016/j.joms.2016.01.052.
92. Arnett, G.W.; Trevisiol, L.; Grendene, E.; McLaughlin, R.P.; D'Agostino, A. Combined Orthodontic and Surgical Open Bite Correction: *Angle Orthod.* **2022**, doi:10.2319/101921-779.1.
93. Viguet-Carrin, S.; Garnero, P.; Delmas, P.D. The Role of Collagen in Bone Strength. *Osteoporos. Int. J. Establ. Result Coop. Eur. Found. Osteoporos. Natl. Osteoporos. Found. USA* **2006**, *17*, 319–336, doi:10.1007/s00198-005-2035-9.
94. El-Zayadi, A.A.; Jones, E.A.; Churchman, S.M.; Baboolal, T.G.; Cuthbert, R.J.; El-Jawhari, J.J.; Badawy, A.M.; Alase, A.A.; El-Sherbiny, Y.M.; McGonagle, D. Interleukin-22 Drives the Proliferation, Migration and Osteogenic Differentiation of Mesenchymal Stem Cells: A Novel Cytokine That Could Contribute to New Bone Formation in Spondyloarthropathies. *Rheumatology* **2016**, kew384, doi:10.1093/rheumatology/kew384.
95. Duvvuru, M.K.; Han, W.; Chowdhury, P.R.; Vahabzadeh, S.; Sciammarella, F.; ElSawa, S.F. Bone Marrow Stromal Cells Interaction with Titanium; Effects of Composition and Surface Modification. *PLOS ONE* **2019**, *14*, e0216087, doi:10.1371/journal.pone.0216087.
96. Tian, F.; Ji, X.-L.; Xiao, W.-A.; Wang, B.; Wang, F. CXCL13 Promotes Osteogenic Differentiation of Mesenchymal Stem Cells by Inhibiting MiR-23a Expression. *Stem Cells Int.* **2015**, *2015*, 632305, doi:10.1155/2015/632305.
97. Jiang, H.; Wang, Y.; Meng, J.; Chen, S.; Wang, J.; Qiu, Y.; Zhao, J.; Guo, T. Effects of Transplanting Bone Marrow Stromal Cells Transfected with CXCL13 on Fracture Healing of Diabetic Rats. *Cell. Physiol. Biochem. Int. J. Exp. Cell. Physiol. Biochem. Pharmacol.* **2018**, *49*, 123–133, doi:10.1159/000492848.
98. De Filippo, K.; Dudeck, A.; Hasenberg, M.; Nye, E.; van Rooijen, N.; Hartmann, K.; Gunzer, M.; Roers, A.; Hogg, N. Mast Cell and Macrophage Chemokines CXCL1/CXCL2 Control the Early Stage of Neutrophil Recruitment during Tissue Inflammation. *Blood* **2013**, *121*, 4930–4937, doi:10.1182/blood-2013-02-486217.
99. Lazennec, G.; Richmond, A. Chemokines and Chemokine Receptors: New Insights into Cancer-Related Inflammation. *Trends Mol. Med.* **2010**, *16*, 133–144, doi:10.1016/j.molmed.2010.01.003.
100. Pu, Y.; Wang, M.; Hong, Y.; Wu, Y.; Tang, Z. Adiponectin Promotes Human Jaw Bone Marrow Mesenchymal Stem Cell Chemotaxis via CXCL1 and CXCL8. *J. Cell. Mol. Med.* **2017**, *21*, 1411–1419, doi:10.1111/jcmm.13070.
101. Asokan, S.; Bandapalli, O.R. CXCL8 Signaling in the Tumor Microenvironment. *Adv. Exp. Med. Biol.* **2021**, *1302*, 25–39, doi:10.1007/978-3-030-62658-7\_3.

102. Wang, S.; Umrath, F.; Cen, W.; Reinert, S.; Alexander, D. Angiogenic Potential of VEGF Mimetic Peptides for the Biofunctionalization of Collagen/Hydroxyapatite Composites. *Biomolecules* **2021**, *11*, 1538, doi:10.3390/biom11101538.
103. Giachelli, C.M.; Steitz, S. Osteopontin: A Versatile Regulator of Inflammation and Biomineralization. *Matrix Biol. J. Int. Soc. Matrix Biol.* **2000**, *19*, 615–622, doi:10.1016/s0945-053x(00)00108-6.
104. Holladay, C.; Power, K.; Sefton, M.; O'Brien, T.; Gallagher, W.M.; Pandit, A. Functionalized Scaffold-Mediated Interleukin 10 Gene Delivery Significantly Improves Survival Rates of Stem Cells In Vivo. *Mol. Ther.* **2011**, *19*, 969–978, doi:10.1038/mt.2010.311.
105. Komori, T. Regulation of Proliferation, Differentiation and Functions of Osteoblasts by Runx2. *Int. J. Mol. Sci.* **2019**, *20*, E1694, doi:10.3390/ijms20071694.
106. Tang, W.; Li, Y.; Osimiri, L.; Zhang, C. Osteoblast-Specific Transcription Factor Osterix (Osx) Is an Upstream Regulator of Satb2 during Bone Formation. *J. Biol. Chem.* **2011**, *286*, 32995–33002, doi:10.1074/jbc.M111.244236.
107. Lefebvre, V.; Dvir-Ginzberg, M. SOX9 and the Many Facets of Its Regulation in the Chondrocyte Lineage. *Connect. Tissue Res.* **2017**, *58*, 2–14, doi:10.1080/03008207.2016.1183667.
108. Loebel, C.; Czekanska, E.M.; Bruderer, M.; Salzmann, G.; Alini, M.; Stoddart, M.J. In Vitro Osteogenic Potential of Human Mesenchymal Stem Cells Is Predicted by Runx2/Sox9 Ratio. *Tissue Eng. Part A* **2015**, *21*, 115–123, doi:10.1089/ten.TEA.2014.0096.
109. Johnson, D.; Iseki, S.; Wilkie, A.O.; Morriss-Kay, G.M. Expression Patterns of Twist and Fgfr1, -2 and -3 in the Developing Mouse Coronal Suture Suggest a Key Role for Twist in Suture Initiation and Biogenesis. *Mech. Dev.* **2000**, *91*, 341–345, doi:10.1016/s0925-4773(99)00278-6.
110. Rice, D.P.; Aberg, T.; Chan, Y.; Tang, Z.; Kettunen, P.J.; Pakarinen, L.; Maxson, R.E.; Thesleff, I. Integration of FGF and TWIST in Calvarial Bone and Suture Development. *Dev. Camb. Engl.* **2000**, *127*, 1845–1855.
111. Bildsoe, H.; Loebel, D.A.F.; Jones, V.J.; Chen, Y.-T.; Behringer, R.R.; Tam, P.P.L. Requirement for Twist1 in Frontonasal and Skull Vault Development in the Mouse Embryo. *Dev. Biol.* **2009**, *331*, 176–188, doi:10.1016/j.ydbio.2009.04.034.
112. el Ghouzzi, V.; Le Merrer, M.; Perrin-Schmitt, F.; Lajeunie, E.; Benit, P.; Renier, D.; Bourgeois, P.; Bolcato-Bellemin, A.L.; Munnich, A.; Bonaventure, J. Mutations of the TWIST Gene in the Saethre-Chotzen Syndrome. *Nat. Genet.* **1997**, *15*, 42–46, doi:10.1038/ng0197-42.
113. Quarto, N.; Senarath-Yapa, K.; Renda, A.; Longaker, M.T. TWIST1 Silencing Enhances In Vitro and In Vivo Osteogenic Differentiation of Human Adipose-Derived Stem Cells by Triggering Activation of BMP-ERK/FGF Signaling and TAZ Upregulation. *Stem Cells Dayt. Ohio* **2015**, *33*, 833–847, doi:10.1002/stem.1907.

114. Nguyen, V.; Meyers, C.A.; Yan, N.; Agarwal, S.; Levi, B.; James, A.W. BMP-2-Induced Bone Formation and Neural Inflammation. *J. Orthop.* **2017**, *14*, 252–256, doi:10.1016/j.jor.2017.03.003.
115. Wu, S.; Xiao, Z.; Song, J.; Li, M.; Li, W. Evaluation of BMP-2 Enhances the Osteoblast Differentiation of Human Amnion Mesenchymal Stem Cells Seeded on Nano-Hydroxyapatite/Collagen/Poly(l-Lactide). *Int. J. Mol. Sci.* **2018**, *19*, E2171, doi:10.3390/ijms19082171.
116. Kausar, T.; Nayeem, S.M. Correlating Interfacial Water Dynamics with Protein-Protein Interaction in Complex of GDF-5 and BMPRI Receptors. *Biophys. Chem.* **2018**, *240*, 50–62, doi:10.1016/j.bpc.2018.05.006.
117. Wang, H.; Xie, Z.; Hou, T.; Li, Z.; Huang, K.; Gong, J.; Zhou, W.; Tang, K.; Xu, J.; Dong, S. MiR-125b Regulates the Osteogenic Differentiation of Human Mesenchymal Stem Cells by Targeting BMPRIb. *Cell. Physiol. Biochem. Int. J. Exp. Cell. Physiol. Biochem. Pharmacol.* **2017**, *41*, 530–542, doi:10.1159/000457013.
118. Labour, M.-N.; Riffault, M.; Christensen, S.T.; Hoey, D.A. TGFβ1 – Induced Recruitment of Human Bone Mesenchymal Stem Cells Is Mediated by the Primary Cilium in a SMAD3-Dependent Manner. *Sci. Rep.* **2016**, *6*, 35542, doi:10.1038/srep35542.
119. Singh, A.; Gill, G.; Kaur, H.; Amhmed, M.; Jakhu, H. Role of Osteopontin in Bone Remodeling and Orthodontic Tooth Movement: A Review. *Prog. Orthod.* **2018**, *19*, 18, doi:10.1186/s40510-018-0216-2.
120. Cukierman, E.; Pankov, R.; Stevens, D.R.; Yamada, K.M. Taking Cell-Matrix Adhesions to the Third Dimension. *Science* **2001**, *294*, 1708–1712, doi:10.1126/science.1064829.
121. Lee, E.J.; Park, S.J.; Kang, S.K.; Kim, G.-H.; Kang, H.-J.; Lee, S.-W.; Jeon, H.B.; Kim, H.-S. Spherical Bullet Formation via E-Cadherin Promotes Therapeutic Potency of Mesenchymal Stem Cells Derived From Human Umbilical Cord Blood for Myocardial Infarction. *Mol. Ther.* **2012**, *20*, 1424–1433, doi:10.1038/mt.2012.58.
122. Rettinger, C.L.; Fourcaudot, A.B.; Hong, S.J.; Mustoe, T.A.; Hale, R.G.; Leung, K.P. In Vitro Characterization of Scaffold-Free Three-Dimensional Mesenchymal Stem Cell Aggregates. *Cell Tissue Res.* **2014**, *358*, 395–405, doi:10.1007/s00441-014-1939-0.
123. Bou-Ghannam, S.; Kim, K.; Grainger, D.W.; Okano, T. 3D Cell Sheet Structure Augments Mesenchymal Stem Cell Cytokine Production. *Sci. Rep.* **2021**, *11*, 8170, doi:10.1038/s41598-021-87571-7.
124. New Biomimetic Strategies for Regeneration of Load-Bearing Bones. In *Bio-Inspired Regenerative Medicine*; Tampieri, A., Sprio, S., Eds.; Jenny Stanford Publishing, 2016 ISBN 978-0-429-08417-1.
125. Bailey, S.; Karsenty, G.; Gundberg, C.; Vashishth, D. Osteocalcin and Osteopontin Influence Bone Morphology and Mechanical Properties. *Ann. N. Y. Acad. Sci.* **2017**, *1409*, 79–84, doi:10.1111/nyas.13470.
126. Anderson, R.M.; Lawrence, A.R.; Stottmann, R.W.; Bachiller, D.; Klingensmith, J. Chordin and Noggin Promote Organizing Centers of Forebrain Development in the Mouse. *Development* **2002**, *129*, 4975–4987, doi:10.1242/dev.129.21.4975.

127. Itoh, Y.; Saitoh, M.; Miyazawa, K. Smad3–STAT3 Crosstalk in Pathophysiological Contexts. *Acta Biochim. Biophys. Sin.* **2018**, *50*, 82–90, doi:10.1093/abbs/gmx118.
128. Yang, Q.; Teng, B.-H.; Wang, L.-N.; Li, K.; Xu, C.; Ma, X.-L.; Zhang, Y.; Kong, D.-L.; Wang, L.-Y.; Zhao, Y.-H. Silk Fibroin/Cartilage Extracellular Matrix Scaffolds with Sequential Delivery of TGF-B3 for Chondrogenic Differentiation of Adipose-Derived Stem Cells. *Int. J. Nanomedicine* **2017**, *12*, 6721–6733, doi:10.2147/IJN.S141888.
129. Li, Y.; Qiao, Z.; Yu, F.; Hu, H.; Huang, Y.; Xiang, Q.; Zhang, Q.; Yang, Y.; Zhao, Y. Transforming Growth Factor-B3/Chitosan Sponge (TGF-B3/CS) Facilitates Osteogenic Differentiation of Human Periodontal Ligament Stem Cells. *Int. J. Mol. Sci.* **2019**, *20*, 4982, doi:10.3390/ijms20204982.
130. Sasaki, H.; Rothrauff, B.B.; Alexander, P.G.; Lin, H.; Gottardi, R.; Fu, F.H.; Tuan, R.S. In Vitro Repair of Meniscal Radial Tear With Hydrogels Seeded With Adipose Stem Cells and TGF-B3. *Am. J. Sports Med.* **2018**, *46*, 2402–2413, doi:10.1177/0363546518782973.
131. Grafe, I.; Alexander, S.; Peterson, J.R.; Snider, T.N.; Levi, B.; Lee, B.; Mishina, Y. TGF- $\beta$  Family Signaling in Mesenchymal Differentiation. *Cold Spring Harb. Perspect. Biol.* **2018**, *10*, a022202, doi:10.1101/cshperspect.a022202.
132. Deng, M.; Mei, T.; Hou, T.; Luo, K.; Luo, F.; Yang, A.; Yu, B.; Pang, H.; Dong, S.; Xu, J. TGF $\beta$ 3 Recruits Endogenous Mesenchymal Stem Cells to Initiate Bone Regeneration. *Stem Cell Res. Ther.* **2017**, *8*, 258, doi:10.1186/s13287-017-0693-0.
133. Ripamonti, U.; Nathaniel Ramoshebi, L.; Teare, J.; Renton, L.; Ferretti, C. The Induction of Endochondral Bone Formation by Transforming Growth Factor-B3: Experimental Studies in the Non-Human Primate Papio Ursinus. *J. Cell. Mol. Med.* **2008**, *12*, 1029–1048, doi:10.1111/j.1582-4934.2008.00126.x.
134. Ripamonti, U.; Duarte, R.; Ferretti, C. Re-Evaluating the Induction of Bone Formation in Primates. *Biomaterials* **2014**, *35*, 9407–9422, doi:10.1016/j.biomaterials.2014.07.053.
135. Del Angel-Mosqueda, C.; Gutiérrez-Puente, Y.; López-Lozano, A.P.; Romero-Zavaleta, R.E.; Mendiola-Jiménez, A.; Medina-De la Garza, C.E.; Márquez-M, M.; De la Garza-Ramos, M.A. Epidermal Growth Factor Enhances Osteogenic Differentiation of Dental Pulp Stem Cells in Vitro. *Head Face Med.* **2015**, *11*, 29, doi:10.1186/s13005-015-0086-5.
136. Hojo, H.; Ohba, S.; Yano, F.; Saito, T.; Ikeda, T.; Nakajima, K.; Komiyama, Y.; Nakagata, N.; Suzuki, K.; Takato, T.; et al. Gli1 Protein Participates in Hedgehog-Mediated Specification of Osteoblast Lineage during Endochondral Ossification. *J. Biol. Chem.* **2012**, *287*, 17860–17869, doi:10.1074/jbc.M112.347716.
137. Chi, B.; Liu, G.; Xing, L.; Tian, F. [RESEARCH PROGRESS OF Hedgehog SIGNALING PATHWAY IN REGULATING BONE FORMATION AND OSTEOGENIC DIFFERENTIATION OF BONE MESENCHYMAL STEM CELLS]. *Zhongguo Xiu Fu Chong Jian Wai Ke Za Zhi Zhongguo Xiufu Chongjian Waike Zazhi Chin. J. Reparative Reconstr. Surg.* **2016**, *30*, 1545–1550, doi:10.7507/1002-1892.20160318.

138. Milner, J.M.; Cawston, T.E. Matrix Metalloproteinase Knockout Studies and the Potential Use of Matrix Metalloproteinase Inhibitors in the Rheumatic Diseases. *Curr. Drug Targets - Inflamm. Allergy* **4**, 363–375.
139. Sasano, Y.; Zhu, J.-X.; Tsubota, M.; Takahashi, I.; Onodera, K.; Mizoguchi, I.; Kagayama, M. Gene Expression of MMP8 and MMP13 during Embryonic Development of Bone and Cartilage in the Rat Mandible and Hind Limb. *J. Histochem. Cytochem. Off. J. Histochem. Soc.* **2002**, *50*, 325–332, doi:10.1177/002215540205000304.
140. Calabrese, G.; Giuffrida, R.; Fabbi, C.; Figallo, E.; Furno, D.L.; Gulino, R.; Colarossi, C.; Fullone, F.; Giuffrida, R.; Parenti, R.; et al. Collagen-Hydroxyapatite Scaffolds Induce Human Adipose Derived Stem Cells Osteogenic Differentiation In Vitro. *PLOS ONE* **2016**, *11*, e0151181, doi:10.1371/journal.pone.0151181.
141. Hippler, M.; Lemma, E.D.; Bertels, S.; Blasco, E.; Barner-Kowollik, C.; Wegener, M.; Bastmeyer, M. 3D Scaffolds to Study Basic Cell Biology. *Adv. Mater. Deerfield Beach Fla* **2019**, *31*, e1808110, doi:10.1002/adma.201808110.
142. Barnes, P.J.; Adcock, I.M. Glucocorticoid Resistance in Inflammatory Diseases. *The Lancet* **2009**, *373*, 1905–1917, doi:10.1016/S0140-6736(09)60326-3.
143. Buckley, L.; Humphrey, M.B. Glucocorticoid-Induced Osteoporosis. *N. Engl. J. Med.* **2018**, *379*, 2547–2556, doi:10.1056/NEJMcp1800214.
144. Weinstein, R.S. Glucocorticoid-Induced Osteonecrosis. *Endocrine* **2012**, *41*, 183–190, doi:10.1007/s12020-011-9580-0.
145. Nisi, M.; La Ferla, F.; Graziani, F.; Gabriele, M. Osteonecrosis of the Jaws Related to Corticosteroids Therapy: A Case Report. *Ann. Stomatol. (Roma)* **2014**, *5*, 29–30.
146. Silva, A.P.; Patrício, É.; Lemos, C.A.; Alves, F.A. Jaw Osteonecrosis Caused by Prolonged Use of Corticosteroids in a Patient With Mycosis Fungoides: Case Report. *Oral Surg. Oral Med. Oral Pathol. Oral Radiol.* **2014**, *117*, e167, doi:10.1016/j.oooo.2013.12.089.
147. Eijken, M.; Koedam, M.; van Driel, M.; Buurman, C.J.; Pols, H.A.P.; van Leeuwen, J.P.T.M. The Essential Role of Glucocorticoids for Proper Human Osteoblast Differentiation and Matrix Mineralization. *Mol. Cell. Endocrinol.* **2006**, *248*, 87–93, doi:10.1016/j.mce.2005.11.034.
148. Hanna, H.; Mir, L.M.; Andre, F.M. In Vitro Osteoblastic Differentiation of Mesenchymal Stem Cells Generates Cell Layers with Distinct Properties. *Stem Cell Res. Ther.* **2018**, *9*, 203, doi:10.1186/s13287-018-0942-x.
149. Li, J.; Zhang, N.; Huang, X.; Xu, J.; Fernandes, J.C.; Dai, K.; Zhang, X. Dexamethasone Shifts Bone Marrow Stromal Cells from Osteoblasts to Adipocytes by C/EBPalpha Promoter Methylation. *Cell Death Dis.* **2013**, *4*, e832–e832, doi:10.1038/cddis.2013.348.
150. MacArthur, B.D.; Please, C.P.; Oreffo, R.O.C. Stochasticity and the Molecular Mechanisms of Induced Pluripotency. *PLoS ONE* **2008**, *3*, e3086, doi:10.1371/journal.pone.0003086.
151. Marciano, D.P.; Kuruvilla, D.S.; Boregowda, S.V.; Asteian, A.; Hughes, T.S.; Garcia-Ordóñez, R.; Corzo, C.A.; Khan, T.M.; Novick, S.J.; Park, H.; et al. Pharmacological



Repression of PPAR $\gamma$  Promotes Osteogenesis. *Nat. Commun.* **2015**, *6*, 7443, doi:10.1038/ncomms8443.

152. Brust, R.; Shang, J.; Fuhrmann, J.; Mosure, S.A.; Bass, J.; Cano, A.; Heidari, Z.; Chrisman, I.M.; Nemetcheck, M.D.; Blayo, A.-L.; et al. A Structural Mechanism for Directing Corepressor-Selective Inverse Agonism of PPAR $\gamma$ . *Nat. Commun.* **2018**, *9*, 4687, doi:10.1038/s41467-018-07133-w.
153. Gardner, O.F.W.; Alini, M.; Stoddart, M.J. Mesenchymal Stem Cells Derived from Human Bone Marrow. In *Cartilage Tissue Engineering: Methods and Protocols*; Doran, P.M., Ed.; Methods in Molecular Biology; Springer: New York, NY, 2015; pp. 41–52 ISBN 978-1-4939-2938-2.

## **9. SCIENTIFIC CONTRIBUTION**

During these years, I published 15 scientific articles in high-impact/peer-reviewed international journals in the fields of cell biology, molecular genetics, epigenetics and molecular biology, as reported below:

1. Oton-Gonzalez, L.; Mazziotta, C.; Iaquinta, M.R.; Mazzoni, E.; Nocini, R.; Trevisiol, L.; D'Agostino, A.; Tognon, M.; Rotondo, J.C.; Martini, F. Genetics and Epigenetics of Bone Remodeling and Metabolic Bone Diseases. *IJMS* 2022, 23, 1500, doi:10.3390/ijms23031500. Impact Factor (IF): 5.923
2. Oton-Gonzalez, L.; Rotondo, J.C.; Lanzillotti, C.; Mazzoni, E.; Bononi, I.; Iaquinta, M.R.; Cerritelli, L.; Malagutti, N.; Ciorba, A.; Bianchini, C.; et al. Serum HPV16 E7 Oncoprotein Is a Recurrence Marker of Oropharyngeal Squamous Cell Carcinomas. *Cancers* 2021, 13, 3370, doi:10.3390/cancers13133370. IF: 6.639
3. Iaquinta, M.R.; Torreggiani, E.; Mazziotta, C.; Ruffini, A.; Sprio, S.; Tampieri, A.; Tognon, M.; Martini, F.; Mazzoni, E. In Vitro Osteoinductivity Assay of Hydroxylapatite Scaffolds, Obtained with Biomorphic Transformation Processes, Assessed Using Human Adipose Stem Cell Cultures. *IJMS* 2021, 22, 7092, doi:10.3390/ijms22137092. IF: 5.923
4. Mazziotta, C.; Lanzillotti, C.; Torreggiani, E.; Oton-Gonzalez, L.; Iaquinta, M.R.; Mazzoni, E.; Gaboriaud, P.; Touzé, A.; Silvagni, E.; Govoni, M.; et al. Serum Antibodies Against the Oncogenic Merkel Cell Polyomavirus Detected by an Innovative Immunological Assay With Mimotopes in Healthy Subjects. *Front. Immunol.* 2021, 12, 676627, doi:10.3389/fimmu.2021.676627. IF: 7.561
5. Iaquinta, M.R.\*; Lanzillotti, C.\*; Mazziotta, C.\*; Bononi, I.; Frontini, F.; Mazzoni, E.; Oton-Gonzalez, L.; Rotondo, J.C.; Torreggiani, E.; Tognon, M.; et al. The Role of MicroRNAs in the Osteogenic and Chondrogenic Differentiation of Mesenchymal Stem Cells and Bone Pathologies. *Theranostics* 2021, 11, 6573–6591, doi:10.7150/thno.55664. IF: 11.556
6. Mazziotta, C.\*; Lanzillotti, C.\*; Iaquinta, M.R.\*; Taraballi, F.; Torreggiani, E.; Rotondo, J.C.; Oton-Gonzalez, L.; Mazzoni, E.; Frontini, F.; Bononi, I.; et al. MicroRNAs Modulate Signaling Pathways in Osteogenic Differentiation of Mesenchymal Stem Cells. *IJMS* 2021, 22, 2362, doi:10.3390/ijms22052362. IF: 5.923

7. Mazzoni, E.; Iaquinta, M.R.; Lanzillotti, C.; Mazziotta, C.; Maritati, M.; Montesi, M.; Sprio, S.; Tampieri, A.; Tognon, M.; Martini, F. Bioactive Materials for Soft Tissue Repair. *Front. Bioeng. Biotechnol.* 2021, 9, 613787, doi:10.3389/fbioe.2021.613787. IF: 5.890
8. Mazzoni, E.; Mazziotta, C.; Iaquinta, M.R.; Lanzillotti, C.; Fortini, F.; D'Agostino, A.; Trevisiol, L.; Nocini, R.; Barbanti-Brodano, G.; Mescola, A.; et al. Enhanced Osteogenic Differentiation of Human Bone Marrow-Derived Mesenchymal Stem Cells by a Hybrid Hydroxylapatite/Collagen Scaffold. *Front. Cell Dev. Biol.* 2021, 8, 610570, doi:10.3389/fcell.2020.610570. IF: 6.684
9. Rotondo, J.C.; Oton-Gonzalez, L.; Mazziotta, C.; Lanzillotti, C.; Iaquinta, M.R.; Tognon, M.; Martini, F. Simultaneous Detection and Viral DNA Load Quantification of Different Human Papillomavirus Types in Clinical Specimens by the High Analytical Droplet Digital PCR Method. *Front Microbiol* 2020, 11, 591452, doi:10.3389/fmicb.2020.591452. IF: 5.640
10. Sprio, S.; Dapporto, M.; Preti, L.; Mazzoni, E.; Iaquinta, M.R.; Martini, F.; Tognon, M.; Pugno, N.M.; Restivo, E.; Visai, L.; et al. Enhancement of the Biological and Mechanical Performances of Sintered Hydroxylapatite by Multiple Ions Doping. *Front. Mater.* 2020, 7, 224, doi:10.3389/fmats.2020.00224. IF: 3.515
11. Mazzoni, E.; Pellegrinelli, E.; Mazziotta, C.; Lanzillotti, C.; Rotondo, J.C.; Bononi, I.; Iaquinta, M.R.; Manfrini, M.; Vesce, F.; Tognon, M.; et al. Mother-to-Child Transmission of Oncogenic Polyomaviruses BKPyV, JCPyV and SV40. *Journal of Infection* 2020, 80, 563–570, doi:10.1016/j.jinf.2020.02.006. IF: 6.072
12. Iaquinta, M.R.\*; Mazzoni, E.\*; Bononi, I.; Rotondo, J.C.; Mazziotta, C.; Montesi, M.; Sprio, S.; Tampieri, A.; Tognon, M.; Martini, F. Adult Stem Cells for Bone Regeneration and Repair. *Front Cell Dev Biol* 2019, 7, 268, doi:10.3389/fcell.2019.00268. IF: 6.684
13. Iaquinta, M.R.\*; Mazzoni, E.\*; Manfrini, M.; D'Agostino, A.; Trevisiol, L.; Nocini, R.; Trombelli, L.; Barbanti-Brodano, G.; Martini, F.; Tognon, M. Innovative Biomaterials for Bone Regrowth. *International Journal of Molecular Sciences* 2019, 20, 618, doi:10.3390/ijms20030618. IF: 5.923

14. Mazzoni, E.; D'Agostino, A.; Iaquinta, M.R.; Bononi, I.; Trevisiol, L.; Rotondo, J.C.; Patergnani, S.; Giorgi, C.; Gunson, M.J.; Arnett, G.W.; et al. Hydroxylapatite-Collagen Hybrid Scaffold Induces Human Adipose-Derived Mesenchymal Stem Cells to Osteogenic Differentiation in Vitro and Bone Regrowth in Patients. *Stem Cells Transl Med* 2020, 9, 377–388, doi:10.1002/sctm.19-0170. IF: 6.940
15. Torreggiani, E.; Rossini, M.; Bononi, I.; Pietrobon, S.; Mazzoni, E.; Iaquinta, M.R.; Feo, C.; Rotondo, J.C.; Rizzo, P.; Tognon, M.; et al. Protocol for the Long-term Culture of Human Primary Keratinocytes from the Normal Colorectal Mucosa. *Journal of Cellular Physiology* 2019, 234, 9895–9905, doi:10.1002/jcp.28300. IF: 6.384

Together with already published articles/reviews, other scientific articles have been accepted/submitted:

1. Iaquinta MR\*, Martini F\*, D' Agostino A, Trevisiol L, Bersani M, Torreggiani E, Tognon M, Rotondo JC and Mazzoni E. Stem cell fate and immunomodulation promote bone regeneration *via* composite Bio-Oss<sup>®</sup>/Avitene<sup>™</sup> biomaterial. *Accepted*.
2. Bononi I, Mazzoni E, Pietrobon S, Iaquinta MR, Caselli A, Torreggiani E, Pugliatti M, Casetta I, Castellazzi M, Granieri E, Martini F, Tognon M. Neurological diseases affected patients including multiple sclerosis are poor responder to BKPyV, a human neurotropic polyomavirus. *Submitted*.